

Validation of UARS MLS "ClO Measurements

J.W. Waters, W.G. Read, L. Froidevaux, T.A. Lungu, V.S. Perun, R.A. Stachnik, R.F. Jar-not, R.E. Cofield, E.F. Fishbein, D.A. Flower, J.R. Burke, J.C. Hardy, L.L. Nakamura, B.P. Ridenoure, Z. Shippony, R.P. Thurstans
Jet Propulsion Laboratory, California Institute of Technology, Pasadena

L.M. Avallone, D.W. Toohy
University of California at Irvine, Earth System Science Department

R.J. deZafra, D.T. Shindell
State University of New York at Stony Brook, Physics Department

Abstract. Validation of stratospheric ClO measurements by the Microwave Limb Sounder (MLS) on the Upper Atmosphere Research Satellite (UARS) is described. Credibility of the measurements is established by (1) examination of the measured ClO spectral emission line and its consistency with the retrieved ClO profiles, and (2) comparisons of MLS results with other ClO measurements by balloon-based, ground-based, and aircraft-based techniques. It is concluded that MLS Version 3 ClO data, the first version publicly released, are useful for scientific analyses at retrieval surfaces between 46 and 1 hPa (approximately 20 to 50 km height). Estimated values of 'noise' (random), 'scaling' (multiplicative) and 'bias' (additive) uncertainties are obtained for the Version 3 data. 'Noise' uncertainties range from 0.4 ppbv at 46 hPa to 1.3 ppbv at 1 hPa for individual profile retrievals, and can be reduced by averaging. 'Scaling' uncertainties in the Version 3 data are 15% over most of the useful vertical range. 'Bias' uncertainties are ~0.2 ppbv over most of the range, but under conditions of enhanced lower stratospheric ClO, degrade to -0.4 ppbv at 46 hPa. Known problems in the MLS Version 3 ClO data are identified, and include bias errors of -0.1 to -0.2 ppbv between 10 and 46 hPa for typical mid-latitude ClO conditions and ~+0.2 ppbv for conditions of depleted gas-phase HNO₃ which are typical of the Antarctic winter vortex. An estimated scaling error of ~+8% is present in the Version 3 data for enhanced lower stratospheric ClO. Further work is planned to correct these problems.

1. Introduction

The Microwave Limb Sounder on the Upper Atmosphere Research Satellite is performing the first global measurements of stratospheric chlorine monoxide (ClO), the predominant form of reactive chlorine which destroys stratospheric ozone (O₃). Knowing the amount and global distribution of stratospheric ClO is important since the rate of O₃ destruction by chlorine chemistry can be inferred from the abundance of ClO, and the primary source of stratospheric chlorine is industrially-produced chlorofluorocarbons (CFCs) [Molina and Rowland, 1974]. Chlorine destruction of O₃ in the upper stratosphere is proportional to [ClO], the ClO number density. Large springtime loss of Antarctic ozone [Farman et al., 1985] is caused, primarily, by a process proportional to [ClO]² [e.g., Solomon, 1990] where reaction of ClO with itself [Molina and Molina, 1987] controls the overall rate.

Techniques which have been developed to measure

stratospheric ClO include *in situ* and remote methods. The *in situ* technique observes 1189A fluorescence from Cl atoms which have been converted from ClO by reaction with NO in a fast flow reactor cell. It has been deployed on parachutes released from balloon [Anderson et al., 1977], reel-down from balloon [Brune et al., 1985], piloted aircraft [Brune et al., 1988], and recently developed for remotely-piloted aircraft [Toohy et al., 1993a]. Remote techniques include heterodyne measurements of millimeter, submillimeter and infrared spectral lines, as well as interferometric observations of submillimeter lines. The millimeter-wavelength heterodyne technique — used on UARS MLS — has been used previously from aircraft [Waters et al., 1979], ground [e.g., Parrish et al., 1981], and balloon [e.g., Waters et al., 1981]. Submillimeter heterodyne techniques have been used from balloon [Stachnik et al., 1992] and aircraft [Crewell et al., 1994], and submillimeter interferometric techniques from balloon [Carli et al., 1988]. The millimeter and submillimeter techniques measure atmospheric thermal

emission. Infrared heterodyne measurements were of atmospheric absorption of solar radiation, and conducted from balloon [Menzies; 1979, 1983].

This paper describes validation of the UARS MLS CIO measurements. Here 'validation' is defined as establishing the credibility of the measurements and their estimated uncertainty (both accuracy and precision). It involves (1) quantifying contributions to the overall uncertainty from various sources --- such as instrument noise, calibration and pointing, approximations made in the data processing algorithms, spectroscopic data base, etc. --- to the overall uncertainty, and (2) comparing the results from MLS with other measurements and 'known' behavior of stratospheric CIO to determine whether there is agreement to within the expected uncertainties. Companion papers in this issue describe calibration of the MLS instrument [Jarnot et al., 1994], and validation of MLS O₃ [Froidevaux et al., 1994], H₂O [Lahoz et al., 1994], and temperature/pressure [Fishbein et al., 1994]. Froidevaux et al. [1994] give details of the algorithms used for retrieving geophysical parameters from the radiances measured by MLS. The 'forward model' used for MLS retrievals will be described in a future publication [W. G. Read et al., in preparation].

The data discussed here are, mainly, the UARS Central Data Handling Facility (CDHF) Version 3 MLS data --- the first version publicly released. Results already published using these data include Douglass et al. [1993]; Elson and Froidevaux [1993]; Geller et al. [1993]; Schoeberl et al. [1993]; Waters et al. [1993ab, 1994]; Bell et al. [1994]; Manney et al. [1994]; Ricaud et al. [1994]; Santee et al. [1994]. MLS data are available electronically from the Earth Observing System Distributed Active Archive Center at the NASA Goddard Space Flight Center. The 'Standard Formatted Data Units (SFDU) Documentation' made available with these data describe the format and content of the data files. Names used in the SFDU Document are indicated by typewriter font (e.g., MMAF.STAT) in this paper,

2. Measurement Description

UARS MLS measurements are obtained from observations of millimeter-wavelength thermal emission as the instrument field-of-view (FOV) is vertically-scanned through the atmospheric limb. Several references exist which describe the general technique of microwave remote sensing [e.g., Staelin, 1969; Njoku, 1982; Ulaby et al., 1981, 1986; Janssen, 1993]. A general description of microwave limb sounding and its features is given by Waters [1989, 1993]. The UARS MLS instrument is described by Barath et al. [1993].

CIO is measured from the spectral line for the $J = \frac{11}{2} + \frac{9}{2}$ rotational transition (J is the quantum number

for total angular momentum) of the ³⁵CIO isotope in the ground vibrational ($v = 0$) and electronic ($^2\Pi_{3/2}$) states. Stratospheric emission from this transition is centered near 204,352 MHz frequency (1.47 mm wavelength) and, due to nuclear quadrupole effects, is split into 8 hyperfine components. The hyperfine components are spread over a range of ~25 MHz, and frequencies of all have been measured with ~0.02 MHz accuracy [Pickett et al., 1981]. The ³⁵CIO dipole moment for the $v = 0$, $^2\Pi_{3/2}$ state has been measured to better than 0.1% accuracy [Yaron et al., 1988]. The linewidth parameter for pressure broadening of these transitions by both N₂ and O₂ has been measured with 3% accuracy as a function of temperature between 200 and 300 K [Pickett et al., 1981; Oh and Cohen, 1994].

The top panel of Figure 1 shows atmospheric emission over the spectral region covered by the MLS 205 GHz radiometer which measures CIO. The bottom panel shows an expanded region of the spectrum covered by the 205 GHz radiometer in MLS spectral bands B2 and 133 which are used for CIO. It indicates individual filter positions in the two bands, and includes contributions from both sidebands of the double-sideband radiometer. B3 was originally included in MLS to measure H₂O₂, when H₂O₂ was predicted to be a major odd-hydrogen reservoir in the middle stratosphere, with abundances >10 ppbv [e.g., Wofsy 1978]. Refinements to parameters used for the theoretical predictions, and measurements [e.g., Chance et al., 1991], now indicate only ~0.1 ppbv H₂O₂ in the stratosphere. The UARS MLS design was 'frozen' before discovery of severe ozone loss in the lower stratosphere over Antarctica, and when the major concerns were chlorine depletion of ozone in the upper stratosphere. Consequently, the instrument is principally designed for measurements in the middle and upper stratosphere. Lower stratospheric measurements are more difficult because the MLS filter banks do not have sufficient bandwidth to cover as wide a spectral region around the broad spectral lines in the lower stratosphere as would be desired. The additional spectral coverage provided by B3, however, improves MLS measurements of CIO in the lower stratosphere. The double-sideband system noise temperature for bands B2/B3 is 990 K; the corresponding 1 σ noise on individual 1.8s radiance measurements is 0.07 K for the wide 128 MHz filters at the end of bands and 0.5 K for the narrow 2 MHz filters at band center, and it has been demonstrated that the noise in averages decreases inversely as the square root of the number of measurements averaged --- down to at least 0.01 K.

The calculated spectra shown in Figure 1 include signals expected for both upper stratospheric and enhanced lower stratospheric CIO. The calculation uses spectroscopic data from the JPL catalog [Poynter and Pickett,

1985; *Pickett et al.*, 1992] and includes spectral lines of all molecules (and states) which are thought to be significant. *Waters [1992, 1993]* gives a general method of quantifying the expected strength of molecular emissions at millimeter and submillimeter wavelengths. ClO is the strongest contributor to daytime stratospheric emission in MLS bands B2 and B3, but there are minor contributions from lines of HNO_3 , $^{18}\text{O}_3$, SO_2 and H_2O_2 . MLS measurements of the SO_2 line have been used to obtain vertical profiles of enhanced SO_2 injected into the stratosphere by the Pinatubo volcano [*Read et al.*, 1993]. Lower stratospheric HNO_3 can also be retrieved [*W.G. Read et al.*, paper in preparation; see also *Santee et al.*, 1994] from its signature in band 114 used for the 205 GHz ozone measurement, but this was not done for Version 3 processing. Measurements in B2 have also been used to obtain upper tropospheric H_2O [*Read et al.*, 1994], which is important for climate change research.

Thermal emission from the ClO line is only a weak function of atmospheric temperature. Accurate temperatures are not required for the ClO measurement. This is because (1) the Planck function at millimeter wavelengths is a weak (linear) increasing function of temperature, and (2) the energies of the ClO states involved in the transition ($\sim 14 \text{ cm}^{-1}$) are much less than kT , where k is Boltzmann's constant. The state energies being less than kT means that the number of molecules in that state decreases with increasing temperature; this is a larger effect than the temperature-dependence of the Planck function. A +5 K change in atmospheric temperature, for example, produces $\sim -3\%$ change in 204 GHz ClO emission.

It can be shown [*Waters*, 1993] that the relative contribution (per unit amount of the emitting species) to the measured limb emission, for optically-thin situations such as the ClO line, has a Gaussian distribution along the observation path - with center at the tangent point and width approximately equal to the geometric mean of the scale height of atmospheric pressure and the diameter of the Earth. This sets the horizontal resolution along the line of sight -- perpendicular to the UARS velocity -- to $\sim 400 \text{ km}$. MLS, under normal operations, performs a complete limb scan with radiometric calibrations every 65.536s -- the MLS Major Frame (MMAF) period. The limb scan covers tangent heights of ~ 0 to $\sim 90 \text{ km}$, and consists of discrete steps. The scan step spacing used for normal operations (see *Jarnot et al.* [1994]) varies between $\sim 1 \text{ km}$ in the lower stratosphere to $\sim 5 \text{ km}$ in the mesosphere. A single MLS measurement period is referred to as an MLS Minor Frame (MMIF), which is of 2.048s duration (1/32 of an MMAF). Atmospheric spectra are measured within an MMIF, during 1.8s dwells of the FOV between steps. The UARS or-

bit motion during the time of a limb scan smears the measurement over $\sim 400 \text{ km}$ in a direction perpendicular to the MLS line-of-sight. The horizontal resolution of the ClO measurement is thus $\sim 400 \times 400 \text{ km}$. The FOV vertical extent (full width at half maximum) at the tangent point for the ClO measurements is 3 km, the approximate inherent vertical resolution of the measurements. As discussed below, the Version 3 data are produced on a vertical grid with points spaced each factor of $10^{1/3} = 2.15$ change in atmosphere pressure, giving a vertical resolution of $\sim 5 \text{ km}$.

Atmospheric pressure at the tangent point of the observation path is simultaneously measured by observations of thermal emission from molecular oxygen, and this provides the vertical coordinate on which ClO profiles are retrieved. Validation of the MLS tangent pressure (and temperature) measurements is described by *Fishbein et al.* [1994].

The latitudinal coverage of measurements is from 34° on one side of the equator to 80° on the other. UARS performs a yaw maneuver at ~ 36 day intervals (a 'UARS month'), when MLS high latitude coverage switches between north and south. Within each UARS month, the UARS orbit plane precesses slowly with respect to the Earth-sun line, and local solar time of MLS measurements at a given latitude (on either the 'day' or 'night' side of the orbit) varies by only 20 minutes during a 24-hour period. The orbit precession causes the measurements to 'sweep through' essentially all local solar times during the course of a UARS month, becoming 20 minutes earlier each day at a fixed latitude.

3. Data Processing for Version 3 ClO

MLS data processing produces individual files containing measurements made over a 24 hour period -- from 0 to 24 hours UT on each day. There are two major steps to the processing. The first converts raw 'counts' from the instrument telemetry into calibrated radiances and other engineering diagnostics, and produces a 'Level 1' file. *Jarnot et al.* [1994] describe the MLS Level 1 processing (and instrument calibration). The second processing step converts calibrated radiances from the Level 1 files into geophysical data, producing a 'Level 2' file (geophysical parameters on a vertical grid chosen by the instrument team). The Level 2 processing step for MLS also produces 'Level 3A' files, which are geophysical parameters on a vertical grid common to all UARS instruments producing atmospheric profiles. There are two Level 3A files: (1) Level 3AT which has profiles equally spaced in time intervals of 65.536s, and (2) Level 3AI, which has profiles equally spaced in latitude intervals of 4° . Accompanying each Level 3AT and 3AI files are 'parameter' files, called

Level 3PT and 3PI, files, which contain various parameters providing diagnostics of the data. Additional processing of Level 3AL files by the UARS gridding team [Reber *et al.*, 1994] produces Level 3B files; these contain data commonly-gridded in the horizontal for all UARS instruments producing Level 3A L data.

A complete MLS limb scan (under normal operations) is performed for each 65.536s MMAF and, during Level 2 processing, a ClO profile is retrieved from the radiances measured on each limb scan. Sequential estimation, as first applied to atmospheric remote sensing by Rodgers [1976] is used, and a detailed description of the algorithms as implemented to produce the Version 3 MLS data is given by Froidevaux *et al.* [1994]. Conceptually, estimated values of a 'state vector' \mathbf{x} and its covariance matrix S are sequentially updated from a measurement vector \mathbf{y} according to the recursion formulae

$$\hat{\mathbf{x}}_i = \hat{\mathbf{x}}_{i-1} + \hat{S}_{i-1} K^T (K \hat{S}_{i-1} K^T + E)^{-1} \times (\mathbf{y} - \hat{\mathbf{y}}^c - K(\hat{\mathbf{x}}_{i-1} - \hat{\mathbf{x}})), \quad (1)$$

$$\hat{S}_i = \hat{S}_{i-1} - \hat{S}_{i-1} K^T (K \hat{S}_{i-1} K^T + E)^{-1} K \hat{S}_{i-1}, \quad (2)$$

where $\hat{\mathbf{x}}$ is a value about which the retrieval is linearized, $\hat{\mathbf{y}}^c$ is the value of \mathbf{y} calculated from $\hat{\mathbf{x}}$ using a 'forward model' and E is the error covariance of \mathbf{y} . K is a matrix of calculated partial derivatives of \mathbf{y}^c with respect to \mathbf{x} , having elements $K_{\alpha\beta} = \partial y_\alpha^c / \partial x_\beta$ where y_α is element α of \mathbf{y}^c , x_β is element β of \mathbf{x} , the partial derivatives are evaluated at $\mathbf{x} = \hat{\mathbf{x}}$, and superscript T indicates transpose. It should be noted that the MLS Version 3 algorithms assume linearity between the measured radiances and ClO mixing ratio, and that there is only a single 'pass' through the radiances, with no iteration. Improved non-linear algorithms are being developed for future data processing; preliminary results from some of these will be mentioned later in this paper.

Vertical variation of the ClO profile, for MLS Version 3 data, is represented as piecewise-linear in mixing ratio versus logarithm of atmospheric pressure, with breakpoints at $10^{(6-n)/3}$ hPa where n is an integer, ranging from 0 to 7 (100 to 0.46 hPa) for the vertical range over which meaningful ClO retrievals are performed. Retrieved mixing ratio values at the breakpoints of this representation (i.e., at pressures of 100, 46, 22, 10, 4.6, ... 0.46 hPa) constitute a subset of the elements of $\hat{\mathbf{x}}$; additional elements of $\hat{\mathbf{x}}$ include all other parameters (e.g., O_3 , temperature, tangent pressure, etc) retrieved

from the MLS data, and a description of the complete MLS state vector is given by Froidevaux *et al.* [1994]. It should be emphasized that the values retrieved for the breakpoints of the piecewise-linear representation should not be interpreted as 'point' measurements at that location; rather the entire profile should be interpreted as that which 'best-fits' the observed radiances, within the limitations of the retrieval algorithms and representation bases.

Radiances measured in MLS spectral bands B2 and B3 during one limb scan constitute the elements of \mathbf{y} which are used for the ClO retrievals. The radiance error covariance E is diagonal, to an adequate approximation, with diagonal elements obtained from the measured instrument noise and produced routinely as part of MLS Level 1 Processing [Jarnot *et al.*, 1994]. Values of the partial derivative matrix K and the calculated radiances $\hat{\mathbf{y}}^c$ are produced, for each 'UARS month' and selected latitude bins, from the MLS forward model, as described by Read *et al.* [paper in preparation]. The forward model accounts for the instrumental frequency and angular smearing of the radiances (including refraction), using measured values for the FOV and filter responses obtained during instrument calibration. It accounts for the hyperfine splitting in the 204 GHz ClO line, and the temperature-dependent populations of the rotational states involved -- including the fraction of ClO in the $^2\Pi_{1/2}$ spin state (11% at 220 K); excited vibrational states have negligible population (about 0.4% at 220K; see discussion in Waters *et al.* [1979]). Numerical errors resulting from software implementation of the forward model contribute less than 0.02 K accumulated uncertainty in the calculated spectral variation of the signals measured by MLS bands B2 and B3.

HNO_3 , and to a lesser extent N_2O , have a small effect on the ClO signal, and are accounted for in the Version 3 algorithm by assuming (latitudinal and seasonal dependent) climatological values [Gille *et al.*, 1989; Taylor *et al.*, 1989]. The effects of the ozone isotope ^{18}OOO are accounted for by multiplying the retrieved O_3 profile by 4.06×10^{-3} based on the 2.04×10^{-3} relative abundance of ^{18}O [Craig, 1957]; variations in the relative isotopic abundance with altitude [Mauersberger, 1987] are not included. The effects of SO_2 on ClO are included, since the Version 3 algorithms simultaneously retrieve SO_2 and ClO.

An independent retrieval is done for each limb scan, with the retrieval algorithm given no 'memory' of results from any other limb scan. The processing of data for each limb scan starts with *a priori* values of S and \mathbf{x} . The ClO retrieval is done after retrievals for all other elements of the state vector \mathbf{x} have been completed, so that values of S and \mathbf{x} at the beginning of the ClO retrieval have been updated for all 'non-ClO' elements.

This accounts, through non-diagonal elements of S , for effects of other retrieved parameters on the retrieved values of CIO and its uncertainty. The *a priori* values used for the 'pure CIO' elements of S are diagonal, with values corresponding to 3 ppbv 1σ uncertainty in CIO for atmospheric pressures between 100 and 0.46 hPa - intentionally very conservative to reduce effects of the *a priori* on the MLS result for CIO. The CIO profile below 100 hPa is also formally 'retrieved' as part of the sequential estimation process, but MLS does not provide significant information at these low altitudes and the retrieval is more tightly constrained to the *a priori* (an *a priori* uncertainty of 0.5 ppbv is used at 215 hPa, and 0.1 ppbv at 464 hPa). The CIO *a priori* values depend upon latitude, 'UARS month', whether the measurement was made during day or night, and are from a gas-phase model prediction (provided by D.J. Wuebbles and colleagues) which includes no heterogeneous chemistry enhancement of lower stratospheric CIO.

A 'spectral baseline' - consisting of a constant offset and a linear variation with frequency - is fitted to the combined radiances measured in bands B2 and 113 on each MMIF; this eliminates effects not adequately accounted for by the forward model. The 'spectral baseline' is part of the state vector x , and its uncertainty is included in the overall uncertainty estimated for CIO. To further eliminate tropospheric effects which could have spectral curvature and may not be adequately accounted for in the forward model, no radiances are used from observations for which the inferred atmospheric pressure at the FOV tangent point is greater than 100 hPa. Also, the algorithms check to ensure that no radiances are used when the inferred optical depth for the observation path is greater than unity (although this should not happen for bands B2 and B3 at tangent heights above 100 hPa).

The retrieved ^{35}ClO mixing ratios are then multiplied by 1.32 to give the total CIO mixing ratio in both ^{35}ClO and ^{37}ClO isotopes. This assumes 75.8% of chlorine is in the ^{35}Cl isotope [Shields *et al.*, 1962].

UARS Level 3A files have values on pressure surfaces of $10^{(6-n)/6}$ hPa where n is an integer - the spacing between Level 3A surfaces being half that of the MLS Version 3 Level 2 surfaces (i.e., there are twice as many Level 3A surfaces as MLS Level 2 surfaces). Averages of the two values on adjacent MLS Level 2 surfaces are put in the Version 3 MLS Level 3A files for the UARS surfaces on which MLS retrievals are not performed. Level 3AL files are produced by interpolating the MLS Level 3AT data to the 3AL latitudes (0, $\pm 4^\circ$, $\pm 8^\circ$, ...).

An estimated uncertainty is placed in the MLS Level 2 and 3 files for each value retrieved for CIO. This uncertainty is from the appropriate diagonal element of \hat{S} at the end of each profile retrieval, and its value is

made negative if it is not at least 2x smaller than the *a priori* uncertainty. Only retrievals having positive values of the estimated uncertainty should be used for scientific analyses unless otherwise endorsed by the MLS team. Several additional diagnostics are routinely produced during data processing and placed in the Level 2 files. The extent to which the retrieved profile 'fits' the measured radiances is described by a χ^2 diagnostic. This [see Froidevaux *et al.*, 1994] is the ratio, normalized to the number of degrees of freedom, of (1) the observed variance between measured and calculated radiances to (2) the predicted variance due to instrument noise - where the calculated radiances are from a linearized forward model operating on the retrieved parameters. The χ^2 diagnostic has a value near unity if the retrieved parameters fit the measured radiances to within the noise. The χ^2 diagnostics are produced for each MLS band, and both for radiances (1) measured during each 1.8s MMIF (χ_{mi}^2), and (2) measured over a complete 65s MMAF (χ_{ma}^2). A quality indicator for each CIO retrieval (QUALITY-CIO), based on χ_{ma}^2 for band B2, is placed in the MISL3PT and L3PL files. Only data having QUALITY-CIO=4, corresponding to $\chi_{ma}^2 \leq 2.0$, should be used for scientific analyses. Another important parameter placed in the MLS 3PT and 3PL files is MMAF_STAT, which gives the overall status of MLS data for that MMAF. Only data having MMAF_STAT=G (good) should be used for scientific analyses.

The retrieved CIO profile points have not been constrained to positive values and, since the signal-to-noise ratio for individual CIO measurements is generally less than unity, negative values often occur. This is required for maintaining a linear relation between the retrieved profile points and the measured radiances - which allows individual retrieved profiles to be averaged together to reduce noise. If the retrieved CIO profiles were not allowed to go negative (which would have been the case, for example, if logarithm of mixing ratio had been retrieved) and the actual amount of atmospheric CIO were zero, for example, then averaging the retrieved profiles would necessarily produce an incorrect non-zero result since instrument noise would only be allowed to produce positive values. Tests have shown that the same result for CIO is obtained by averaging the individual retrieved profiles as is obtained by performing a retrieval on averaged radiances. Much less effort is required in averaging the available individual profiles than in averaging the radiances and then doing additional retrievals; this is a major benefit of appropriately allowing negative values in individual retrievals.

Averaging kernels [Rodgers, 1990], which describe the vertical resolution of the Version 3 CIO retrievals, and their dependence upon the *a priori*, are shown in Figure 2. Summations over the averaging kernel columns

have value near unity, which indicate the **MIS CIO retrievals** between 100 and 0.46 hPa are virtually independent of the *a priori*; their width indicates the vertical resolution is approximately equal to that of the retrieval grid spacing (factor of $10^{1/3}$ change in atmospheric pressure, or ~ 5 km). The **MIS averaging kernels** are much narrower (especially in the lower stratosphere), and have peak values much closer to unity than those given in *Aellig et al.* [1993] for CIO measured by the same technique. The difference is due, mainly, to differences in the assumed *a priori* uncertainties. *Aellig et al.* [1993] assume an *a priori* CIO uncertainty ranging from less than 0.1 ppbv below 30 km and above 56 km to 0.7 ppbv at 40 km --- this causes the *a priori* to have a much larger effect (which reduces the peak values of the averaging kernels, and broadens them) in their retrievals than in ours where an *a priori* uncertainty of 3 ppbv is used at all altitudes between 100 and 0.46 hPa.

4. Radiances and Closure

An important aspect of validating **MIS CIO** is examination of the measured radiances, and the extent to which these are 'fit' by radiances calculated from the retrieved profiles. There are 30 spectral channels (in **MIS spectra**) bands **B2** and **B3**) which are used for retrieving CIO from **MIS**. These channels resolve the CIO emission line at all altitudes throughout the stratosphere, allowing clear identification of the CIO signal. Approximately 500 spectral points in each limb scan are used to retrieve the 8 CIO profile values, the 4 SO_2 profile values and approximately 36 'spectral baseline' values (offset and slope for each measured spectrum used in the CIO retrievals). Since there are many more measurements than retrieved parameters, examination of the residuals is a meaningful exercise.

Figure 3 shows averages of measured lower stratospheric radiances and residuals for conditions of enhanced lower stratospheric CIO in the Antarctic vortex in mid-August, where largest CIO abundances are measured by **MIS** [*Waters et al.* 1993 b]. Also shown are the radiances calculated from the Version 3 retrieved profiles, and the residuals (measured minus calculated radiances). The radiance is given as double-sideband 'brightness temperature' — a quantity which, when multiplied by Boltzmann's constant, gives the average spectral power density (Watts/Hz) received through each filter. It should be noted that the full Planck function

and not the Rayleigh-Jans approximation which is sometimes used for microwave calculations — is used for the **MIS** calculation. The 'double-sideband' units are due to the fact that the blackbody radiometric calibration used for **MIS** gives signals in both sidebands of the double-sideband radiometers, whereas the CIO spectral

line appears in only one of the sidebands; the 'single-sideband' CIO signals would be approximately twice as strong as the double-sideband signals shown here. The good fit between measurement and calculation is evident in Figure 3, and there is closure to within ~ 0.2 K brightness temperature.

The narrower spectral feature from upper stratospheric CIO is shown in Figure 4. Also shown are averages of the radiances calculated from the retrieved CIO and the residuals. The closure is within 0.05 K brightness temperature. The extent to which the lack of closure introduces errors in the retrievals is discussed in the next section of this paper.

Figure 5 shows averages of spectra measured at tangent height above ~ 65 km where the CIO signal (if present at all) would be confined to the narrow center channels, and illustrate residual artifacts in the measured radiances. These artifacts have a spectral variation of ~ 0.05 K brightness temperature, which yield artifacts in retrieved CIO abundances of ~ 0.05 ppbv. They appear sufficiently stable that day-night differences are expected to reduce the instrumental artifacts to approximately 0.01 K brightness temperature, corresponding to CIO abundance of approximately 0.01 ppbv (see also discussion in *Jarnot et al.*, [1994]).

Figure 6 shows daily zonal averages of χ^2_{ma} for bands **B2** and **B3** for the first three years of **MIS** operations. Values are generally in the 1.25-1.75 range, indicating reasonable fits to the measured radiances, but also indicating room for improvement. The gaps in Junc 1992 are due to **MIS** being off during an emergency with the **UARS** solar array drive. In the latter part of June, and early part of July 1992, **MIS** band **B3** was off while **B2** remained on; the improved χ^2_{ma} values in **B2** when **B3** was off are expected since there are fewer pieces of spectral data to fit. The large χ^2_{ma} values at northern mid-latitudes in October and November 1992 are due to development of excess noise induced by the **MIS** switching mirror movement at times near sunrise on the spacecraft when the **UARS** power supply voltage was at its lowest. The **MIS** instrument was determined to be sufficiently stable that calibration is not needed on each limb scan; its operation was then adapted to sense low-voltage situations, and the switching mirror was not moved in those situations. This adaptation was implemented between 18 November 1992 and 2 June 1993 -- after which performance, as measured by the χ^2_{ma} diagnostic, improved. The occurrences of occasional large χ^2_{ma} values after June 1993 are when there were abnormal operations. The one-day gaps in April-May 1994 and July 1994 are when **MIS** was operated every other day during 'summer **UARS** months' -- done to conserve lifetime of the antenna scan actuator which developed problems starting in late December 1993.

5. Uncertainties in Version 3 CIO

Uncertainties in the MLS CIO data, for use in scientific analyses, are conveniently grouped into three categories:

1. Noise --- a random contribution which can be reduced by averaging (this is the 'precision' of the measurement),
2. Scaling --- a 'multiplicative' uncertainty which gives the 'percentage' uncertainty in the measurements,
3. Bias -- an 'additive' uncertainty which can sometimes be reduced by taking appropriate differences.

We describe in detail below the MLS CIO uncertainties grouped into these categories. First, however, Figure 7 shows the '*a priori*' and 'measurement' contributions to uncertainties in individual MLS retrievals as obtained from the formalism developed by Rodgers [1990]. The '*a priori*' contribution is what has sometimes been called the 'null space' error, and we use the new terminology per the recommendation of Marks and Rodgers [1993]. The '*a priori*' contribution is considered a scaling uncertainty for CIO, as will be discussed later. The 'measurement' contribution shown in Figure 7 is the uncertainty due to measurement noise as given by this formalism.

The three categories of uncertainties mentioned above will now be discussed in detail.

'Noise' Uncertainties

The estimated noise uncertainty ($\pm 1\sigma$) associated with each retrieved CIO profile point is obtained from the appropriate diagonal element of the estimated covariance matrix computed by the retrieval algorithms, and is stored along with the retrieved values in the MLS data files. It includes the effects of noise uncertainties associated with temperature, pointing (tangent pressure of the observation path), water vapor, fitted spectral baseline and other parameters which are part of the overall state vector for the MLS retrievals. As stated earlier, the resulting uncertainty is multiplied by -1 if it is not at least 2x lower than the assumed *a priori* uncertainty -- to produce negative estimated uncertainties in the data files when the *a priori* has more than 25% influence on the result, so that these situations can easily be identified.

Figure 8 compares the 1σ noise uncertainties predicted by the retrieval algorithms with the 1σ variation observed in retrieved CIO profiles under conditions when instrument noise is expected to dominate. Each panel shows results for a full UARS month (summer in each hemisphere) of retrievals from measurements made

at night with local solar times between midnight and 6 am (no retrievals were included for which the solar zenith angle at the time and place of measurements was less than 95°). More than 10,000 independent retrievals were included for the results shown in each panel. The standard deviation of the measurements agrees closely with the predicted 1σ noise, except at the lowest altitude (100 hPa). Part of the discrepancy at 100 hPa is due to the fact that the predicted uncertainty includes a contribution from the assumed 3 ppbv *a priori* uncertainty, whereas a constant *a priori* value (0.0 ppbv at 100 hPa) with no noise is actually used when doing the retrievals. The Version 3 retrieval algorithms, therefore, 'think' there is noise on the *a priori* and include its contribution in the overall predicted uncertainty, whereas the *a priori* noise is not actually present (in the sense of introducing variability in the result) and the variability in the result is less than predicted. This effect is not so noticeable at higher altitudes where the measurements have more sensitivity relative to the assumed *a priori* uncertainty. Without the contribution from a *a priori* 'noise', the predicted CIO noise at 100 hPa is reduced from 1.7 ppbv to 1.4 ppbv. The remaining discrepancy of ~0.4 ppbv between the estimated and observed CIO noise at 100 hPa is still under investigation. The formal error estimates in Figure 7 show smaller uncertainties than predicted by the Version 3 algorithms at 100 hPa, and even smaller than variations in the retrieved values; this is also under investigation.

Figure 9 shows the distribution, on each retrieval pressure surface, of values of the nighttime CIO retrievals which were included in Figure 8 (a total of more than 20,000 retrievals). The distribution is seen to be Gaussian, as expected for random noise, and supports our understanding of the noise uncertainties in MLS CIO. Schoeberl et al. [1993] also found a Gaussian distribution of night-time and extra-vertical CIO values from MLS which are consistent with that expected from the noise.

'Scaling' Uncertainties

Figure 10 summarizes the estimated scaling uncertainties for the Version 3 CIO data. The bases for these estimates are given below.

CIO is retrieved from optically-thin radiance measurements and there is, to within a good approximation, a linear relationship between the CIO abundances, absorption coefficient and radiances: the same scaling uncertainties in radiances and absolute values of the CIO absorption coefficient thus apply to the retrieved profiles.

An overall instrument calibration uncertainty of 3% is used [Jarnot et al., 1994]. 'Calibration uncertainty' is here defined as the combined systematic uncertainty in

the calibrated radiances from each instrument channel *and* that introduced by instrument parameters in the forward model calculations of the radiance (which use the measured instrument spectral and field-of-view response). It should be noted that the same radiometer, optics path and calibration are used for the MLS/CIO measurements as for its 205 GHz ozone measurements, so that validation of the ozone measurements [Froidevaux et al., 1994], contributes confidence to calibration of the instrument for CIO measurements.

Uncertainties in the absolute value of the absorption coefficient are due to uncertainties in the measured dipole moment of CIO and in the calculated matrix element for the particular transition observed by MLS. The 0.1% uncertainty in the dipole moment [Yaron et al., 1988] introduces an 0.2% error since the square of the dipole moment appears in the expression for the absorption coefficient. The uncertainty in the calculation of the transition matrix element is estimated to be 0.5% [H.M. Pickett, private communication].

MLS spectrally resolves the CIO atmospheric emission feature, and its measurements provide information on the CIO line shape and width. An 'off-line' retrieval scheme was implemented which allowed retrieval of the CIO pressure-broadening linewidth parameter, simultaneously with the other parameters normally retrieved. Results gave a value somewhat smaller than the N₂ broadening parameter measured by Pickett et al. [1981]. The CIO line broadening, by both O₂ and N₂, were then measured over a temperature range of 200-300 K in the laboratory by J.J. Oh and E.A. Cohen at JPL, who found values for N₂ in agreement with those of Pickett et al. [1981], but significantly smaller broadening by O₂. The new laboratory measurements [Oh and Cohen, 1994] have an estimated accuracy of 3%, and are consistent with the broadening parameter retrieved from the MLS data. Due to the smaller broadening by O₂, the new linewidth parameter for 'air' is ~10% lower than the N₂ value of Pickett et al. [1981]. The new Oh and Cohen [1994] linewidth parameter was used in the production of MLS Version 3 CIO data. The effect of the estimated 3% uncertainty of the linewidth parameter on the retrieved profiles was determined by propagating the uncertainty through the retrieval algorithm, which resulted in the 'Δν(CIO)' curve shown in Figure 10.

The scaling error due to the *a priori* can be estimated as follows. Neglecting off-diagonal terms in the covariance matrix, the retrieved value \hat{x} is obtained from the *a priori* value x_a and the 'measured' value x_m according to $\hat{x} := \hat{\sigma}^2(x_m/\sigma_m^2 + x_a/\sigma_a^2)$, where σ_m is the uncertainty associated with the measurement, σ_a is the uncertainty associated with the *a priori*, and $\hat{\sigma}$ is the resulting overall uncertainty predicted by the retrieval algorithm: $U^{-2} = \sigma_m^{-2} + \sigma_a^{-2}$. For $x_a = 0$, the 'measure-

ment' is thus seen to be scaled by $\hat{\sigma}^2/\sigma_m^2$. The scaling error is then $1 - \hat{\sigma}^2/\sigma_m^2 = \hat{\sigma}^2/\sigma_a^2$. The *a priori* 'scaling uncertainty' shown in Figure 10 is $\hat{\sigma}^2/\sigma_a^2$, where $\hat{\sigma}$ is taken from Figure 8 and $\sigma_a = 3$ ppbv is the *a priori* uncertainty assumed by the Version 3 algorithms. This is considered an upper limit, since the actual *a priori* value used by the retrievals is expected to be closer to the true value than an *a priori* of zero, and the *a priori* scaling error is proportional to the difference between the *a priori* and true values.

Figure 11 shows results of simulations (without noise on the radiances) where the 'true' CIO was made to cycle between 0, 1 and 2 ppbv separately at all retrieval surfaces. Except at 100 hPa (and to some extent at 0.46 hPa) where effects of the *a priori* are expected as discussed above, the retrieval 'closure' is seen (by comparing the retrieved values with the 'true' values) to be within ~10%. Based on this, we use 10% as an estimated scaling uncertainty due to lack of closure, and this value is shown in Figure 10.

The 'P_{tan}' curve in Figure 10 is the uncertainty in CIO due to 6% systematic uncertainty [Fishbein et al., 1994] in the MLS tangent pressure measurement. Additional systematic uncertainties in the MLS FOV direction and shape, filter shapes, etc., are thought too small to contribute significantly to the overall scaling uncertainty for CIO. See Froidevaux et al. [1994] for a discussion of their magnitude and effect on uncertainties in MLS ozone.

'Bias' Uncertainties

Bias uncertainties can be introduced in the retrievals due to lack of adequately fitting the measured radiances within the noise. This 'residual uncertainty' can be caused by inadequacies in the non-iterative linear algorithm used for producing Version 3 data (which can also introduce a 'scaling' uncertainty), and effects of interfering species which are not adequately accounted for in the retrieval scheme. Molecules which have a small effect on the CIO signal, and which are accounted for only by climatological values in producing the Version 3 data, include HNO₃ and N₂O. The effects of the ozone isotope ¹⁸O are included by using values for its abundance obtained from multiplying the retrieved O₃ profile by 4.08x 10⁻³, based on the 2.04x 10⁻³ relative abundance of ¹⁸O [Craig, 1957]; variations in the relative isotopic abundance with altitude [Mauersberger, 1987] are not included. The effects of SO₂ are included, since the Version 3 algorithms simultaneously retrieve SO₂ and CIO.

Figure 12 shows the residual error associated with retrievals of CIO for typical mid-] altitude conditions and for enhanced lower stratospheric CIO conditions encountered over Antarctica. The curves in Figure 12 were determined by taking the differences between averages of

radiances measured in **MLS** bands **B2** and **B3** and average of radiances calculated from the retrieved profiles. The averaging sufficiently reduced instrument noise to where it did not contribute significantly to the resulting radiance residuals. These residuals were then propagated through the retrieval algorithms to determine the resulting uncertainty in **CIO**. Simulation tests, described below, were performed to determine how the Version 3 'residual' uncertainties should be partitioned between 'bias' and 'scaling' effects.

Figure 13 shows results of simulation tests for an enhanced lower stratospheric **CIO** situation. The solid curve is 'truth'; radiances for the simulations were calculated from it using climatological **HNO₃** and not including effects of **N₂O**. The dashed curve gives retrievals from the Version 3 algorithms, which also use climatological **HNO₃** and do not account for **N₂O**; agreement with 'truth' to better than 0.1 ppbv is obtained. The dotted curves in Figure 13 show results obtained from the same simulated radiances, but when **HNO₃** and **N₂O** are changed between zero and climatological values. The results indicate that complete removal (at all altitudes) of **HNO₃** can cause the retrieved **CIO** to be up to 0.3 ppbv too large (at 46 hPa), and complete removal of **N₂O** can cause the retrieved **CIO** to be up to 0.2 ppbv too small (at 100 hPa). The effect of **N₂O** i.e. <0.05 ppbv at 46 hPa and above for this simulation. The 'day minus night' differences for **CIO** show negligible effect of **HNO₃** or **N₂O**.

Figure 14 shows results from similar tests to determine the effects of **HNO₃** and **N₂O**, but using measured radiances. Radiances used in these tests were measured in the Antarctic vortex on 17 August and 17 September 1992. These days were chosen to be representative of (a) mid-August when **MLS** observes greatly enhanced **CIO** on both the 22 and 46 hPa retrieval surfaces, and (b) mid-September when greatly enhanced **CIO** is present only at 46 hPa [Waters et al., 1993b]. Retrievals giving largest **CIO** abundances were selected for examination, and the solid curves in Figure 14 are the averages of ~20 Version 3 profiles on 17 August and ~40 profiles on 17 September. The dashed curve shows results from a test where the radiances were averaged first and retrievals performed on the averaged radiances, with iterations to account for non-linearities. The iterative retrievals on averaged radiances give ~0.1 ppbv less enhanced **CIO** at 46 hPa, and ~0.2 ppbv less at 22 hPa. At 100 hPa there is a discrepancy with the Version 3 values of ~0.8 ppbv for the 17 August daytime **CIO** profile, and ~0.3 ppbv for the 17 September profiles. The situation at 100 hPa will be discussed below in more detail. In regards to the effects of **HNO₃** and **N₂O** on **CIO**, similar results are obtained as for those shown in Figure 13. The effect of setting **HNO₃** to zero is to re-

duce the **CIO** peak values by ~0.4 ppbv, and change the 100 hPa **CIO** value by ~0.5 ppbv. The effect of **N₂O** is less than ~0.1 ppbv at 46 hPa and above, but can be ~0.5 ppbv at 100 hPa. These differences are consistent with values expected from the residual uncertainties shown in Figure 12. All day-night differences agree to within ~0.1 ppbv at 46 hPa and above.

To further investigate the extent to which effects of **HNO₃** contribute to uncertainties in the Version 3 **CIO** for the extremes of situations actually encountered in the atmosphere, we examined an ensemble of **MLS** measurements made during 14–29 August 1992 at locations in the Antarctic vortex where gas-phase **HNO₃** was simultaneously observed to be greatly depleted. The **HNO₃** observations used here are from preliminary algorithms which retrieve **HNO₃** from the **MLS** radiances, and which will be incorporated into future reprocessing of **MIS** data. **MLS** **HNO₃** is obtained primarily from its signature in the 205 GHz ozone band (see upper panel of Figure 1) and not from its much weaker feature which affects the **CIO** measurement (see lower panel of Figure 1). This ensemble of measurements was chosen to be representative of 'worst case' effects of **HNO₃** on **CIO**: where <~1 ppbv **HNO₃** at 46 hPa was retrieved but the Version 3 algorithms assume ~10 ppbv **HNO₃**.

Table 1 compares the Version 3 **CIO** values with the preliminary values obtained with the **HNO₃** retrievals. With **HNO₃** retrieved, the **CIO** values at 22 hPa are reduced by 0.1 ppbv and the values at 46 hPa are reduced by 0.2 ppbv, for both day and night measurements. The day-night differences in 22 and 46 hPa **CIO** are unchanged. At 100 hPa, the night value retrieved for **CIO** is unchanged, but the day value is increased by 0.2 ppbv. The **HNO₃** effects on 100 hPa **CIO** appear to arise through its effects at 46 hPa: with **HNO₃** forced to climatological values, the Version 3 algorithms give (1) ~0.2 ppbv too much **CIO** at 46 hPa when fitting the radiances measured where 46 hPa **HNO₃** is depleted, then (2) too little **CIO** at 100 hPa — when 46 hPa **CIO** is enhanced — to compensate for retrieving too large a value at 46 hPa. Table 2 compares Version 3 **CIO** from regions in the January 1992 Arctic vortex where largest **CIO** was observed [Waters et al., 1993a] with the same data set but with **HNO₃** retrievals included. The effect here of **HNO₃** is to slightly (~0.1 ppbv which is only marginally significant) increase the **MLS** Arctic enhanced **CIO** values. The **HNO₃** retrieved from these Arctic **MLS** data was slightly higher than the Version 3 climatological values, as is expected due to **HNO₃**-rich air from evaporating **PSCs** in the warmer Arctic vortex.

The results described above indicate that if **HNO₃** is completely removed from the atmosphere at all altitudes, then the Version 3 **MLS** enhanced **CIO** peak abundances will be artificially large by ~0.4 ppbv. Complete removal

of N_2O can affect ClO by ~ 0.5 ppbv at 100 hPa, but its effect at higher altitudes is negligible. For HNO_3 profiles actually encountered in the polar vortices, we expect errors in the Version 3 data of $\sim +0.1$ ppbv at 22 hPa and $\sim +0.2$ ppbv at 46 hPa in the Antarctic, and ~ 0.1 ppbv or less at these altitudes in the Arctic. Taking day night differences effectively removes the bias errors due to HNO_3 and N_2O at 46 hPa and higher altitudes.

As can be seen from the values in Tables 1 and 2, and in Figure 14 for 17 August 1992, there are differences at 100 hPa which are significant in the day ClO values obtained between the retrievals with and without HNO_3 included, but not in the night ClO values. To investigate the cause of this behavior we averaged MIS radiances measured in the Antarctic vortex for the 14-29 August 1992 period, and compared averages from Version 3 data with those from an improved algorithm which uses the averaged radiances and iterates to account for non-linearities. The improved algorithm accounts for HNO_3 . It also uses pointing (tangent pressure) retrievals obtained with an updated 63 GHz O_2 pressure-broadening parameter [Liebe *et al.*, 1992] which is 6% smaller than that used in the Version 3 retrievals (from Liebe *et al.* [1991b] --- essentially the same as in Liebe *et al.* [1991a]). Results are shown in Figure 15 for the retrievals, and in Figure 16 for the radiances and residuals obtained from the retrieved profiles. Note the significantly smaller residuals which are obtained with the improved algorithms.

The discrepancies in 100 hPa ClO as obtained with different retrievals described above was found from these tests to be due to small non-linearities affecting the 100 hPa retrieval which are encountered when ClO is enhanced at 22 and/or 46 hPa. The results from the tests with the improved algorithms showed HNO_3 effects on ClO of $\sim 0.2-0.3$ ppbv, consistent with previous results. They additionally showed (from the day-night differences) that non-linearities cause the Version 3 values of enhanced ClO to be too large (a 'scaling' error) by 9% at 22 hPa and 7% at 46 hPa, consistent with the 10% scaling uncertainty estimated for lack of closure from the simulation results described earlier. From these tests, we conclude it is likely that the MLS Version 3 results for enhanced ClO at 22 and 46 hPa are too large by (1) a bias error up to ~ 0.2 ppbv for depleted gas-phase HNO_3 conditions typical of those encountered in the Antarctic winter vortex, and (2) an additional scaling error up to $\sim 8\%$. Due to non-linearities, the Version 3 100 hPa ClO (including day-night differences) should not be considered reliable when 46 and/or 22 hPa ClO is greatly enhanced.

To further investigate the behavior of Version 3 enhanced lower stratospheric ClO, we examined its variation with respect to local solar zenith angle (sza). Fig-

ure 17 shows enhanced ClO abundances for the same measurement ensemble as used for the results in Table 1 (Antarctic vortex during 14-29 August 1992 where gas-phase HNO_3 is greatly depleted) averaged in bins according to the sza at the time and location of measurements (local solar time of these measurements ranged from 8am through 11 pm). The variation with solar zenith angle shown in Figure 17, which includes measurements made between $\sim 60^\circ$ S and 80° S, should not be interpreted as diurnal variation at a single location. The variation of sza with latitude must be considered for quantitatively interpreting the shape of the curve, especially for values of sza near 90° . Figure 18 shows the statistical distributions of values which went into the averages, separately for 'day' and 'night' measurements. The observed distribution is closely Gaussian, with width approximately equal to the uncertainty predicted by the Version 3 algorithms (except narrower than predicted at 100 hPa, as discussed earlier in regards to other data samples). This distribution suggests the samples are all from the same 'population', and that it is reasonable to take averages as done for the results shown in Figure 17 and Table 1.

The variation of lower stratospheric polar vortex ClO with solar zenith angle, when there is little available NO_2 (as should be the case for the data shown in Figure 17, since the measurements were selected where HNO_3 --- thought to be the dominant source of NO_2 in these circumstances --- is depleted), is expected to be due to ClO-ClOOCl photochemistry, with ClO going to ClOOCl at night [e.g., Molina and Molina, 1987; Solomon, 1990]. For 3 ppbv total chlorine in ClO and ClOOCl, the nighttime value of ClO calculated to be in equilibrium with ClOOCl is ~ 0.05 ppbv at 46 hPa (188 K) and ~ 0.03 ppbv at 22 hPa (180 K), where the numbers in parentheses are the average temperatures at which the measurements in Figure 17 were made. However, the expected decay after sunset at 22 hPa is sufficiently slow that equilibrium is not expected to be reached at the time past sunset (0-7 hours) at which the measurements in Figure 17 were made, and ~ 0.4 ppbv ClO at 22 hPa is expected for the largest solar zenith angles shown in Figure 17. Averages of MLS measurements made well into the polar night (not shown here) give smaller 22 hPa ClO abundances of ~ 0.1 ppbv, in better agreement with the expected equilibrium values. The nighttime ClO values at 22 and 46 hPa in Figure 17 thus appear, within their uncertainties, to be consistent with expected behavior. The Version 3 100 hPa ClO behavior with respect to solar zenith angle shown in Figure 17 is not realistic, and is an artifact due to the non-linearity mentioned above.

The daytime 46 and 22 hPa values shown in Figure 17 are typical of the largest ClO abundances ob-

served by **MIS**. When the **estimated bias** error of 0.2 ppbv due to **HNO₃** and scaling error of 8% in the Version 3 data are corrected for, the maximum values become 2.4 ppbv for the retrieval value at 22 hPa and 2.1 ppbv for the value at 46 hPa with an estimated uncertainty of ~ 0.2 ppbv. These values, if interpreted as **CIO** abundances at the indicated pressures, imply (using nominal rate parameters for **C1QC1OOC1** photochemistry [DeMore et al., 1992; Nickolaisen et al., 1994]) 3.5 ± 0.4 ppbv total chlorine in **C1O** and **C1OOC1** at 46 hPa and 2.8 ± 0.3 ppbv at 22 hPa, where the uncertainties given here do **not** include uncertainties in the **photochemical** parameters. The total stratospheric chlorine in 1992, obtained from the **ATMOS** experiment [Gunsontal., 1994], is 3.44 ± 0.30 ppbv. The maximum values for chlorine in **C1O** and **C1OOC1** implied from the **MIS** measurements are within the range of what is 'allowable', given the total amount of chlorine in the stratosphere, but the 46 hPa values leave **essentially** 'no room' for any other forms. More work is needed to account for effects of the **MIS** vertical resolution on the **implications** of its large **C1O** measurements for the total chlorine in **C1O** and **C1OOC1**.

To investigate the solar zenith angle behavior of Version 3 **C1O** when lower stratospheric **C1O** is **not** greatly enhanced, averages of summer measurements of **C1O** binned by solar zenith angle were performed and the results are shown in Figure 19. The artifacts in 100 hPa **C1O** which appear in the Antarctic vortex data are not present in these data -- as expected, since the **non-linearities** causing those artifacts should be significant only during conditions of enhanced lower stratospheric **C1O**. The retrieved summer 100 hPa **C1O** values are zero to within the ~ 0.05 ppbv noise level of the average. Unrealistic negative values of ~ 0.1 - 0.2 ppbv (which are outside the expected noise of the averaged points), however, appear in nighttime values at 10-46 hPa. Figure 20 shows average profiles retrieved from measurements taken between midnight and sunrise during summer in both hemispheres. Between 100 and ~ 4.6 hPa altitudes we expect **C1O** to be essentially zero between midnight and sunrise, so we interpret the negative values in the averages at these altitudes as a bias error in the retrievals. Their magnitude is consistent with the expected residual uncertainties shown in Figure 12. The **C1O** is not expected to decrease so much at night at higher altitudes, and this is seen in the **MIS** data shown in Figure 19. The model results of *Ko and Sze [1984]* predict midnight **C1O** to be (a) $\sim 2\times$ lower than midday **C1O** at 2 hPa, (b) essentially the same as midday **C1O** at 1 hPa, and (c) ~ 0.1 ppbv larger than midday **C1O** at 0.46 hPa. The **MIS** results shown in Figure 19 agree reasonably well with these predictions. Figure 21 shows averages of radiances measured near noon and

midnight for tangent heights of 0.46-1.0 hPa, and 1.0-2.2 hPa, and for four days during the period which the data for Figure 19 were obtained. The **C1O** spectral feature is clearly present in both the noon and midnight spectra at 1.0- 2.2 hPa. However, the feature is not so clear in the 0.46- 1.0 hPa radiances, and more investigation is needed before the 0.46 hPa **C1O** retrievals can be considered adequate for general scientific analyses.

Summary of Estimated Uncertainties

Table 3 summarizes our estimates of the three types of **uncertainties** for the Version 3 **C1O** data, and known problems in these data, based on the analyses described above. The 'noise' uncertainties shown in Figure 22 are typical values for a single profile. Values of uncertainties given in the data files should be used for the noise on any specific individual retrieval (but being aware that the 100 hPa uncertainty in the files overestimates the noise, as discussed above). Values for the bias uncertainties given here are based on the residual uncertainties given in Figure 12, but have been increased by ~ 0.05 ppbv due to non-physical negative nighttime values at 22 hPa (see Figure 20) being up to 0.05 ppbv larger than the uncertainties shown in Figure 12. Figure 22 gives a plot of these estimated uncertainties. We believe the systematic 'bias' and 'scaling' uncertainties given here represent envelopes which are not often exceeded -- that they are, roughly, 90% confidence (2σ) values.

6. Comparisons with Other Measurements

We now compare **MIS** results for **C1O** with those from other measurement techniques. Useful comparisons generally require averaging of **MIS** results because of the low signal-to-noise on individual retrievals of **C1O**.

Comparisons with Balloon Measurements

Many pre-UARS measurements of upper stratospheric **C1O** were made from balloons at mid latitudes in the northern hemisphere. Figure 23 shows 20-40° N monthly zonal mean mid-day profiles from **MIS** for every north-looking UARS month from October 1991 through August 1993. The variation in these monthly zonal means is seen to be small (~ 0.1 ppbv) suggesting that useful comparisons of mid-latitude upper stratospheric **C1O** can be made without regards to the particular season of the measurements. Figure 24 compares the **MIS** monthly zonal means with the summary of mid-latitude upper stratospheric **C1O** measurements given in *Waters et al. [1988]*. There is general agreement to ~ 0.1 ppbv below 35 km. However, some of the earlier measurements shown in Figure 24 give 0.2-0.4 ppbv more **C1O** above ~ 35 km than appear in the **MIS** monthly zonal

means.

Figure 25 shows balloon measurements of CIO made during March and April 1991 at 34° N by the Submillimeter Limb Sounder (SLS) [Stachnik *et al.*, 1992] and by the in situ technique [Avalone *et al.*, 1993a]. These are compared with 30-40° N MLS zonal means (day-night differences) for the MLS north-looking periods in February and March of 1992, 1993 and 1994. The agreement between the MLS monthly zonal averages and the local SLS and in situ measurements is better than 0.1 ppbv at all altitudes. MLS shows slightly larger CIO abundances at 46 hPa (~21 km), which is only marginally significant relative to the expected uncertainty. Such an increase could be due to effects of the Pinatubo volcano which erupted between the sets of measurements. Avalone *et al.* [1993b] have analyzed aircraft in situ data and shown an increase in CIO at ~50 hPa and ~20-40° N between data taken before Pinatubo and that taken in February 1992 (when the first set of MLS measurements shown in Figure 25 were made). Comparisons of MLS results with those from aircraft are in a later subsection of this paper.

CIO profiles coincident with MLS were measured by the balloon-borne SLS as part of the UARS correlative measurements program. SLS measurements at the same time as MLS were obtained on 1 October 1991 (launched from Ft. Sumner, New Mexico), 20 February 1992 (Daggett, California), 29 September 1992 (Ft. Sumner) and 3 April 1993 (Daggett). The estimated accuracy is 0.1 ppbv or better over a vertical range between 50 and 1 hPa. Figure 26 compares MLS 30-40° N zonal mean CIO profiles with those measured on individual flights of SLS. The daily zonal means from MLS agree, to within the estimated uncertainties, with the SLS profiles over the full vertical range of the measurements. The MLS monthly zonal means agree to within 0.1 ppbv or better with SLS over the full vertical range. The 3 April 1993 SLS flight occurred when MLS was looking south, so that MLS profiles are not available on that date for comparison (measurements at the northern extreme of the south-looking orbit were in darkness); data from that flight are included later (Figure 36) in a time series of MLS data.

Comparisons with Ground-based Measurements

Ground-based measurements of stratospheric CIO were first reported by Parrish *et al.* [1981], and typical mid-latitude results obtained prior to UARS are the curve labeled 'Barrett *et al.*' in Figure 24. Measured variation in upper stratospheric CIO throughout a complete diurnal cycle over Hawaii (19° N) during October and December 1982 was reported by Solomon *et al.* [1984]. Figure 27 compares the Solomon *et al.* [1984] results with the 10 30° N zonal mean diurnal variation observed by

MLS during the UARS north-looking months of October 1992 and December 1991. The CIO column abundance above 30 km inferred from the ground based measurement is shown, along with the column above 10 hPa from MLS. The model [Ko and Sze, 1984] predictions given in Solomon *et al.* [1984] are also included in Figure 27. Both the measurements and model results have been normalized in the same manner. There is generally good agreement between MLS and ground-based, but with the MLS measurements fitting more closely the model predictions of a steeper morning rise than is evident in the ground-based measurements. The mid-day column above 30 km from the ground-based measurements is $0.7-0.8 \times 10^{18}$ molecules/m², whereas that inferred from MLS is $1.0-1.2 \times 10^{18}$ molecules/m². The difference of ~50% is consistent with the ~5% per year increase expected in stratospheric chlorine and the time difference of the two measurements.

Enhanced CIO in the lower stratosphere over Antarctica has been measured by ground-based microwave radiometers operating at McMurdo Station (78°S, 166°E) since 1986 [deZafra *et al.*, 1987; Solomon *et al.*, 1987; Barrett *et al.*, 1988; deZafra *et al.*, 1989]. This technique has also been used as part of the UARS correlative measurements program to obtain CIO measurements from McMurdo at the same time as MLS. Figure 28 compares MLS and ground-based [Shindell *et al.*, 1994] CIO measurements over McMurdo during 15-20 September 1992. Day-night differences at 10 hPa and below have been taken for both techniques. MLS maps (map for 17 September 1992 is in Waters *et al.* [1993 b]) show that during this period McMurdo was near the outer edge of enhanced lower stratospheric CIO, and that significantly larger CIO abundances occurred polewards of McMurdo. Both the MLS and ground-based measurements show the 'double-peaked' CIO profile, which is caused by separate regimes of gas-phase chemistry in the upper stratosphere and heterogeneous chemistry in the lower stratosphere. The heights of the CIO peaks obtained from the two techniques are in good agreement, and the peak abundances agree to within 0.1 ppbv. There are, however, differences of ~0.2 ppbv at 22-30 km which may be significant. These are, perhaps, due to the different vertical resolution of the two techniques and the different methods used for representing the vertical variation.

Figure 29 and 30 compare the CIO profiles obtained from ground-based and MLS measurements over McMurdo during 4-7 and 15-17 September 1993 [deZafra *et al.*, 1994 b]. MLS maps of CIO for this period [Waters *et al.*, paper in preparation], and those of potential vorticity [Manney *et al.*, 1993; 1994b] show the region of largest lower stratospheric CIO, and the Antarctic vortex, extending further outward over McMurdo than was the case when the 15-20 September 1992 measure-

ments shown in Figure 28 were made. These maps also show the Antarctic vortex and the region of enhanced CIO to be relatively symmetric about the pole during 4-7 September 1993, but more distorted towards McMurdo during 15-17 September 1993 when the air over McMurdo was representative of that deeper within the vortex than during 4-7 September 1993 (see also Figure 5 of *deZafra et al.* [1994b]). Both the MIS and ground-based measurements show more lower stratospheric CIO over McMurdo in 1993 than in 1992, especially at ~ 22 km (~ 22 hPa) altitude. More CIO over McMurdo in 1993 than in 1992 is expected from the differences in vortex location between 1992 and 1993 for the periods shown in Figures 28-30. MIS shows 46 hPa CIO increasing from 4-7 September 1993 to 15-17 September 1993 (as would be expected from the changes in vortex location between these periods), however, whereas the ground-based technique shows CIO decreasing at that altitude. To ensure the increase observed by MIS was not an artifact of the retrieval technique, retrievals were performed on the same data set but with the radiances first averaged and then an iterative retrieval performed on the averaged radiances. Results from the radiance-averaged iterative retrieval are the thick dashed lines in Figures 29 and 30. The same behavior is seen at 46 hPa as in the Version 3 MIS data, although lower stratospheric CIO peak abundances are ~ 0.2 ppbv smaller. This discrepancy between results from the two techniques, and others such as that at 10 hPa altitude where MIS shows significantly less CIO than the ground-based, are being investigated. There is generally worse agreement between MIS and ground-based results for the 1993 McMurdo measurements than those for 1992.

Figure 31 shows column measurements of CIO over Thule, Greenland, during February and March of 1992 [*deZafra et al.*, 1994a], and compares these with columns obtained from MIS. The ground-based measurements were taken during mid-day and are averages over periods of 3-5 days. Column CIO computed from individual MIS measurements made nearest Thule on both the ascending and descending portions of the orbit are shown, and the MIS data have been smoothed with a 5-day running average. During the period of these comparisons the 'day' side of the orbit for MIS measurements slowly changed from ascending to descending, and the solar zenith angle and local solar time of the MIS measurements are shown in the two bottom panels. The agreement between the day MIS measurements and the ground-based measurements is roughly comparable to the observed variations, all that should be expected given the different horizontal and temporal samplings of the two techniques.

Ground-based column measurements of HCl over Åre

Sweden (63° N), performed as part of the EASOE campaign [*Pyle et al.*, 1994] during the 1991-92 Arctic winter, have been compared with CIO columns over Åre during the same period [*Bell et al.*, 1994]. During early January 1992, when MIS observed a large increase in CIO, the HCl column was greatly decreased as expected, since the January increase in CIO should be at the expense of HCl.

Comparisons with Aircraft Measurements

Enhanced lower stratospheric CIO was measured from the ER-2 aircraft during the 1987 Antarctic campaign [*Anderson et al.*, 1989; 1991]. Figure 32 compares the 1987 ER-2 measurements with averages from MIS data made inside the vortex during the same time of year and centered at the latitude and longitude of the ER-2 measurements. The dates selected for the comparative MIS measurements were chosen to be within the mid-range of corresponding dates for the 1987 ER-2 measurements, and when MIS maps showed the edge of enhanced CIO to be at approximately the same location as observed by the ER-2 in 1987. Although there is acceptable agreement at the highest altitudes measured by the ER-2, the problems with MIS 100 hPa CIO data discussed earlier are evident at the lowest altitudes shown here.

In situ measurements of lower stratospheric CIO were made [*Avallone et al.*, 1993b; *Toohey et al.*, 1993b] from the ER-2 as part of the AASF-II campaign [*Anderson and Toon*, 1993] from September 1991 through March 1992. Their precision is better than 0.01 ppbv. Monthly zonal means of MIS data are required to reduce its noise to a level at which comparisons with the mid-latitude ER-2 data are meaningful, and Figure 33 shows height-latitude contour plots of MIS monthly zonal averages to put in context the more detailed mid-latitude comparisons with the ER-2 measurements shown later. The increase in lower stratospheric CIO between October 1991 and March 1992 at ~ 30 - 50° N seen by the ER-2 is evident in these MIS monthly zonal mean data. We also note that the increase in the upper stratospheric (~ 2.2 - 4.6 hPa) CIO from equator to pole seen in the MIS data agrees qualitatively with the predictions of *Solomon and Garcia* [1984]. (Smaller abundances of upper stratospheric CIO are expected at low latitudes where increased CH_4 quenches reactive chlorine. UARS CLAES measurements [*Kumer et al.*, 1993] show more upper stratospheric CH_4 at low latitudes, as expected due to ascending tropical air.) Figure 34 compares the MIS monthly zonal mean measurements with those from the ER-2 reported in *Fahney et al.* [1993]. The MIS and ER-2 results agree to within the expected MIS precision of ± 0.04 ppbv for the monthly zonal mean.

Figure 35 shows CIO plotted versus ozone for ER-2 measurements [*Avallone et al.*, 1993b] made in October

1991 and February 1992, and for **MLS** monthly zonal (day-night) means from the same time periods and range of latitudes. The upper cross is for the average of **MLS** values at 46 hPa, the middle cross for 68 hPa, and the lower cross for 100 hPa. The October 1991 **MLS** measurements shown in the top panel of Figure 35 were obtained shortly after launch, and before the **MLS** scan was programmed on 31 October 1991 to give more measurements in the lower stratosphere; consequently, the quality of the **MLS** lower stratospheric measurements for October 1991 in the upper panel is not as good as for February 1992 period shown in the lower panel of Figure 35. Despite the very low **ClO** abundances (relative to **MLS** sensitivity), however, the agreement is within the expected **MLS** precision --- and is especially good for the February 1992 measurements.

A time-series of **MLS** 30-50° N monthly zonal mean lower stratospheric **ClO** is shown in Figure 36, and compared with **ER-2** and **SLS** measurements. There is agreement to within the estimated **MLS** precision. Larger abundances of extra-vertical **ClO** in winter, as shown in these **MLS** data, are expected due to greater photolysis of **HNO₃** in summer (producing more **NO₂** which quenches **ClO**) and, perhaps, to faster rates of certain heterogeneous reactions [Rodriguez *et al.*, 1991; Solomon *et al.*, 1993; Tie *et al.*, 1994]. This seasonal variation in **MLS ClO**, which is also observed in the southern hemisphere [Waters *et al.*, paper in preparation], can be quantitatively explained by two-dimensional model results [Harwood *et al.*, paper in preparation].

Comparisons of **MLS ClO** results with **ER-2** measurements of enhanced lower stratospheric **ClO** in the Arctic 1991-92 winter vortex have been made. All show excellent agreement in the location of enhanced **ClO**. Figure 37 is a scatterplot of individual **MLSClO** measurements versus near-coincident **ER-2** measurements, and shows agreement to within the **MLS** noise. Table 4 gives details of the individual measurements which were included in Figure 37.

Figure 38 compares **ClO** profiles measured on the **ER-2** flight into the Arctic vortex on 20 January 1992 [Toohey *et al.*, 1993b], when the largest **ClO** abundances were measured by the **ER-2** during the **AASE-II** campaign, with the average of profiles measured by **MLS** during 9-11 January 1992 in the vortex region where it observed largest **ClO** [Waters *et al.*, 1993a]. (**MLS** turned to north-viewing on 14 January 1992, so there are no measurements from it to compare directly with the 20 January **ER-2** results.) Even though the measurements compared in Figure 38 were obtained 10 days apart, and at different locations in the vortex, there is good agreement between the **MLS ClO** average profile values and the **ER-2** measurements in the upper portion of the **ER-2** profile. Problems with the **MLS** measure-

ments near 100 hPa, as discussed previously, are also indicated here.

Comparisons with the **SUMAS** submillimeter aircraft measurements made in the Arctic vortex in February 1993 [Crewell *et al.*, 1994b] also show excellent agreement in location of the enhanced lower stratospheric **ClO**. The enhanced lower stratospheric **ClO** abundances from **MLS** are ~25% larger than from **SUMAS**, although this difference is about within the expected uncertainties of the two experiments.

Summary of Comparisons with Other Measurements

The comparisons done to date between **MLS** and other measurements of **ClO** indicate general agreement to within the estimated **MLS** uncertainties given earlier in Table 3 (and Figure 22), and the uncertainties of the comparative measurements.

7. Plans for Further Work

Further work is planned to eliminate the known problems in the Version 3 **ClO** data which have been summarized earlier in Table 3. At least two reprocessings of **MLS** data are planned. The first is principally aimed at producing a lower stratospheric **HNO₃** data set from **MLS** and will use the Version 3 algorithm. This processing will give improved **ClO** by accounting for the **HNO₃** effects, using better 'pointing' obtained from the revised 0₂ linewidth parameter, and using better 'space' radiances (from improved Level 1 processing) to improve **ClO** retrievals above 1 hPa. A later reprocessing will use iterative algorithms to account for non-linearities. This later processing should make the **MLS** 100 hPa **ClO** product useful (at least for day-night differences), eliminate the ~8% scaling error which exists in the Version 3 data for enhanced lower stratospheric **ClO**, and reduce residual uncertainties to ~0.1 ppbv.

As well as upper tropospheric **H₂O**, mentioned earlier, additional **MLS** products which may be available from future algorithms include geopotential height, isotopic ozone, **11₂O₂**, and one component of wind in the mesosphere.

Acknowledgments. The **MLS** team thanks C.C. Voge for managing our software development for many years, J. It. Holden, R. It. Lay and M.S. Loo for their contributions to pre-launch testing and in-orbit operations of **MLS**, and G.K. Lau for overall management of our project during its operational phase. We thank E.A. Cohen and J.J. Oh for quickly measuring the oxygen broadening of the **MLS ClO** spectral line as soon as our measurements suggested the need for it, and G. I. Manney, T. Luu, and R.W. Zurek for providing original derived meteorological quantities used operationally on a daily basis in checking the 'reasonableness'

of enhanced ClO distributions observed by M I.S. We are grateful to W.G. Grose and his UARS team for atmospheric model data used in pre-launch testing; to D.J. Wuebbles and his UARS team for model ClO data used as 'climatology', and to R. Seals and colleagues for assembling a 'climatology' for use in UARS data processing. We thank H.M. Pickett, M.R. Schoeberl, A. Ii. Douglass, I., S. Elson, M.L. Santee, R.S. Harwood, W.A. Iahoz, G.E. Peckham and our other MLS colleagues, as well as those mentioned above and many others, for many helpful discussions. Finally, we thank all our UARS colleagues, and especially those responsible for the UARS Central Data Handling Facility, for their support throughout our many years of working together. The research performed at the Jet Propulsion Laboratory, California Institute of Technology, was under contract with NASA and sponsored through its UARS Project.

References

- Aellig, C. P., N. Kampfer, and R. M. Bevilacqua, Error analysis of ClO, O₃, and H₂O abundance profiles retrieved from millimeter wave limb sounding measurements, *J. Geophys. Res.*, **98**, 2975-2983, 1993.
- Anderson, J. G. and O. B. Toon, Airborne Arctic Stratospheric Expedition II: An Overview, *Geophys. Res. Lett.*, **20**, 2499-2502, 1993.
- Anderson, J. G., J. J. Margitan, and D. H. Stedman, Atomic chlorine and the chlorine monoxide radical in the stratosphere: three in situ observations, *Science*, **198**, 501-503, 1977.
- Anderson, J. G., W. H. Brune, and M. H. Proffitt, Ozone destruction by chlorine radicals within the Antarctic vortex: the spatial and temporal evolution of ClO-O₃ anticorrelation based on in situ ER-2 data, *J. Geophys. Res.*, **94**, 11,465-11,479, 1989.
- Anderson, J. G., D. W. Toohey, and W. H. Brune, Free radicals within the Antarctic vortex: the role of CFCs in Antarctic ozone loss, *Science*, **251**, 39-46, 1991.
- Avallone, L. M., D. W. Toohey, W. H. Brune, R. J. Salawitch, A. E. Dessler, and J. G. Anderson, Balloon-borne in situ measurements of ClO and ozone: implications for heterogeneous chemistry and mid-latitude ozone loss, *Geophys. Res. Lett.*, **20**, 1795-1798, 1993a.
- Avallone, L. M., D. W. Toohey, M. H. Proffitt, J. J. Margitan, K. R. Chan, and J. G. Anderson, In-situ measurements of ClO at mid-latitudes: Is there an Effect from Mt. Pinatubo?, *Geophys. Res. Lett.*, **20**, 2519-2522, 1993b.
- Barath, F. T., M. C. Chavez, R. E. Cofield, D. A. Flower, M. A. Frerking, M. B. Gram, W. M. Harris, J. R. Holden, R. F. Jarnot, W. G. Kloezeman, G. J. Klose, G. K. Lau, M. S. Loo, H. J. Maddison, R. J. Matlack, R. P. McKinney, G. E. Peckham, H. M. Pickett, G. Siebes, F. S. Soltis, R. A. Suttie, J. A. Tarsala, J. W. Waters, and W. J. Wilson, The Upper Atmosphere Research Satellite Microwave Limb Sounder Instrument, *J. Geophys. Res.*, **98**, 10,751-10,762, 1993.
- Barrett, J. W., P. M. Solomon, R. L. deZafra, M. Jaramillo, I. Emmons, and A. Parrish, Formation of the Antarctic ozone hole by the ClO dimer mechanism, *Nature*, **336**, 455-458, 1988.
- Bell, W., N. A. Martin, T. D. Gardiner, N. R. Swann, P. T. Woods, P. F. Fogal, and J. W. Waters, Column measurements of stratospheric trace species over Åre, Sweden in the winter of 1991-92, *Geophys. Res. Lett.*, **21**, 1347-1350, 1994.
- Brune, W. H., E. M. Weinstock, M. J. Schwab, R. M. Stimpfle, and J. G. Anderson, Stratospheric ClO: in-situ detection with a new approach, *Geophys. Res. Lett.*, **12**, 441-444, 1985.
- Brune, W. H., E. M. Weinstock, and J. G. Anderson, Mid-latitude ClO below 22 km altitude: measurements with a new aircraft-borne instrument, *Geophys. Res. Lett.*, **15**, 144-147, 1988.
- Carli, R., F. Mencaraglia, M. Carlotti, B. M. Dinelli, and I. Nolt, Submillimeter measurement of stratospheric chlorine monoxide, *J. Geophys. Res.*, **93**, 7063-7068, 1988.
- Chance, K. V., D. G. Johnson, W. A. Traub, and K. W. Jucks, Measurements of the stratospheric hydrogen peroxide profile using far infrared thermal emission spectroscopy, *Geophys. Res. Lett.*, **18**, 1003-1006, 1991.
- Craig, H., Isotopic standards for carbon and oxygen and correction factors for mass-spectrometric analysis of carbon dioxide, *Geochim. Cosmochim. Acta.*, **12**, 133-149, 1957.
- Crewell, S., K. Künzi, H. Nett, T. Wehr, and P. Hartogh, Aircraft measurements of ClO and HCl during FASOF 1991/92, *Geophys. Res. Lett.*, **21**, 1267-1270, 1994a.
- Crewell, S., R. Fabian, K. Künzi, H. Nett, T. Wehr, W. Read, and J. Waters, Comparison of ClO measurements made by airborne and spaceborne microwave radiometers in the arctic winter stratosphere 1993, *Geophys. Res. Lett.*, submitted, 1994b.
- DeMore, W. Et., S. P. Sander, D. M. Golden, R. F. Hampson, M. J. Kurylo, C. J. Howard, A. R. Ravishankara, C. E. Kolb, and M. J. Molina, *Chemical Kinetics and Photochemical Data for Use in Stratospheric Modeling: Evaluation Number 10*, Technical Report 92-20, Jet Propulsion Laboratory, 1992.
- deZafra, R. L., M. Jaramillo, A. Parrish, P. Solomon, B. Connor, and J. Barrett, High concentrations of chlorine monoxide at low altitudes in the Antarctic spring stratosphere: diurnal variation, *Nature*, **328**, 408-411, 1987.
- deZafra, R. L., M. Jaramillo, J. Barrett, L. K. Emmons, P. Solomon, and A. Parrish, New observations of a large concentration of ClO in the springtime lower stratosphere over Antarctica and its implications for ozone-depleting chemistry, *J. Geophys. Res.*, **94**, 11,423-11,428, 1989.
- deZafra, R. L., I. K. Emmons, J. M. Reeves, and D. T. Shindell, An overview of millimeter-wave spectroscopic measurements of chlorine monoxide at Thule, Greenland, February-March, 1992: vertical profiles, diurnal variation and longer-term trends, *Geophys. Res. Lett.*, **21**, 1271-1274, 1994a.
- deZafra, R. L., J. M. Reeves, and D. T. Shindell, Chlorine monoxide in the Antarctic spring vortex I: Evolution of midday vertical profiles of McMurdo Station, 1993, submitted to *J. Geophys. Res.*, 1994b.

- Douglass, A., R. Rood, J. Waters, L. Froidevaux, W. Read, I. Elson, M. Geller, Y. Chi, M. Cerniglia, and S. Steenrod, A 3D simulation of the early winter distribution of reactive chlorine in the north polar vortex, *Geophys. Res. Lett.*, 20, 1271-1274, 1993.
- Elson, I. S. and L. Froidevaux, The use of Fourier transforms for synoptic mapping: early results from the Upper Atmosphere Research Satellite Microwave Limb Sounder, *J. Geophys. Res.*, 98, 23,039-23,049, 1993.
- Fahey, D. H., S. R. Kawa, E. L. Woodbridge, P. Tin, J. C. Wilson, H. H. Jonsson, J. E. Dye, D. Baumgardner, S. Borrmann, D. W. Toohey, L. M. Avallone, M. H. Proffitt, J. Margitan, M. Loewenstein, J. R. Podolske, R. J. Salawitch, S. C. Wofsy, M. K. W. Ko, D. E. Anderson, M. R. Schoeberl, and K. R. Chan, In situ measurements constraining the role of sulphate aerosols in mid-latitude ozone depletions, *Nature*, 363, 509-514, 1993.
- Farman, J. C., B. G. Gardiner, and J. D. Shanklin, Large losses of total ozone in Antarctica reveal seasonal ClO/NO_x interaction, *Nature*, 315, 207-210, 1985.
- Fishbein, E. F., R. E. Cofield, L. Froidevaux, R. F. Jarnot, T. A. Lungu, W. G. Read, Z. Shippony, J. W. Waters, I. S. McDermid, T. J. McGee, U. Singh, M. Gross, A. Hauchecorne, and M. E. Gelman, Validation of UARS MLS temperature/pressure measurements, *J. Geophys. Res.* (special issue on validation of UARS data), submitted 1994.
- Froidevaux, L., W. G. Read, T. A. Lungu, R. E. Cofield, E. F. Fishbein, D. A. Flower, R. F. Jarnot, B. P. Ride-noure, Z. Shippony, J. W. Waters, J. J. Margitan, I. S. McDermid, R. A. Stachnik, G. E. Peckham, G. Braathen, T. Deshler, J. Fishman, D. J. Hofmann, and S. J. Oltmans, Validation of UARS MLS ozone measurements, *J. Geophys. Res.* (special issue on validation of UARS data), submitted 1994.
- Geller, M. A., Y. Chi, R. B. Rood, A. R. Douglass, D. J. Allen, M. Cerniglia, and J. W. Waters, 3-D transport-chemistry studies of the stratosphere using satellite data together with data assimilation, In M.-I. Chanin, editor, *The Role of the Stratosphere in Global Change*, Springer-Verlag (NATO ASI Series, Vol. 18), Berlin, 1993.
- Gille, J. C., P. L. Dailey, and C. A. Craig, Revised reference model for nitric acid, In Keating, G. M., editor, *Middle Atmosphere Program Handbook for MAP Volume 51*, chapter 6, ICSU Scientific Committee on Solar-Terrestrial Physics (SCOSTEP), University of Illinois, Urbana, 1989.
- Gunson, M. R., M. C. Abrams, I. L. Lowes, E. Mahieu, R. Zander, C. P. Rinsland, M. K. W. Ko, N. I. Sze, and D. K. Weisenstein, Increase in levels of stratospheric chlorine and fluorine loading between 1985 and 1992, *Geophys. Res. Lett.*, 21, 2223-2226, 1994.
- Janssen, M. A., editor, *Atmospheric Remote Sensing by Microwave Radiometry*, John Wiley & Sons, New York, 1993.
- Jarnot, R. F., R. E. Cofield, J. W. Waters, and G. E. Peckham, Calibration of UARS MLS, *J. Geophys. Res.* (special issue on validation of UARS data), submitted 1994.
- Ko, M. K. W. and N. I. Sze, Diurnal variation of ClO: implications for the stratospheric chemistries of ClONO₂, HOCl, and HCl, *J. Geophys. Res.*, 89, 11619-11632, 1984.
- Lahoz, W. A., M. R. Suttie, L. Froidevaux, R. S. Harwood, C. L. Lau, T. A. Lungu, G. E. Peckham, H. C. Pumphrey, W. G. Read, Z. Shippony, R. A. Suttie, and J. W. Waters, Validation of UARS MLS 183 GHz H₂O measurements, *J. Geophys. Res.* (special issue on validation of WARS data), submitted 1994.
- Liebe, H. J., G. A. Hufford, and R. O. DeBolt, *The Atmospheric 60-GHz Oxygen Spectrum: Modeling and Laboratory Measurements*, Technical Report NTIA 91-272, National Telecommunications and Information Administration, Institute for Telecommunication Sciences, Boulder, Colorado, 1991.
- Liebe, H. J., G. A. Hufford, and R. O. DeBolt, Measurements of the 60 GHz O₂ spectrum of air, In *URSI Radio Science Meeting*, June 1991.
- Liebe, H. J., P. W. Rosenkranz, and G. A. Hufford, Atmospheric 60 GHz oxygen spectrum: New laboratory measurements and line parameters, *J. Quant. Spectrosc. Radiat. Transfer*, 48, 629-643, 1992.
- Manney, G. L., L. Froidevaux, J. W. Waters, I. S. Elson, E. F. Fishbein, R. W. Zurek, R. S. Harwood, and W. A. Lahoz, The evolution of ozone observed by UARS MLS in the 1992 late winter southern polar vortex, *Geophys. Res. Lett.*, 20, 1279-1282, 1993.
- Manney, G. L., L. Froidevaux, J. W. Waters, and R. W. Zurek, Evolution of MLS ozone and the polar vortex during winter, *J. Geophys. Res.*, in press 1994.
- Manney, G. L., L. Froidevaux, J. W. Waters, R. W. Zurek, W. G. Read, I. S. Elson, J. B. Kumer, J. L. Mergenthaler, A. F. Roche, A. O'Neill, R. S. Harwood, I. MacKenzie, and R. Swinbank, Chemical depletion of ozone in the Arctic lower stratosphere during winter 1992-93, *Nature*, 370, 429-434, 1994.
- Marks, C. J. and C. D. Rodgers, A retrieval method for atmospheric composition from limb emission measurements, *J. Geophys. Res.*, 98, 14939-14953, 1993.
- Mauersberger, K., Ozone isotope measurements in the stratosphere, *Geophys. Res. Lett.*, 14, 80-83, 1987.
- Menzies, R. T., Remote measurement of ClO in the stratosphere, *Geophys. Res. Lett.*, 6, 151-154, 1979.
- Menzies, R. T., A re-evaluation of laser heterodyne radiometer ClO measurements, *Geophys. Res. Lett.*, 10, 729-732, 1983.
- Molina, L. T. and M. J. Molina, Production of Cl₂O₂ from the self-reaction of the ClO radical, *J. Phys. Chem.*, 91, 433-436, 1987.
- Molina, M. J. and F. S. Rowland, Stratospheric sink for chlorofluoromethanes: chlorine atom catalysed destruction of ozone, *Nature*, 249, 810-812, 1974.
- Nickolaisen, S. L., R. R. Friedl, and S. P. Sander, Kinetics and mechanism of the ClO + ClO reaction: pressure and temperature dependence of the bimolecular and termolecular channels and thermal decomposition of chlorine peroxide, *J. Phys. Chem.*, 98, 155-169, 1994.
- Njokkr, E. G., Passive microwave remote sensing of the Earth from space - a review, *Proc. IEEE*, 79, 728-750, 1982.
- Oh, J. J. and E. A. Cohen, Pressure broadening of ClO by N₂ and O₂ near 204 and 649 GHz and new frequency mea-

- measurements between 632 and 725 GHz, *J. Quant. Spectrosc. Radiat. Transfer*, 54, 151-156, 1994.
- Parrish, A., R. L. deZafra, P. M. Solomon, J. W. Barrett, and E. R. Carlson, Chlorine oxide in the stratospheric ozone layer: ground-based detection and measurement, *Science*, 211, 1158-1161, 1981.
- Pickett, H. M., D. E. Brinza, and E. A. Cohen, Pressure broadening of ClO by nitrogen, *J. Geophys. Res.*, 86, 7279-7282, 1981.
- Pickett, H. M., R. L. Poynter, and E. A. Cohen, *Submillimeter, Millimeter and Microwave Spectral Line Catalog*, Technical Report 80-23, Revision 3, Jet Propulsion Laboratory, 1992.
- Poynter, R. L. and H. M. Pickett, Submillimeter, millimeter and microwave spectral line catalog, *Appl. Opt.*, 24, 2235-2240, 1985.
- Pyle, J. A., N. It. P. Harris, J. C. Farman, F. Arnold, G. Braathen, R. A. Cox, P. Faucon, R. L. Jones, G. Megie, A. O'Neill, U. Platt, J. Pommereau, U. Schmidt, and F. Stordal, An overview of the EASOE campaign, *Geophys. Res. Lett.*, 21, 1191-1194, 1994.
- Read, W. G., L. Froidevaux, and J. W. Waters, Microwave Limb Sounder (MLS) measurements of SO₂ from Mt. Pinatubo volcano, *Geophys. Res. Lett.*, 20, 1299-1302, 1993.
- Read, W. G., J. W. Waters, L. Froidevaux, D. A. Flower, R. F. Jarnot, D. L. Hartmann, R. S. Harwood, and R. B. Rood, Upper tropospheric water vapor from UARS MLS, *Run. Amer. Met. Soc.*, to be submitted 1994.
- Reber, C. A. and Others, Validation of UARS Level 3B data, *J. Geophys. Res. (special issue on validation of WARS data)*, submitted 1994.
- Ricaud, P. D., E. S. Carr, L. Froidevaux, R. S. Harwood, J. H. Kumer, W. A. Lahoz, J. L. Mergenthaler, G. E. Peckham, W. G. Read, A. E. Roche, and J. W. Waters, Polar stratospheric clouds as deduced from MLS and CLAIM measurements, *Geophys. Res. Lett.*, submitted 1994.
- Rodgers, C. D., Retrieval of atmospheric temperature and composition from remote measurements of thermal radiation, *Rev. Geophys. and Space Phys.*, 14, 609-624, 1976.
- Rodgers, C. D., Characterization and error analyses of profiles retrieved from remote sounding measurements, *J. Geophys. Res.*, 95, 5587-5595, 1990.
- Rodriguez, J. M., M. K. W. Ko, and N. D. Sze, Role of heterogeneous conversion of N₂O₅ on sulfate aerosols in global ozone losses, *Nature*, 352, 134-137, 1991.
- Santee, M. L., W. G. Read, J. W. Waters, L. Froidevaux, G. I. Manney, D. A. Flower, R. F. Jarnot, R. S. Harwood, and G. E. Peckham, Interhemispheric differences in polar stratospheric HNO₃, H₂O, ClO and O₃ from UARS MLS, *Science*, submitted 1994.
- Schoeberl, M. R., R. S. Stolarski, A. R. Douglass, P. A. Newman, L. R. Lait, J. W. Waters, L. Froidevaux, and W. G. Read, MLS ClO observations and arctic polar vortex temperatures, *Geophys. Res. Lett.*, 20, 2861-2864, 1993.
- Shields, W. R., T. J. Murphy, E. L. Garner, and V. H. Dibelber, Absolute isotopic abundance ratio and the atomic weight of chlorine, *J. Am. Chem. Soc.*, 84, 1519-1522, 1962.
- Shindell, D. T., L. K. Emmons, J. M. Reeves, and R. L. deZafra, Observations of midday evolution and diurnal variation of stratospheric ClO profiles from McMurdo Station, Antarctica, spring 1992, *J. Geophys. Res.*, 1994 submitted.
- Solomon, S., Progress towards a quantitative understanding of Antarctic ozone depletion, *Nature*, 347, 347-354, 1992.
- Solomon, S. and R. R. Garcia, On the distributions of long-lived tracers and chlorine species in the middle atmosphere, *J. Geophys. Res.*, 89, 11,633-11,644, 1984.
- Solomon, P. M., R. deZafra, A. Parrish, and J. W. Barrett, Diurnal variation of chlorine monoxide: a critical test of chlorine chemistry in the ozone layer, *Science*, 224, 1210-1214, 1984.
- Solomon, P. M., B. Conner, R. L. deZafra, A. Parrish, J. Barrett, and M. Jaramillo, High concentrations of chlorine monoxide at low altitudes in the Antarctic spring stratosphere, *Nature*, 328, 411-413, 1987.
- Solomon, S., R. W. Sanders, R. R. Garcia, and J. G. Keys, Increased chlorine dioxide over Antarctica caused by volcanic aerosols from Mount Pinatubo, *Nature*, 363, 245-248, 1993.
- Stachnik, R. A., J. C. Hardy, J. A. Tarsala, J. W. Waters, and N. R. Erickson, Submillimeterwave heterodyne measurements of stratospheric ClO, HCl, O₃, and HO₂: First Results, *Geophys. Res. Lett.*, 19, 1931-1934, 1992.
- Staelin, D. H., Passive remote sensing at microwave wavelengths, *Proc. IEEE*, 57, 427-439, 1969.
- Taylor, F. W., A. Dudhia, and C. D. Rodgers, Proposed reference models for nitrous oxide and methane in the middle atmosphere, In Keating, G. M., editor, *Middle Atmosphere Program Handbook for MAP Volume 31*, chapter 4, ICSU Scientific Committee on Solar-terrestrial Physics (SCOSTEP), University of Illinois, Urbana, 1989.
- Tic, X., G. P. Brasseur, B. Briegleb, and C. Granier, Two-dimensional simulation of Pinatubo aerosol and its effect on stratospheric ozone, *J. Geophys. Res.*, in press 1994.
- Toohey, D. W., L. M. Avallone, N. T. Allen, J. N. Demusz, J. N. Hazen, and J. G. Anderson, The performance of a new instrument for in situ measurements of ClO in the lower stratosphere, *Geophys. Res. Lett.*, 20, 1791-1794, 1993a.
- Toohey, D. W., L. M. Avallone, L. R. Lait, P. A. Newman, M. R. Schoeberl, D. W. Fahey, F. L. Woodbridge, and J. G. Anderson, The seasonal evolution of reactive chlorine in the northern hemisphere stratosphere, *Science*, 261, 1134-1136, 1993b.
- Ulaby, F. T., R. K. Moore, and A. K. Fung, *Microwave Remote Sensing Active and Passive, Volume I: Microwave Remote Sensing Fundamentals and Radiometry*, Addison-Wesley, Reading, Massachusetts, 1981.
- Ulaby, F. T., R. K. Moore, and A. K. Fung, *Microwave Remote Sensing Active and Passive, Volume III: From Theory to Applications*, Addison-Wesley, Reading, Massachusetts, 1986.
- Waters, J. W., Microwave limb-sounding of Earth's upper atmosphere, *Atmospheric Research*, 23, 391-410, 1989.

- Waters, J. W., Submillimeter heterodyne spectroscopy and remote sensing of the upper atmosphere, *IEEE Proceedings*, 80, 1679-1701, 1992.
- Waters, J. W., Microwave Limb Sounding, In Janssen, M. A., editor, *Atmospheric Remote Sensing by Microwave Radiometry*, chapter 8, John Wiley & Sons, New York, 1993.
- Waters, J. W., J. J. Gustincic, R. K. Kakar, H. K. Roacoe, P. N. Swanson, T. G. Phillips, T. DeGraauw, A. R. Kerr, and R. J. Matlack, Aircraft search for millimeter wavelength emission by stratospheric ClO, *J. Geophys. Res.*, 84, 6934, 1979.
- Waters, J. W., J. C. Hardy, R. F. Jarnot, and H. M. Pickett, Chlorine monoxide radical, ozone, and hydrogen peroxide: Stratospheric measurements by microwave limb sounding, *Science*, 214, 61-64, 1981.
- Waters, J. W., R. A. Stachnik, J. C. Hardy, and R. F. Jarnot, ClO and O₃ stratospheric profiles: balloon microwave measurements, *Geophys. Res. Lett.*, 15, 780-783, 1988.
- Waters, J. W., L. Froidevaux, W. G. Read, G. L. Manney, L. S. Elson, D. A. Flower, R. F. Jarnot, and R. S. Harwood, Stratospheric ClO and ozone from the Microwave Limb Sounder on the Upper Atmosphere Research Satellite, *Nature*, 362, 597-602, 1993a.
- Waters, J. W., L. Froidevaux, G. L. Manney, W. G. Read, and L. S. Elson, Lower stratospheric ClO and O₃ in the 1992 southern hemisphere winter, *Geophys. Res. Lett.*, 20, 1219-1222, 1993b.
- Waters, J. W., G. L. Manney, W. G. Read, L. Froidevaux, D. A. Flower, and R. F. Jarnot, UARS MLS observations of lower stratospheric ClO in the 1992-93 and 1993-94 arctic winter vortex, *Geophys. Res. Lett.*, submitted 1994.
- Wofsy, S. C., Temporal and latitudinal variations of stratospheric trace gases: A critical comparison between theory and experiment, *J. Geophys. Res.*, 83, 364-378, 1978.
- Yaron, I., K. Peterson, and W. Klemperer, On the dipole moment functions of ClO and OH, *J. Chem. Phys.*, 88, 4702-4710, 1988.

Table 1. Averages values of lower stratospheric ClO abundances (ppbv) retrieved from MLS data taken in the Antarctic vortex during 14-29 August 1992. 'DAY' values were obtained for solar zenith angles (sza) $\leq 83^\circ$ at 46 and 100 hPa, and $\leq 88^\circ$ for 22 hPa; 'NIGHT' values are for $\text{sza} \geq 100^\circ$. The uncertainties shown here for the 'DAY' and 'NIGHT' values are the measured standard deviation of the values divided by the square root of the number of measurements which were averaged; the uncertainty given for the 'DAY minus NIGHT' values are the rss of 'DAY' and 'NIGHT' uncertainties.

pressure	DAY		NIGHT		DAY minus NIGHT	
	Version 3	with HNO ₃ retrieved (preliminary)	Version 3	with HNO ₃ retrieved (preliminary)	Version 3	with HNO ₃ retrieved (preliminary)
22 hPa	2.81±0.04	2.72±0.04	0.58±0.02	0.48±0.02	2.23±0.05	2.24±0.05
46 hPa	2.52±0.04	2.33±0.04	0.23±0.02	0.06±0.02	2.29±0.05	2.27±0.05
100 hPa	-0.37±0.08	-0.15±0.10	0.39±0.03	0.41±0.04	-0.76±0.09	-0.56±0.10

Table 2. Averages values of lower stratospheric ClO abundances (ppbv) retrieved from MLS data taken in the Arctic vortex during 9-11 January 1992 between 55-65° N and 0-60° E. 'DAY' values were obtained for solar zenith angles (sza) $\leq 85^\circ$ and local solar times between 11 am and 1 pm. 'NIGHT' values are for $\text{sza} \geq 120^\circ$ and local solar times between midnight and 3 am. The uncertainties shown here for the 'DAY' and 'NIGHT' values are the measured standard deviation of the values divided by the square root of the number of measurements which were averaged; the uncertainty given for the 'DAY minus NIGHT' values are the rss of 'DAY' and 'NIGHT' uncertainties.

pressure	DAY		NIGHT		DAY minus NIGHT	
	Version 3	with HNO ₃ retrieved (preliminary)	Version 3	with HNO ₃ retrieved (preliminary)	Version 3	with HNO ₃ retrieved (preliminary)
22 hPa	1.01±0.19	1.09±0.20	0.05±0.05	0.13±0.05	0.96±0.20	0.96±0.21
46 hPa	2.36±0.16	2.48±0.16	0.29±0.09	0.32±0.09	2.07±0.17	2.16±0.17
100 hPa	-0.38±0.33	-0.68±0.26	-0.02±0.17	0.01±0.16	-0.36±0.37	-0.67±0.31

Table 3. Summary of estimated uncertainties and known problems in **MIS** Version 3 **C10**. The 'noise' uncertainty gives the 'precision' of the **measurement**, and can be reduced by averaging. The values given here for the 'bias' and 'scaling' uncertainties, which apply to the 'accuracy' of the **measurements** after accounting for noise, are believed to represent envelopes which are not often exceeded — roughly 90% confidence (2σ) values.

pressure (hPa)	typical single profile 1σ noise (ppbv)	estimated bias uncertainty (ppbv)	estimated scaling uncertainty	known problems
0.46	1.6	0.2	40%	More investigations are required before the Version 3 0.46 hPa values can be considered reliable for general scientific analyses.
1.0	1.3	0.2	20%	
2.2	0.8	0.15	15%	
4.6	0.5	0.15	15%	Version 3 data have a bias error of -0.05 ppbv
10	0.4	0.15	15%	Version 3 data have a bias error of -0.1 ppbv
22	0.3	0.2	15%	Version 3 data have a bias error of -0.15 to -0.2 ppbv when HNO₃ has typical 'climatological' values, and a bias error of $\sim+0.2$ ppbv under conditions of depleted HNO₃ typical of the Antarctic vortex; these bias errors can be removed by taking day-night differences (when conditions permit). There is a scaling error of $\sim+9\%$ for enhanced C10 conditions.
46	0.4	0.2-0.4	15%	Version 3 data have a bias error of -0.1 ppbv when HNO₃ has typical 'climatological' values, and a bias error of $\sim+0.2$ ppbv under conditions of depleted HNO₃ typical of the Antarctic vortex; these bias errors can be removed by taking day-night differences (when conditions permit). There is a scaling error of $\sim+7\%$ for enhanced C10 conditions.
100	1.0	0.4-0.8	40%	Version 3 100 hPa data are not reliable under conditions when 22 and/or 46 hPa C10 is greatly enhanced. More investigations are required before they can generally be considered reliable at the small C10 abundances which are typically expected at 100 hPa

Table 4 Individual MLS ClO measurements and near-coincident ER-2 measurements in the 1991-92 Arctic winter vortex. Universal time (UT), latitude, longitude and potential temperature (θ) of the ER-2 measurements are indicated. The range of ClO values shown here for the ER-2 measurements is the range of values which were measured over a spatial region of the approximate size as that sampled during individual MLS measurements. Also given for the MLS measurements are the record number (in the daily MLS data file), the solar zenith angle (sza) and the local solar time (lst) of the measurements. The MLS data is Version 3, and values are given for the 46 hPa retrieval point, and from the retrieved vertical profile at the potential temperature of the corresponding ER-2 measurement.

date 1992	ER-2					MLS							
	UT h:m	lat 'N	long 'W	θ K	ClO ppbv	UT h:m	lat 'N	long 'W	rec#	sza deg	lst hour	ClO@46hPa ppbv	ClO@ θ ppbv
4 Jan	18:05	58	56	475	0.550.3	17:16	57	48	949	84.1	14.0	0.4±0.4	0.6±0.4
	19:30	51	63	490	0.1±0.02	18:55	51	67	1039	79.8	14.3	-0.24±0.4	0.0±0.4
						18:56	47	65	1040	87.7	14.5	-0.24±0.4	0.2±0.4
6 Jan	16:00	61	44	450	0.8±0.1	15:43	65	42	864	87.8	12.8	1.14±0.4	0.9±0.4
						15:44	62	38	865	85.0	13.0	1.6±0.4	1.0±0.4
	18:30	55	56	475	0.12±0.03	17:22	55	57	955	79.6	13.5	-0.2±0.4	0.2±0.4
8 Jan	16:15	61	44	450	0.4±0.2	15:49	62	50	869	84.4	12.4	1.7±0.4	0.6±0.4
						15:50	59	47	870	81.3	12.6	0.6±0.4	0.4±0.4
	14:10	51	63	465	0.35±0.25	17:28	52	66	960	75.3	12.9	0.2±0.4	0.3±0.4
	19:30	49	65	500	0.14±0.03	17:29	49	64	961	72.3	13.1	0.6±0.4	0.4±0.4
17 Feb	17:20	65	61	450	0.6±0.2	17:30	68	62	961	81.0	13.1	0.5±0.4	0.4±0.4
						15:54	68	37	873	81.3	13.2	-0.3±0.4	0.8±0.4
	17:55	65	63	480	0.75±0.1	17:29	65	66	960	77.4	12.8	0.25±0.4	0.5±0.4
						15:53	65	42	872	77.6	12.9	1.0±0.4	0.6±0.4
	18:30	61	65	485	0.7±0.1	17:28	61	70	959	73.8	12.6	0.6±0.4	0.6±0.4
						15:52	62	45	871	74.0	12.6	-0.15±0.4	0.2±0.4
	19:00	58	66	495	0.3±0.1	17:27	58	73	958	70.2	12.4	0.6±0.4	0.75±0.4
						15:51	58	48	870	70.5	12.4	0.1±0.4	0.26±0.4
	19:30	55	67	510	0.17±0.06	17:26	55	75	957	66.7	12.2	0.7±0.4	0.4±0.4
						15:50	55	51	869	66.9	12.2	0.3±0.4	0.3±0.4
	20:20	51	67	500	0.10±0.02	17:25	51	78	956	63.2	12.0	0.4±0.4	0.1±0.4
						15:49	51	53	868	63.5	12.0	0.3±0.4	0.2±0.4

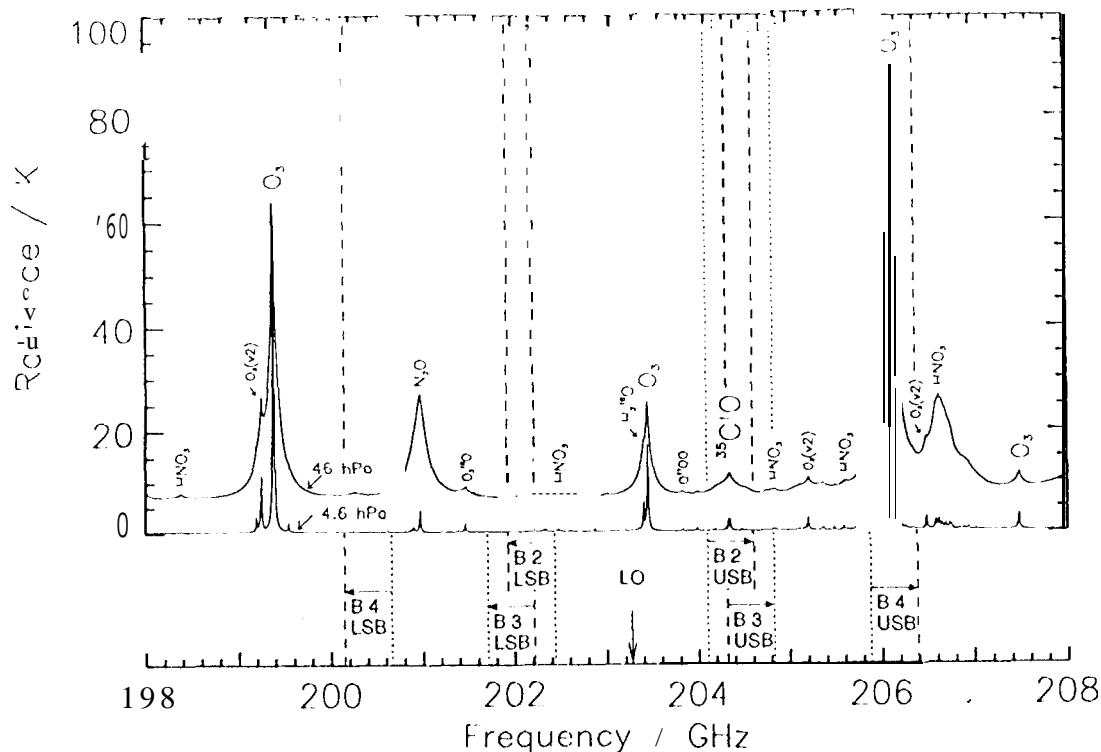


Figure 1. Calculated atmospheric limb radiance for the spectral region containing the 205 GHz ClO line measured by UARS/MLS. The upper panel shows the spectrum over the 198-208 GHz region, and indicates locations of the 205 GHz radiometer local oscillator (LO) and upper (USB) and lower (LSB) sidebands for MLS bands B2, B3 and B4. The lower panel shows a more detailed view of the region covered by bands B2 and B3 used for ClO, and is a 'double sideband' (DSB) calculation --- the average (and folded about the LO frequency) of contributions from the LSB and USB. Locations of the 15 filters in B2 and B3 are indicated in the lower panel. The 'IF frequency' axis on the bottom panel gives the frequency after the first heterodyne conversion in the 205 GHz radiometer; filter channels in B3 increase in the opposite direction than in B2 because of different second-heterodyne conversions in these two bands [Barathetal., 1993]. The vertical scale is the equivalent brightness temperature of the radiance. The two calculated spectra in each panel are for observation paths through the limb with tangent pressures of 4.6 hPa (upper stratosphere) and 46 hPa (lower stratosphere). The ClO profile used for these calculations was double-peaked to represent lower stratospheric ClO enhanced by heterogeneous chemistry, and upper stratospheric ClO due to pure gas-phase chemistry; peak values of 1 ppbv were assumed for both the lower and upper stratospheric ClO.

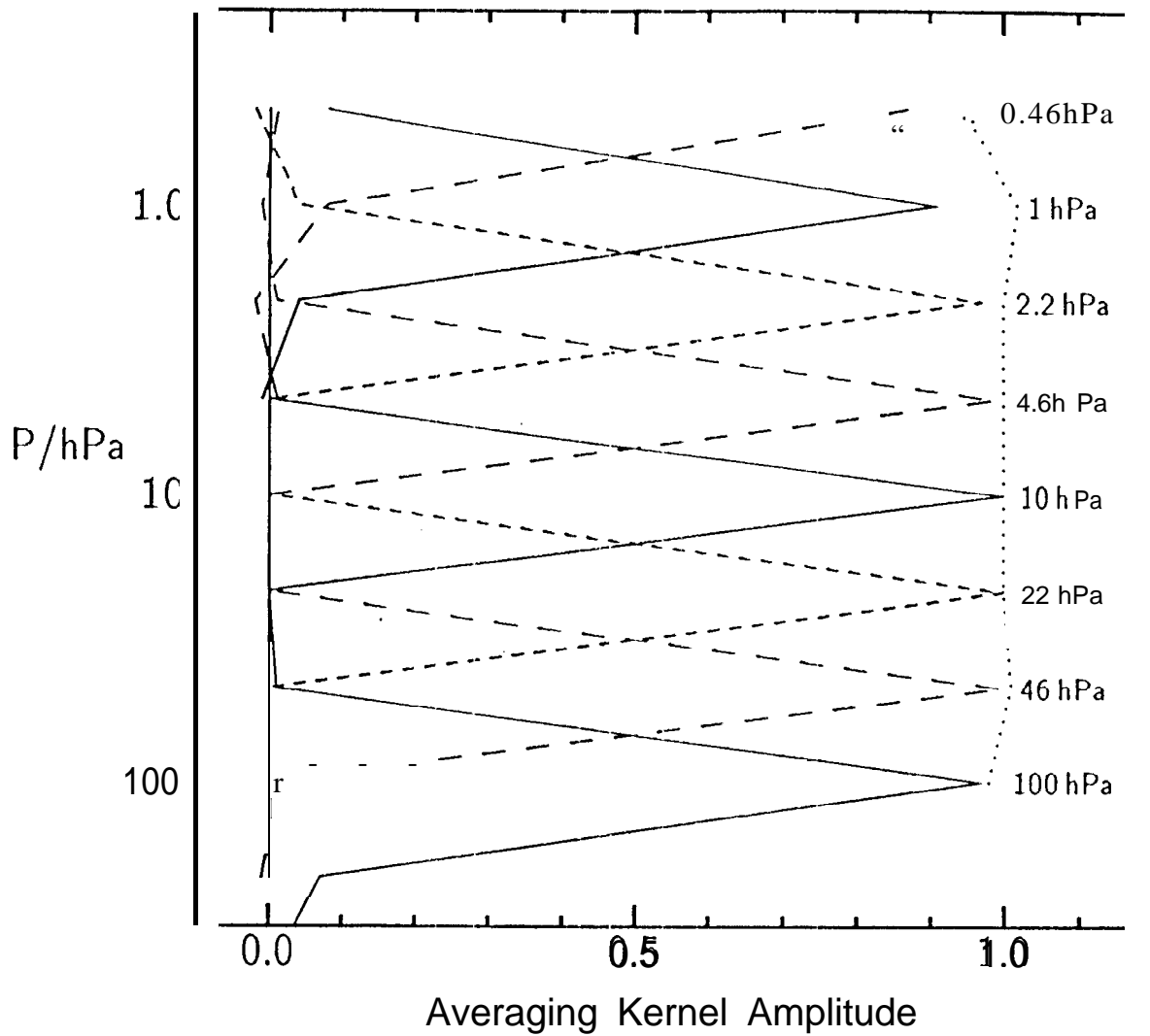


Figure 2. Averaging kernels (see *Rodgers [1990]; Marks and Rodgers [1993]*) for MLS Version 3 CIO retrievals of individual profiles. The solid and dashed curves are the rows of the averaging kernel matrix, and give the vertical resolution in the retrieved profile. The number printed to the right of each peak is the pressure of the retrieval surface associated with that kernel. The dotted line is the sum of the columns of the averaging kernel matrix for that height, and gives the relative amount of information which comes from the MLS measurement, as opposed to coming from the *a priori*.

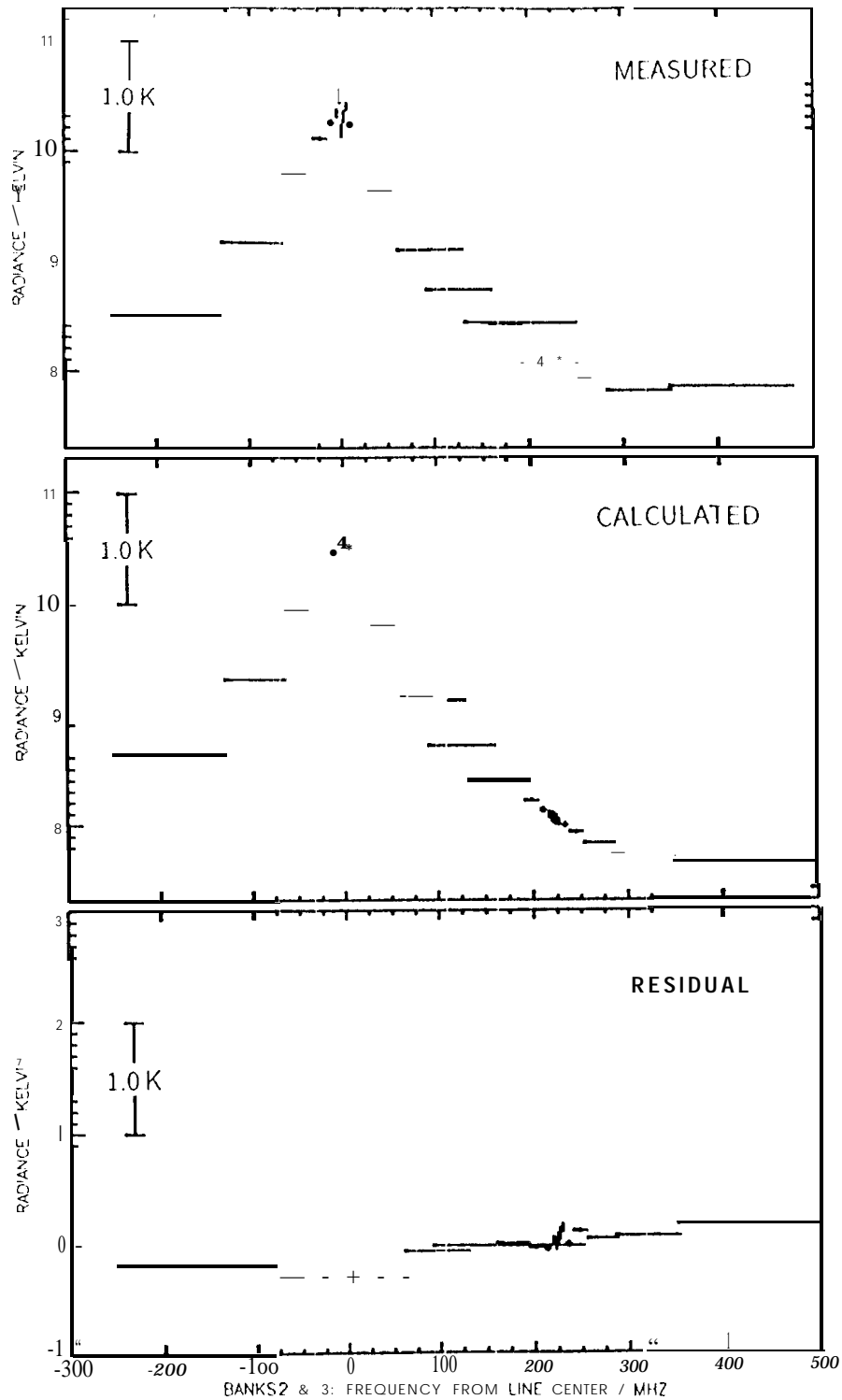


Figure 3. Lower stratospheric ClO spectra from the Antarctic vortex. Top panel is the average of measurements made with the MLSFOV between 22 and 100 hPa tangent pressures (-13–22 km) on 16 separate limb scans occurring during daylight (at local solar zenith angles less than 85°) on 16 August 1992. The limb scans were selected from the region where largest ClO abundances are retrieved, and only data having MMAF_STAT=G and QUALITY_CLO=4 have been included. Middle panel is the average of spectra for the same tangent heights calculated from the individual retrievals. Bottom panel shows the residuals (measured minus calculated). Horizontal bars indicate the different filter channels, and the width of each bar gives the width of that filter. The vertical bars give the expected noise of the average.

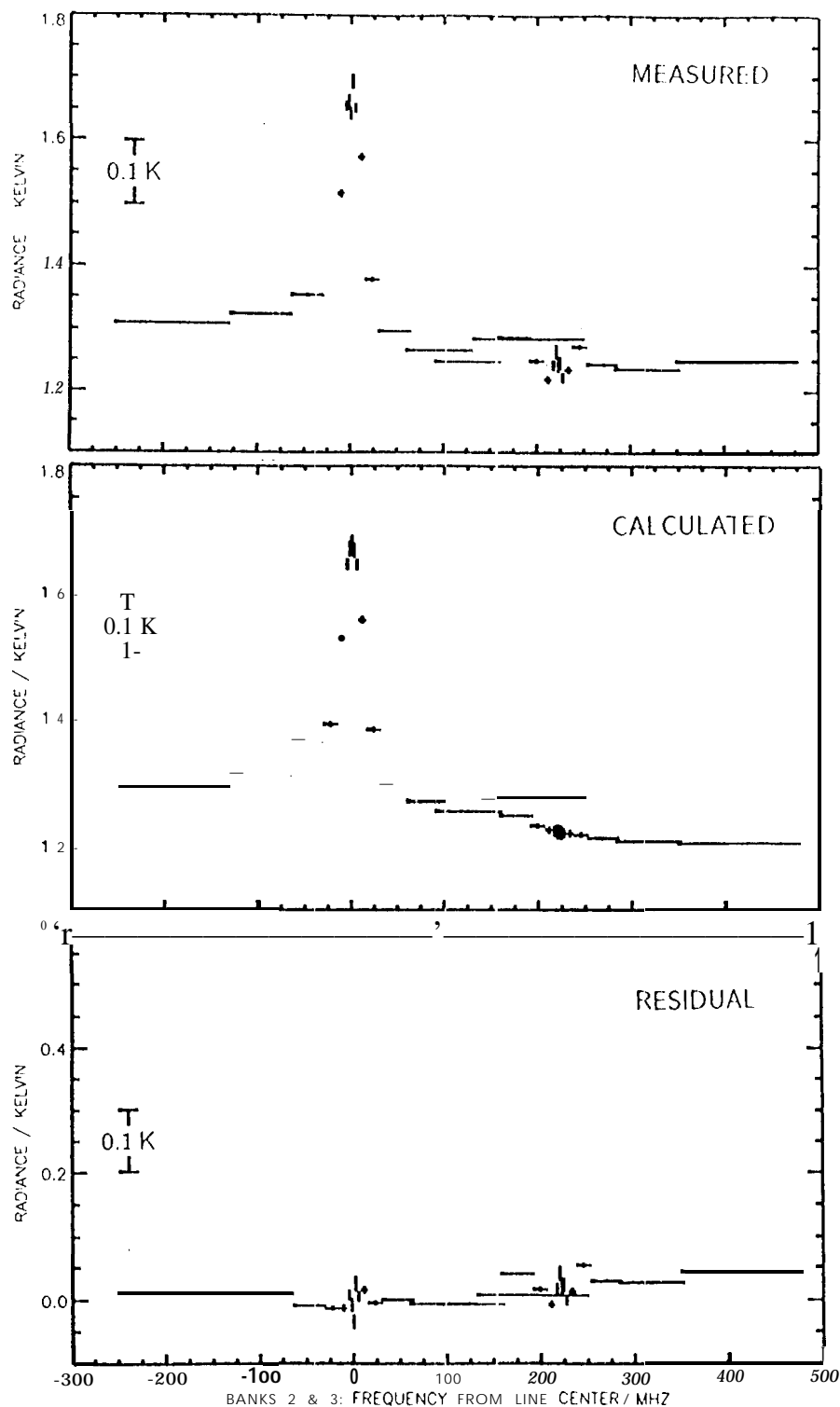


Figure 4. Mid-upper stratospheric ClO spectra. Top panel is the average of measurements made with the MLS FOV between 2.2 and 10 hPa tangent pressures (~ 31 – 42 km) on 548 separate limb scans occurring during daylight (at local solar zenith angles less than 80°) on 11 July 1993. Only data having `MMAF_STAT=G` and `QUALITY_CL0=4` have been included. Middle panel is the average of spectra for the same tangent heights calculated from the individual retrievals. Bottom panel] shows the residuals (measured minus calculated). Horizontal bars indicate the different filter channels, and the width of each bar gives the expected noise of that filter. The vertical bars give the expected noise of the average. Note that the vertical scale has been greatly expanded from that in the previous figure.

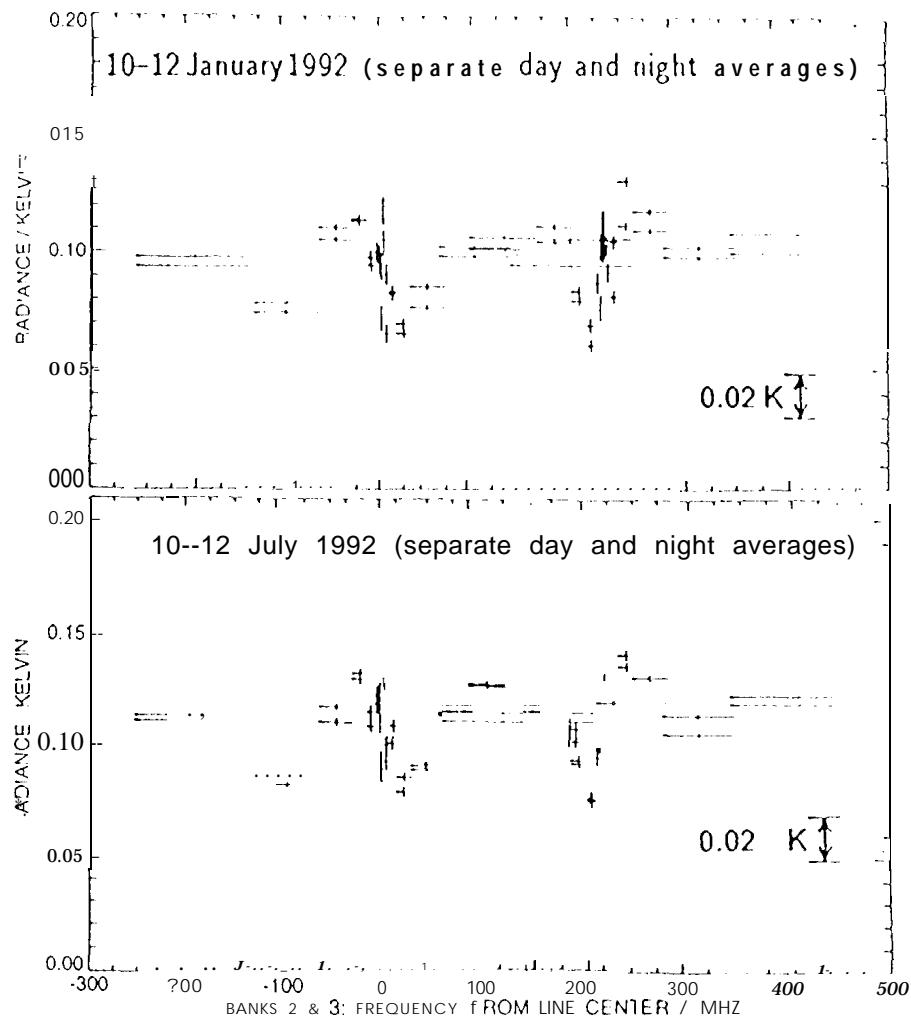


Figure 5. MIS 'space radiances' for two 3-day periods averaged separately for day and night. Only radiances having inferred tangent pressure less than 0.1 hPa (heights above about 65 km) are included in the average. The top panel is for 10-12 January 1992 (north looking), and the bottom panel is for 10-12 July 1992 (south-looking). The two spectra in each panel are the separate averages for 'day' (solar zenith angle less than 90°) and 'night' (solar zenith angle greater than 90°). The spectra pattern for these high altitudes shown here is thought to be due to residual instrumental artifacts. Note that the peak-to-peak variation in its amplitude is approximately 0.05 Kelvin in brightness temperature, which corresponds to the amplitude of signal from a CIO abundance of approximately 0.05 ppbv. Also note that the pattern between day and night repeats to within approximately 0.01 Kelvin brightness temperature, which corresponds to the amplitude of signal from a CIO abundance of approximately 0.01 ppbv. Averages are of approximately 9000 individual spectra, each measured with an instrument integration time of 2s, and only data having MMAF_STAT=G and QUALITY_CIO=4 have been included.

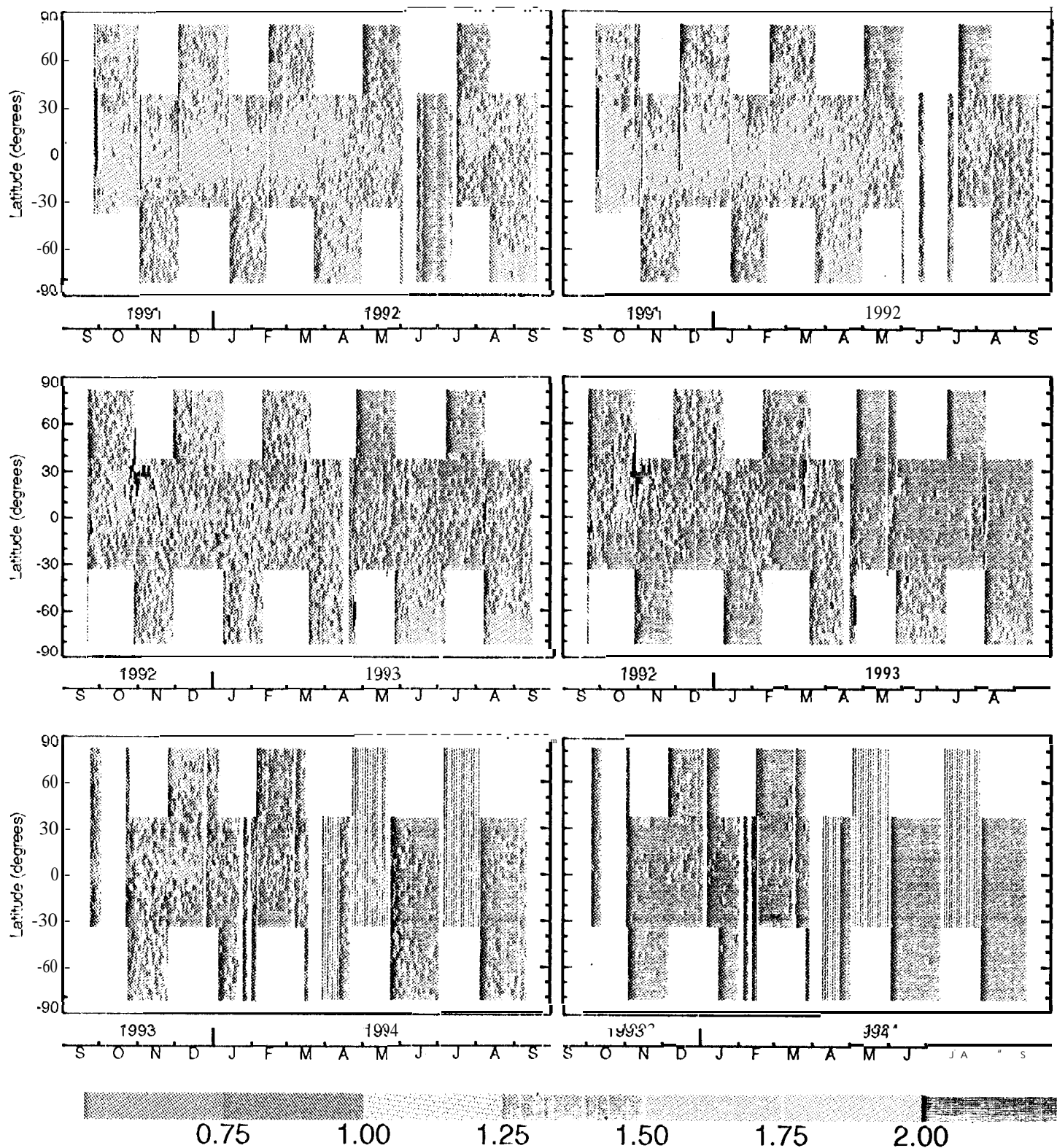


Figure 6. Daily zonally-averaged χ^2_{ma} for MLS CIO retrievals for the first three years of MLS measurements. Values are shown separately for MLS band 2 (left) and band 3 (right). Gaps occur where there were no measurements; the alternating gaps during April-May and July 1994 are when MLS was operated every other day.

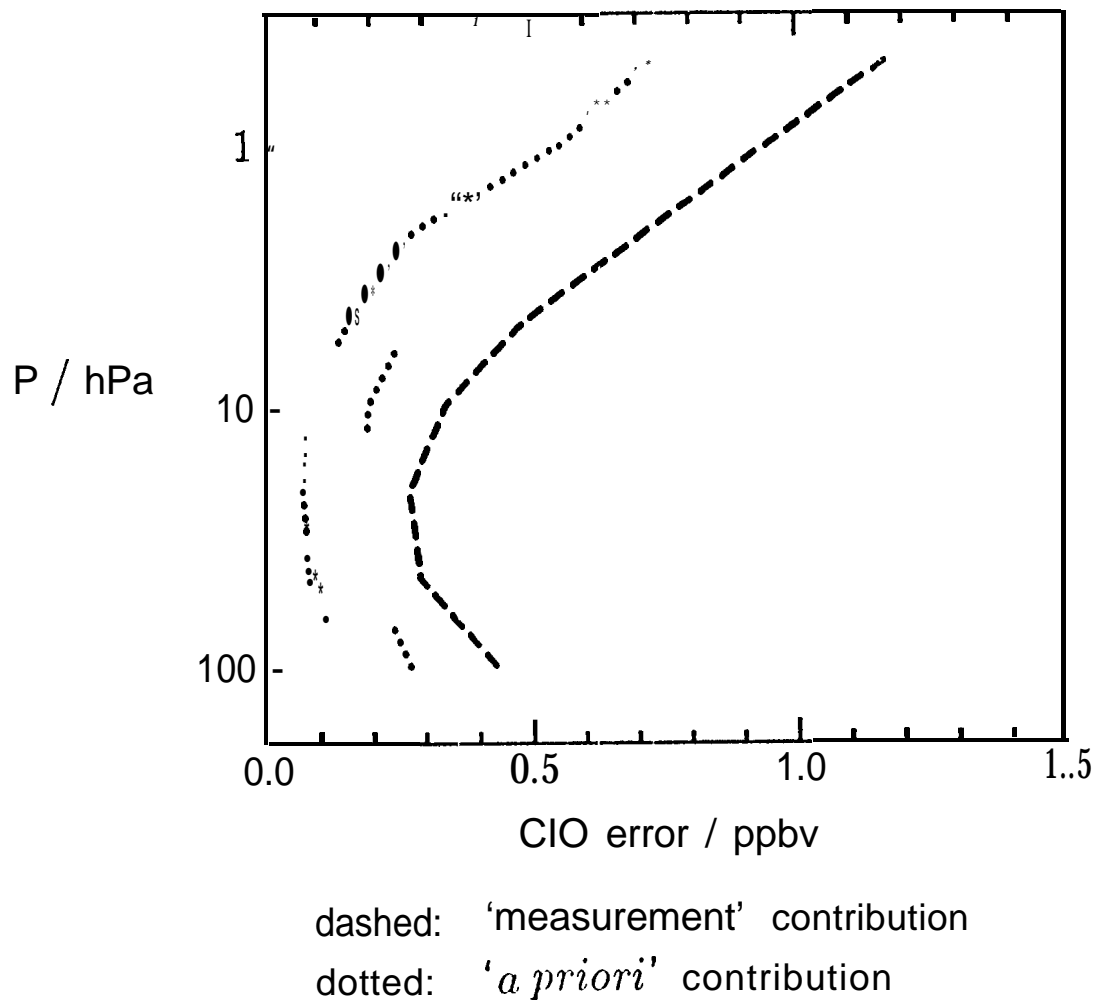
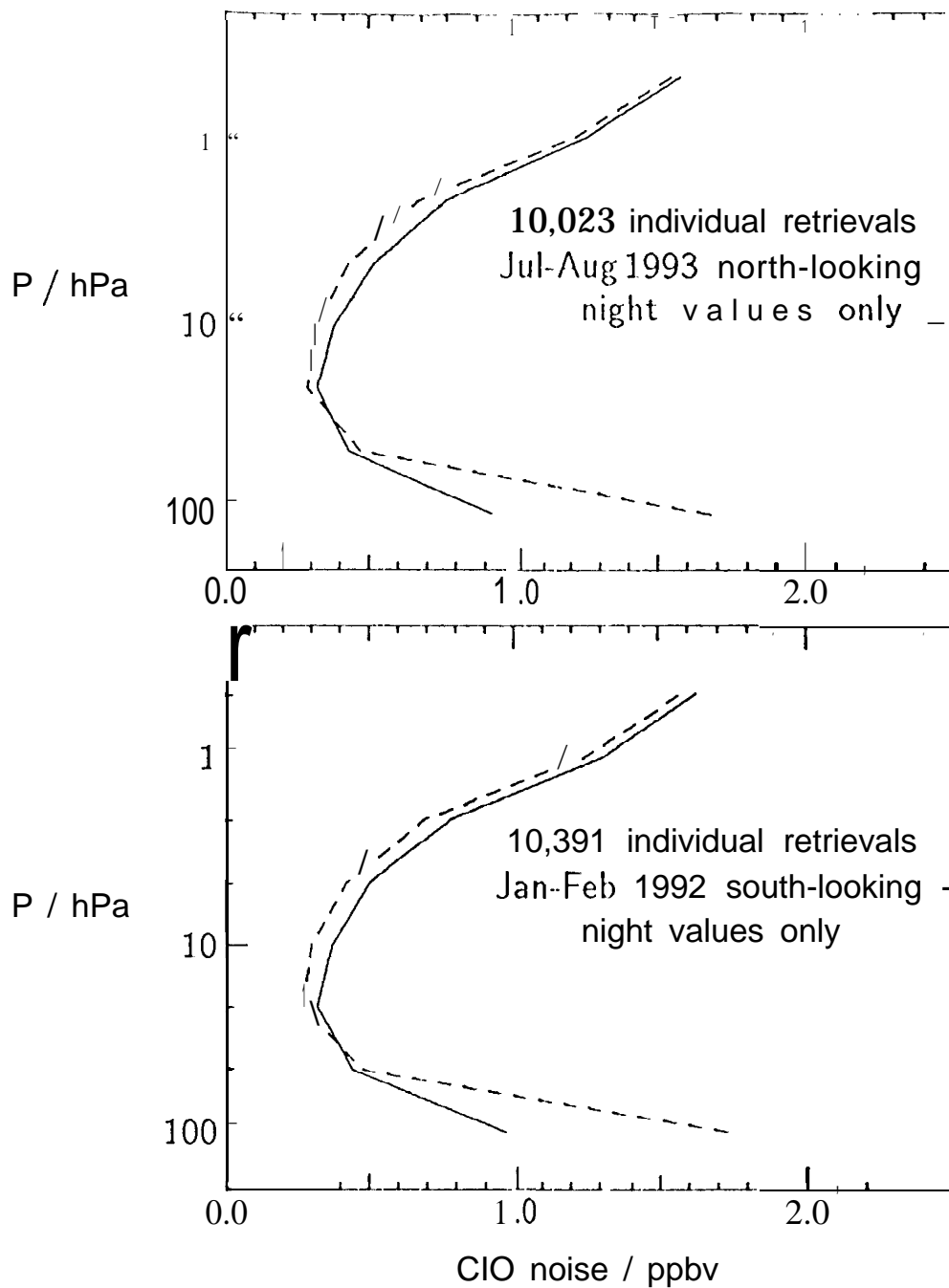


Figure 7. 'Measurement' and 'a priori' contributions to uncertainties in the individual MLS CIO retrievals as described by the formalism of Rodgers [1990].



solid: Standard deviation of measurements
dashed: Predicted 1σ noise

Figure 8. Measured and predicted noise in individual MLS ClO retrievals. The data sample here included only retrievals made in early morning (solar zenith angles greater than 95° and local solar times between midnight and 6 am) during the 9 July to 8 August 1993 north-looking period (top) and the 15 January to 14 February 1992 south-looking period (bottom). This sample covers times when ClO is expected to be a minimum, and variations in the retrieved values are expected to be dominated by measurement noise. The predicted 1σ noise shown by the dashed curves is the average value for each data ensemble of the values produced by the algorithms for the Version 3 data. Only data having `MMAF_STAT=G` and `QUALITY_CL0=4` have been included.

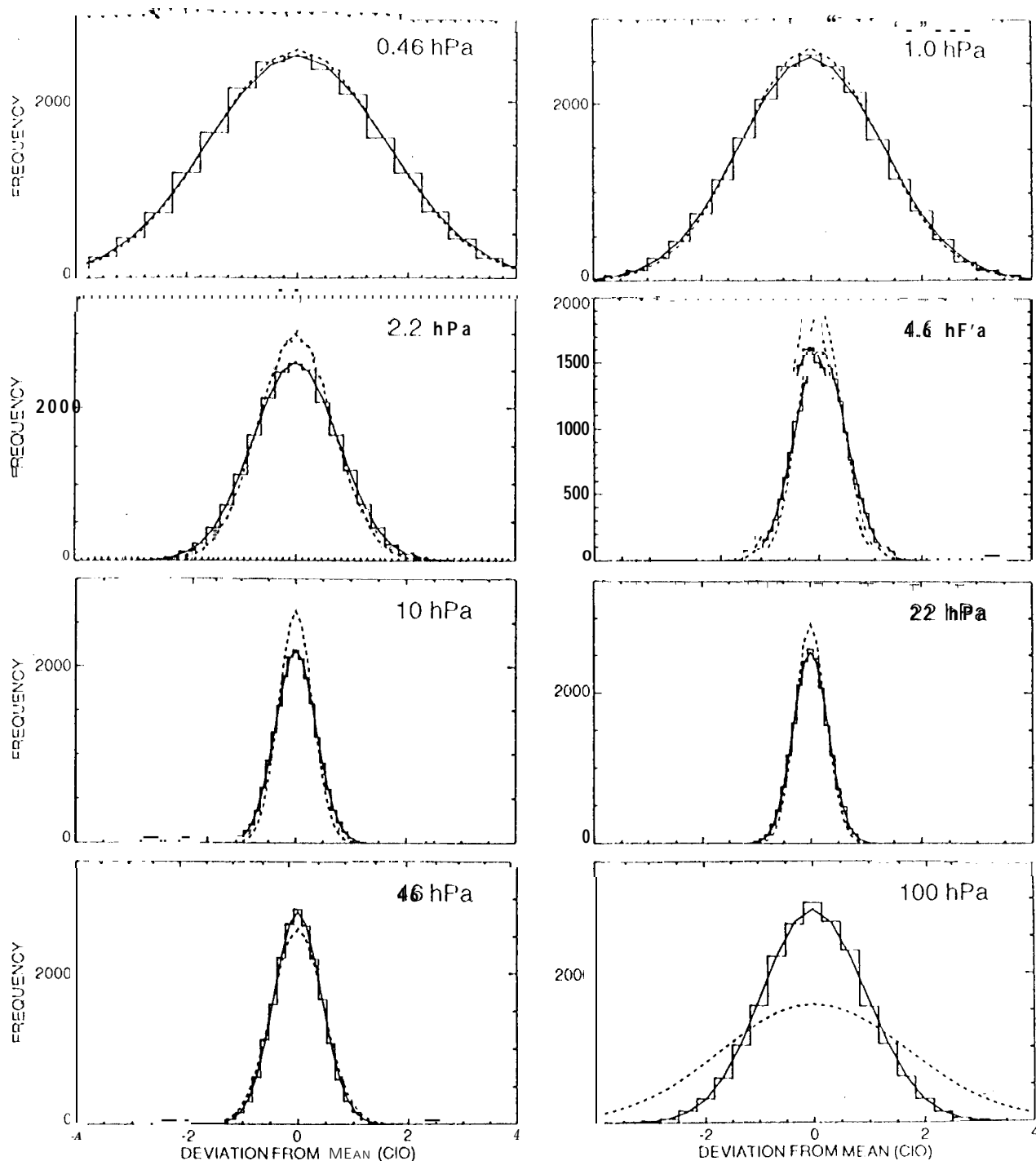
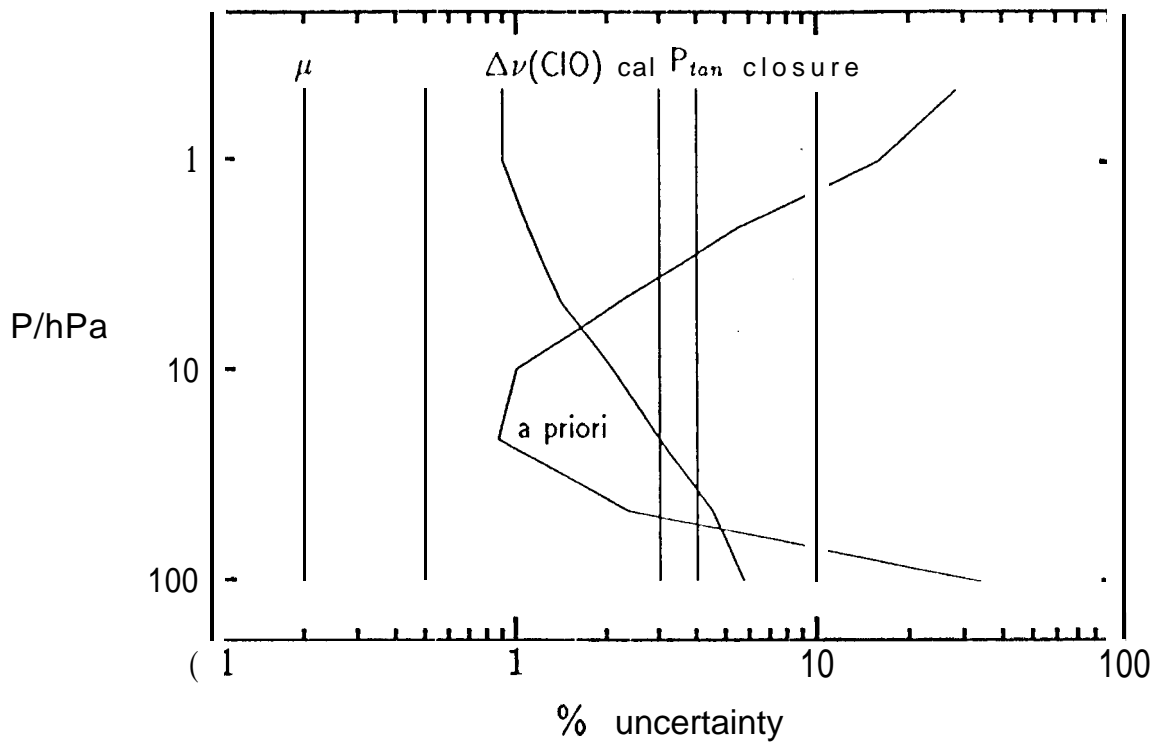


Figure 9. The distribution of nighttime CIO profiles retrieved from MLS. The data ensemble used here includes 20,414 individual profiles retrieved between midnight and 6am for the UARS months of Jan-Feb 1992 (south-looking summer) and Jul-Aug 1993 (north-looking summer) when stratospheric CIO is expected to be minimum, and the retrieved distribution is expected to be dominated by instrument noise. The 'staircase' histograms in each panel give show the measured distribution of the retrieved values. Only data having **MMAF_STAT=6** and **QUALITY_CIO=4** have been included. The horizontal axis is deviation from the mean (in ppbv), and the vertical axis is the number of values within the 0.25 ppbv increments chosen for the histogram. The smooth curves are Gaussians having approximately the same enclosed area as the histograms. The solid Gaussian has width equal to the measured standard deviation of the data, and the dashed has width equal to the average of the uncertainties predicted by the Version 3 algorithm.



μ	due to molecular dipole moment
ϕ	due to transition matrix element
$\Delta\nu(ClO)$	due to ClO linewidth
P_{tan}	due to tangent pressure
cal	due to instrument calibration
closure	due to lack of retrieval closure
a priori	maximum effect of a priori

Figure 10. Estimated 'scaling' uncertainties for MLS Version 3 ClO.

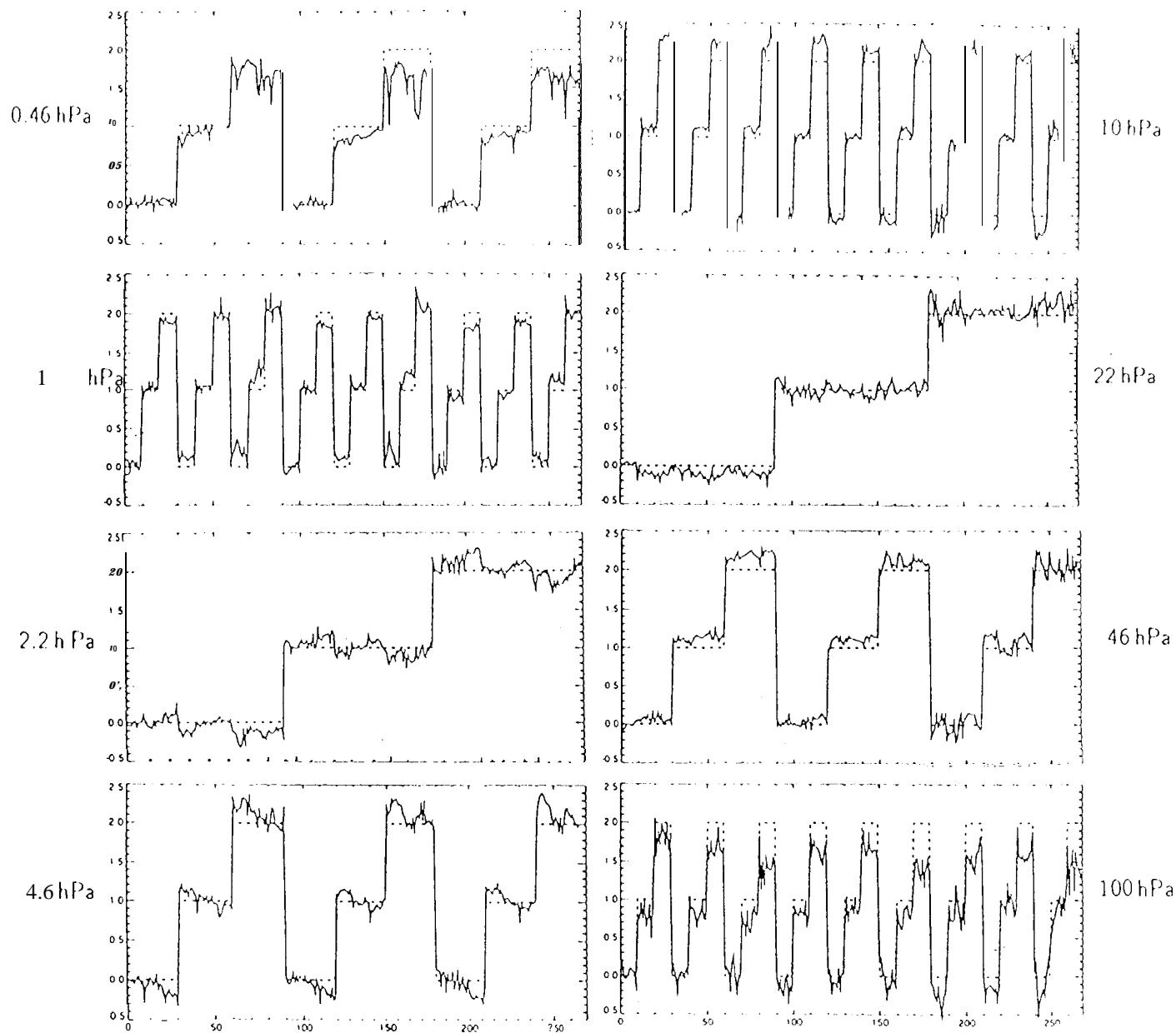


Figure 11. Results of simulations using the Version 3 CIO retrieval algorithms. A total of 270 simulations were performed for this test, and the horizontal axis gives the index of individual retrievals. The dashed lines are the 'truth' and the solid lines are the simulated retrieval results. The 'truth' was made to cycle between 0, 1 and 2 ppbv CIO at the various levels. The 'noise' in the retrievals is due to other than measurement noise, as noise was not added to the simulated radiances used in these tests (although nominal radiance uncertainties were assumed by the algorithms) in order to see the effects more precisely. Underestimates of CIO at 0.46 and 100 hPa are expected due to effects of the a priori. [This figure will be redrawn before publication.]

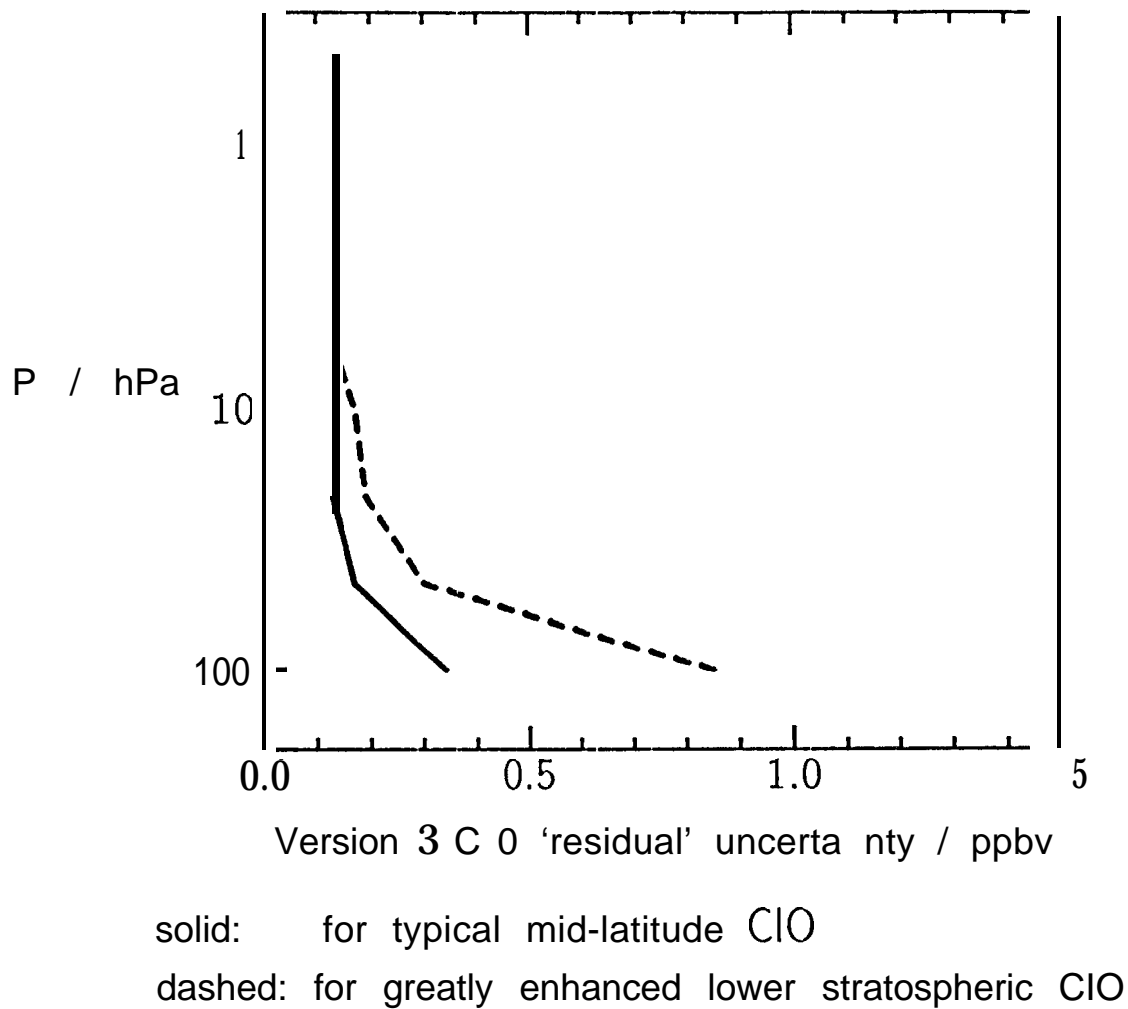


Figure 12. Uncertainties in MIS Version 3 ClO retrievals due to lack of closure in fitting the measured radiances.

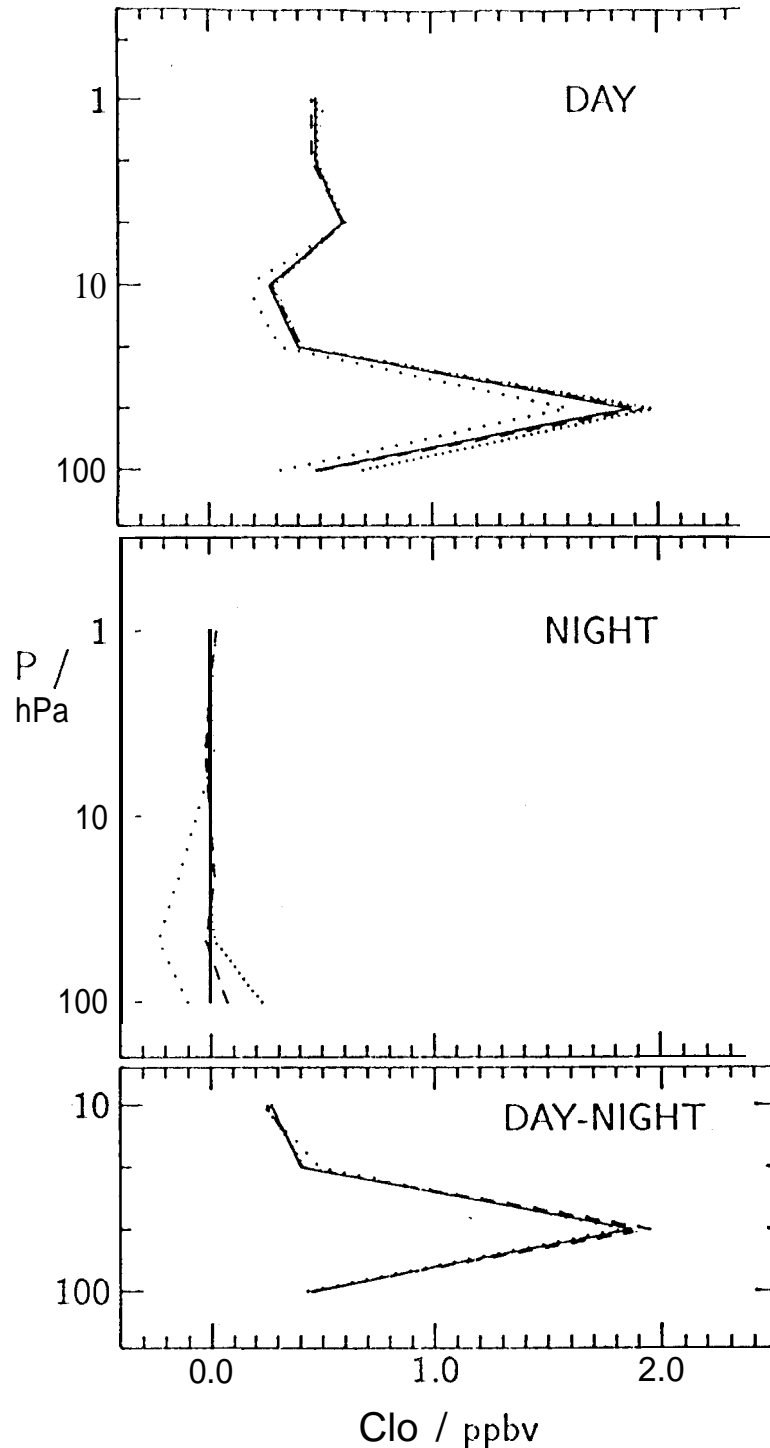


Figure 13. Results of ClO retrieval simulations for conditions of enhanced ClO in the lower stratosphere. 'True profiles' are the solid curves, from which radiances were calculated and used in simulations to produce results shown in the other curves. The dashed curves give results from algorithm producing the MLS Version 3 data. The dotted curves show the effects of changing HNO_3 and N_2O between climatological profiles and zero. The curve with dense dots is with both N_2O and HNO_3 set to zero, while that with sparse dots is with climatological N_2O and zero HNO_3 . The results shown here are the averages of approximately 40 individual retrievals for both 'day' and 'night' conditions. Curves in the bottom panel are day minus night differences for retrievals at 10 hPa and below.

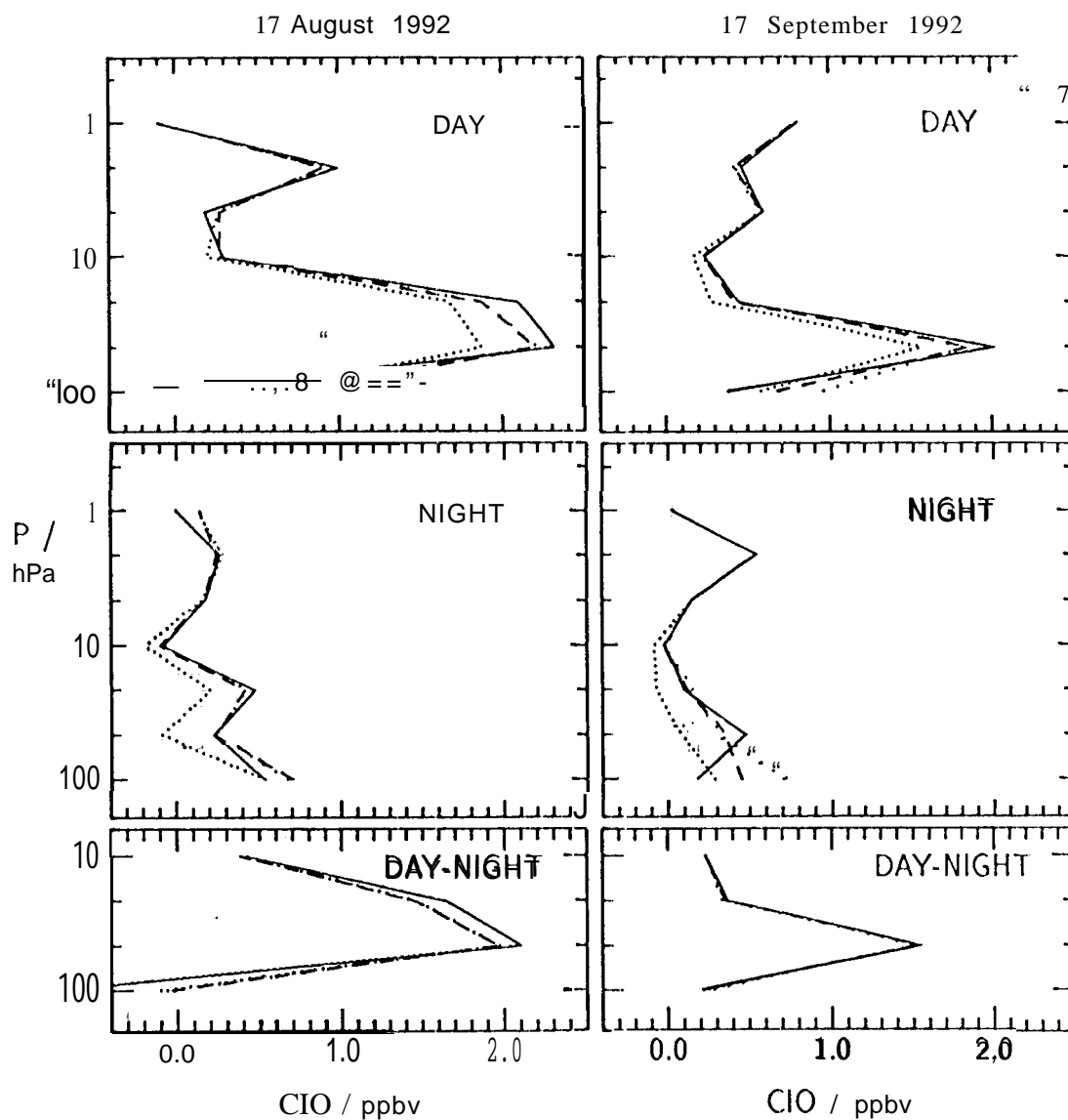


Figure 14. Results from different retrieval schemes used on MLS radiances measured over Antarctica on 17 August 1992 (left) and 17 September 1992 (right). The averages of approximately 20 individual retrievals are shown. The solid curves are from the algorithm producing the MLS Version 3 data. The dashed curves are from retrievals made on averaged radiances with an iterative scheme to handle non-linearities, but which treats HNO_3 and N_2O in the same way as the production algorithms. Dotted curves show the effects of changing HNO_3 and N_2O from climatological profiles to zero. The curve with dense dots has climatological N_2O and zero HNO_3 ; that with sparse dots has zero N_2O and climatological HNO_3 . Only radiances having $\text{MAF_STAT}=G$ were included.

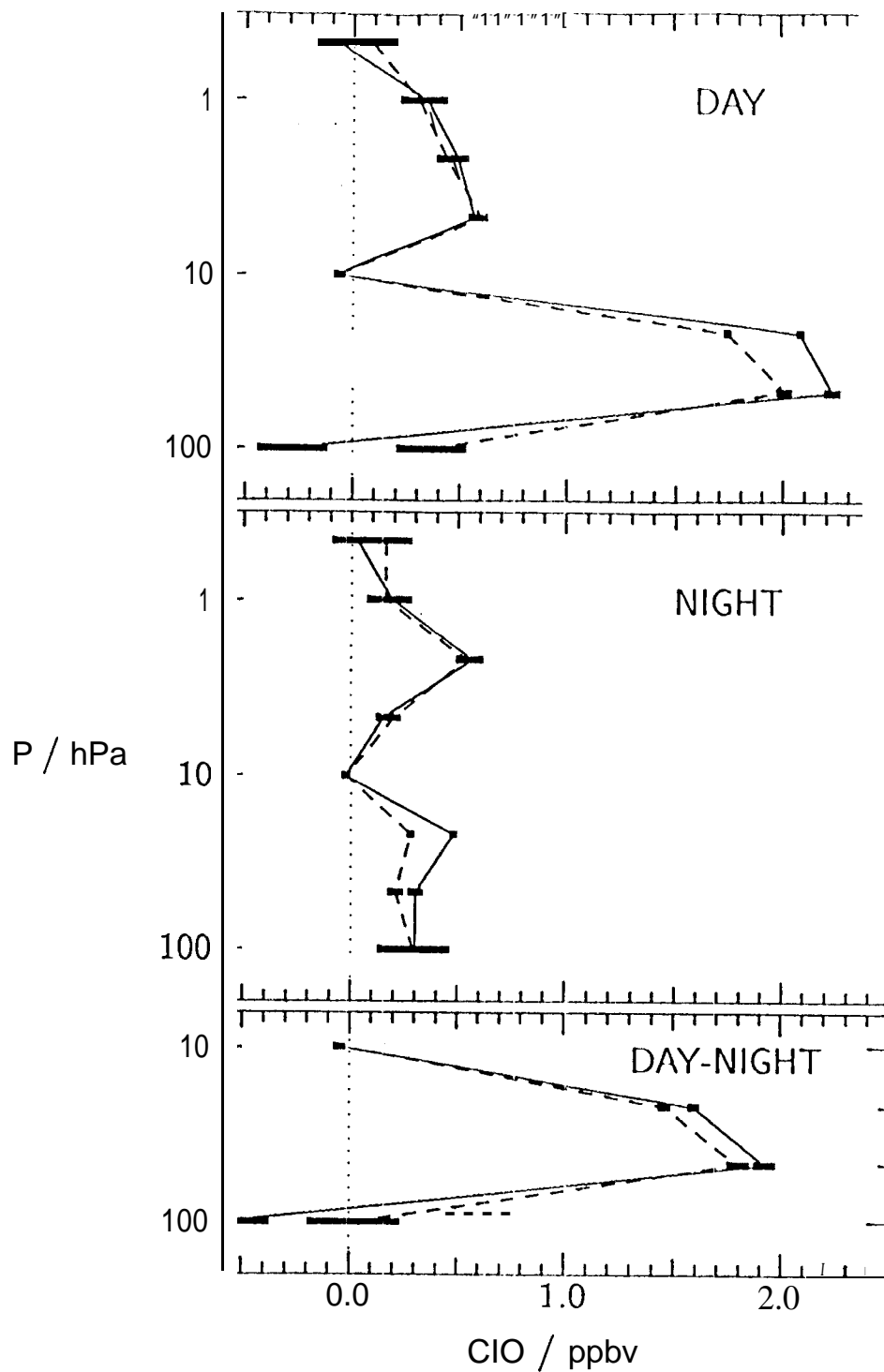
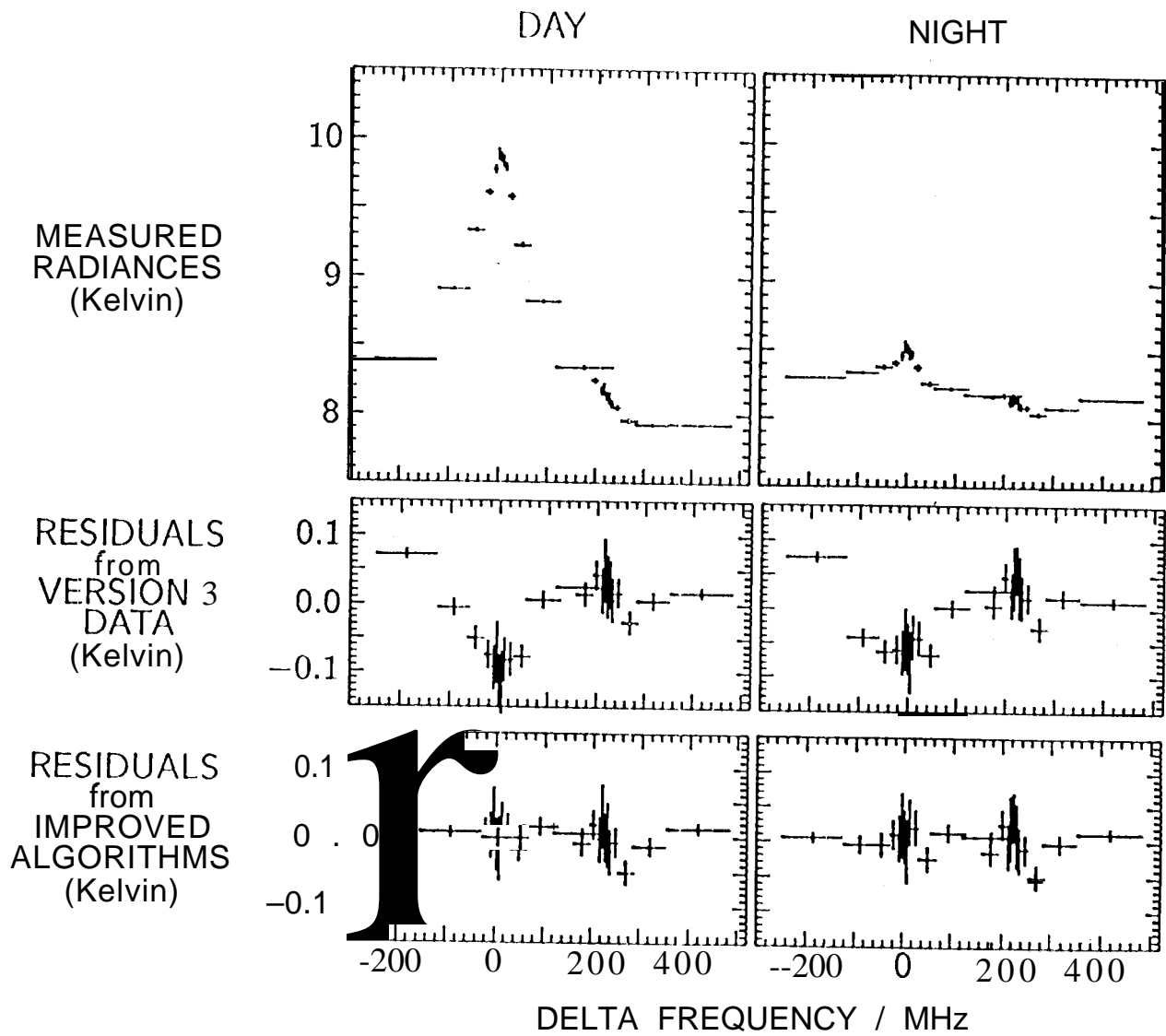


Figure 15. Average of ClO retrievals from MIS measurements made 14-29 August 1992 in the Antarctic vortex between 65-75 S and 0-90 E. Solid lines are from Version 3 data. Dashed lines are from an improved algorithm which accounts for non-linearities, includes effects of HNO₃, and uses the revised O₂ linewidth parameter. Horizontal bars give the $\pm 1\sigma$ predicted precision of the averages. The 'day' average consisted of 178 individual measurements which had local solar zenith angles between 78 and 91° and local solar times between 8:40 am and 2:40 pm. The 'night' average consisted of 187 individual measurements which had local solar zenith angles between 96 and 127°, and local solar times between 5:10 and 11:00 pm. Only data having MMAF_STAT=G and QUALITY_CLO=4 were included.



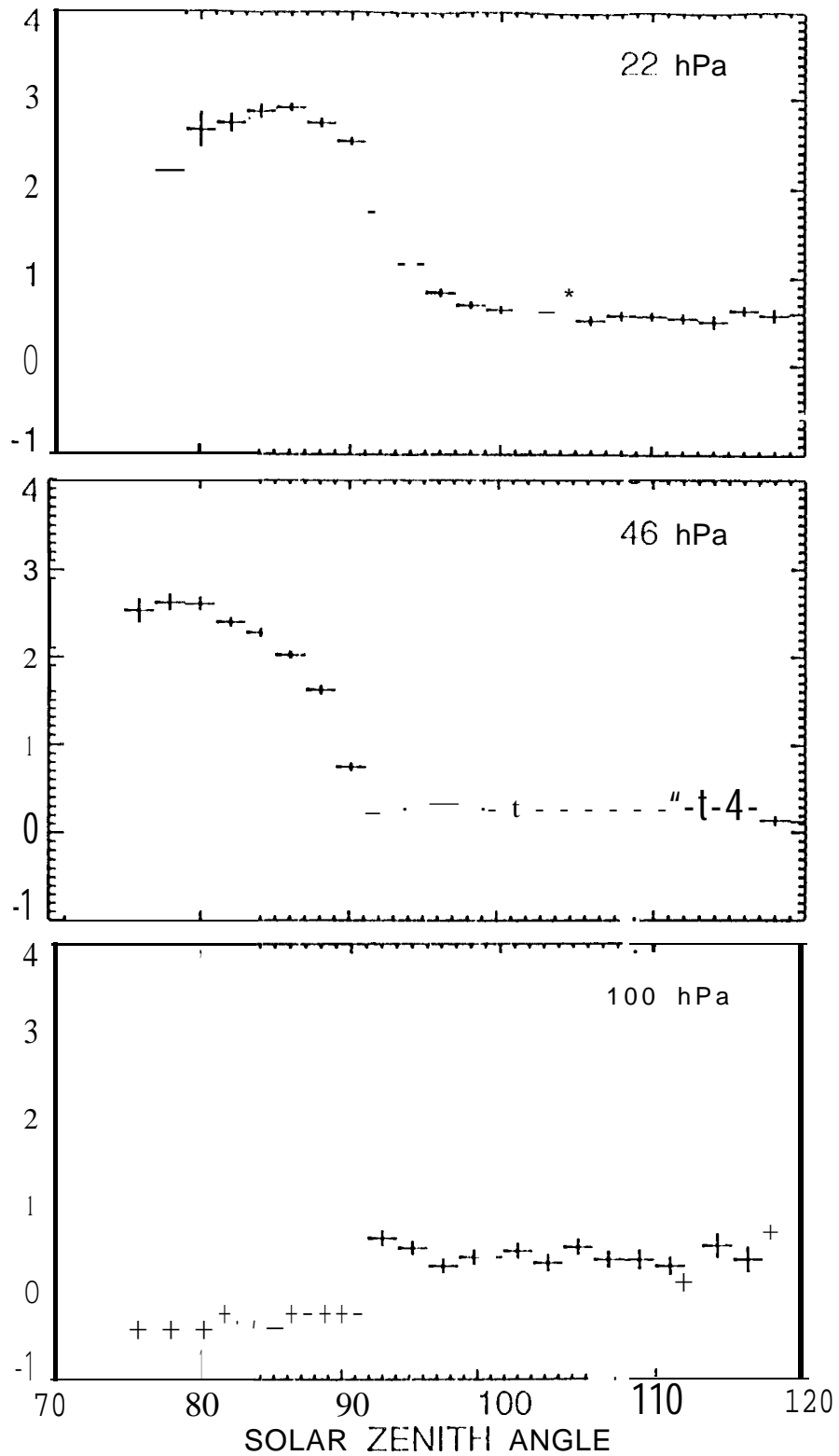


Figure 17. Lower stratospheric Version 3 ClO as a function of zenith angle, for time and location of largest ClO abundances measured by MLS. Shown here are averages of measurements made in the Antarctic vortex during 14-29 August 1992, and are plotted as a function of solar zenith angle (sza) at the time and location of the measurements. The vertical scale is ppbv and the data have been averaged in 2° sza bins, and only data with MMAF_STAT=G and QUALITY_CLO=4 have been included. The unrealistic behavior at 100 hPa ClO is an artifact, as discussed in the text.

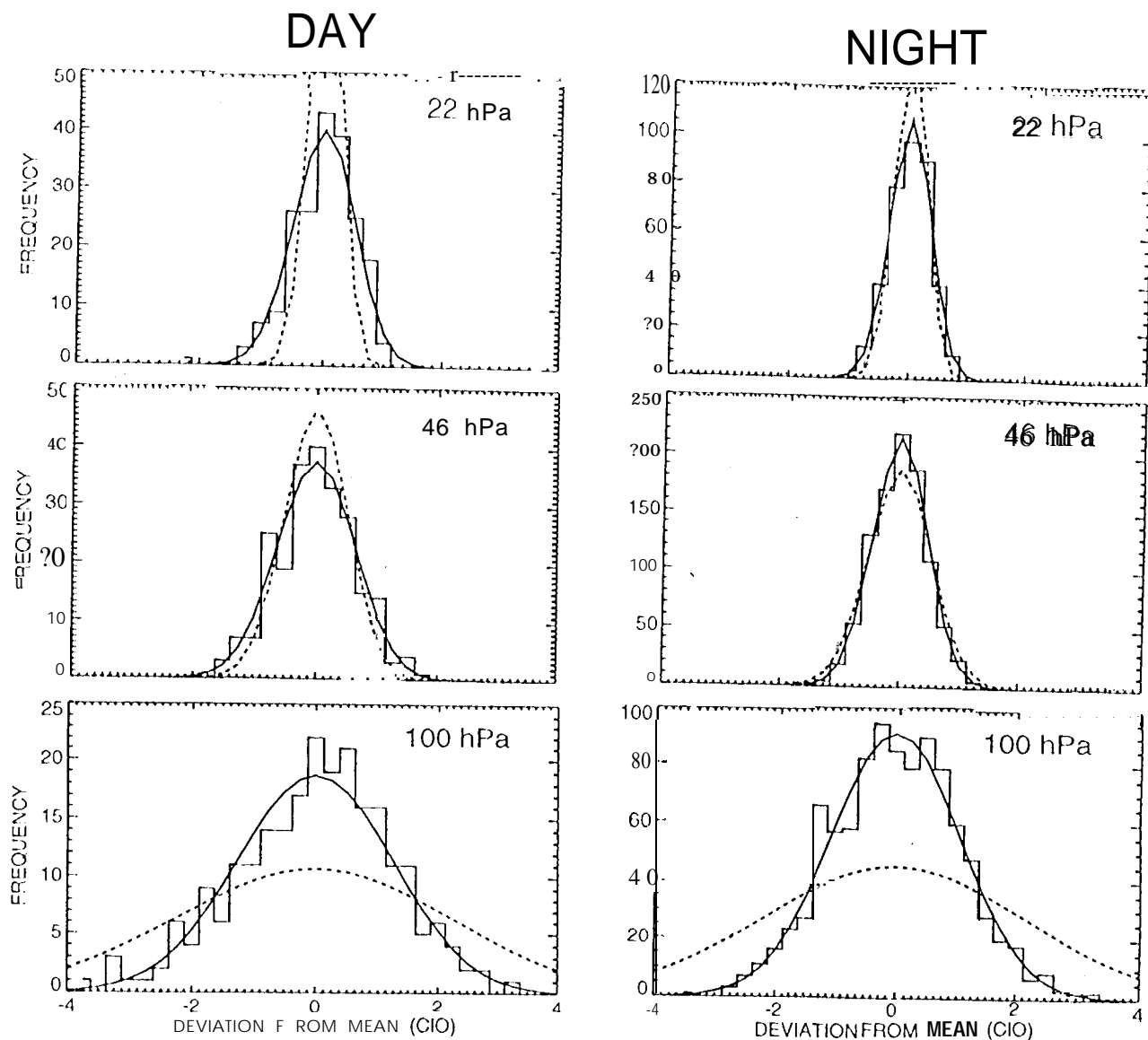


Figure 18. Statistical distribution of the CIO values which have been averaged for Figure ?? . 'Day' is defined as solar zenith angle (sza) $\leq 83^\circ$ for 46 and 100 hPa, and $\leq 88^\circ$ for 22 hPa. 'Night' is defined as $sza > 100^\circ$. The horizontal axis is variation from the mean in ppbv; the vertical axis is number of occurrences of that value. Histograms give the distribution of retrieved values, binned in 0.25 ppbv increments. Only data having MMAF_STAT=G and QUALITY_CIO=4 have been included. The smooth curves are Gaussians having approximately the same enclosed area as the histograms. The solid Gaussian has width equal to the measured standard deviation of the data, and the dashed has width equal to the average of the uncertainties predicted by the Version 3 algorithms.

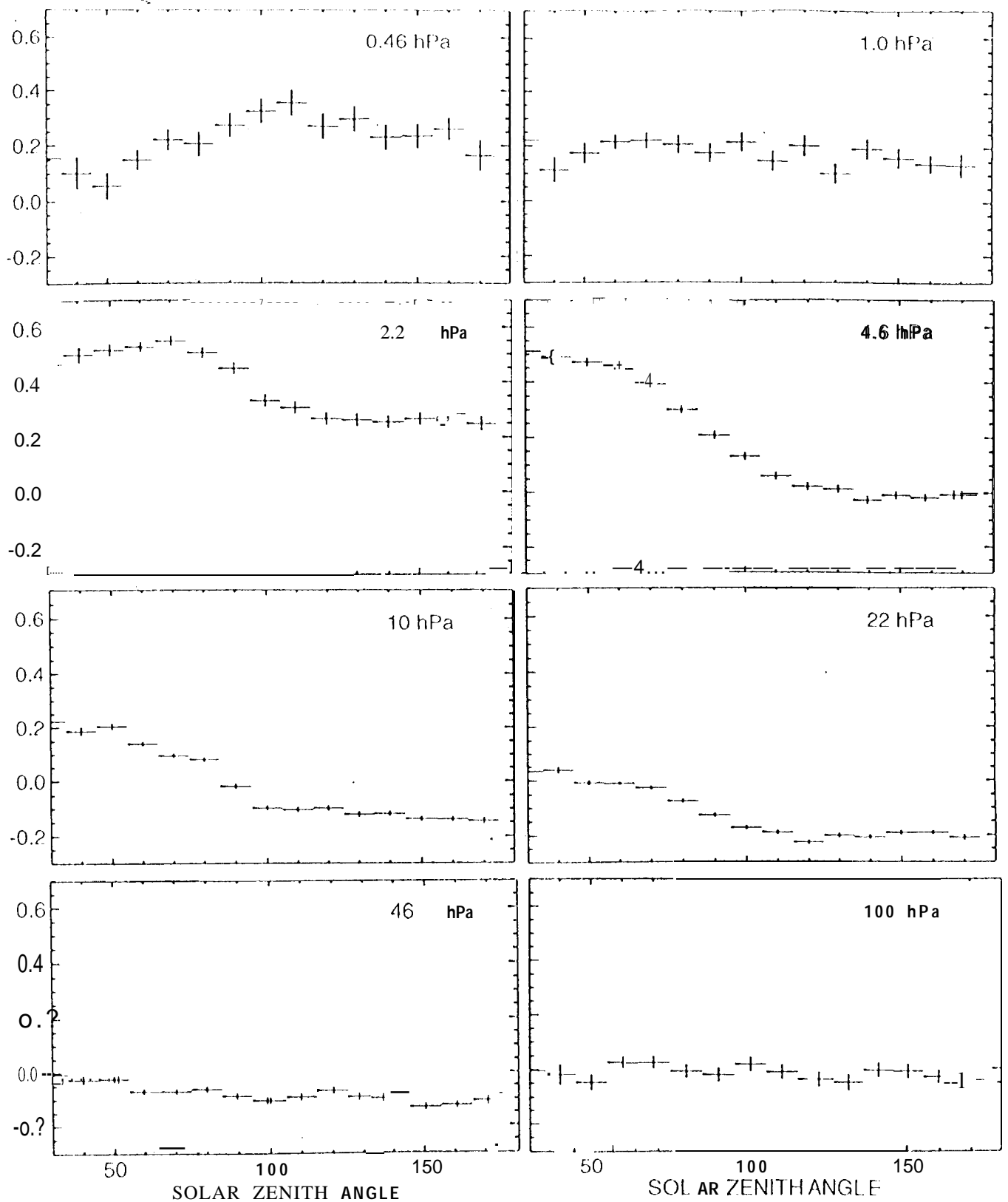


Figure 19. Variation with solar zenith angle (sza) of Version 3 CIO for measurements made during the summer south-looking period from 15 January through 14 February 1992. Individual retrievals were binned by sza, and then averaged over all latitudes to produce the results shown here. The vertical scale is ppbv, and vertical bars show the expected precision of the average. Only data having MMAP_STAT=G and QUALITY_CIO=4 have been included.

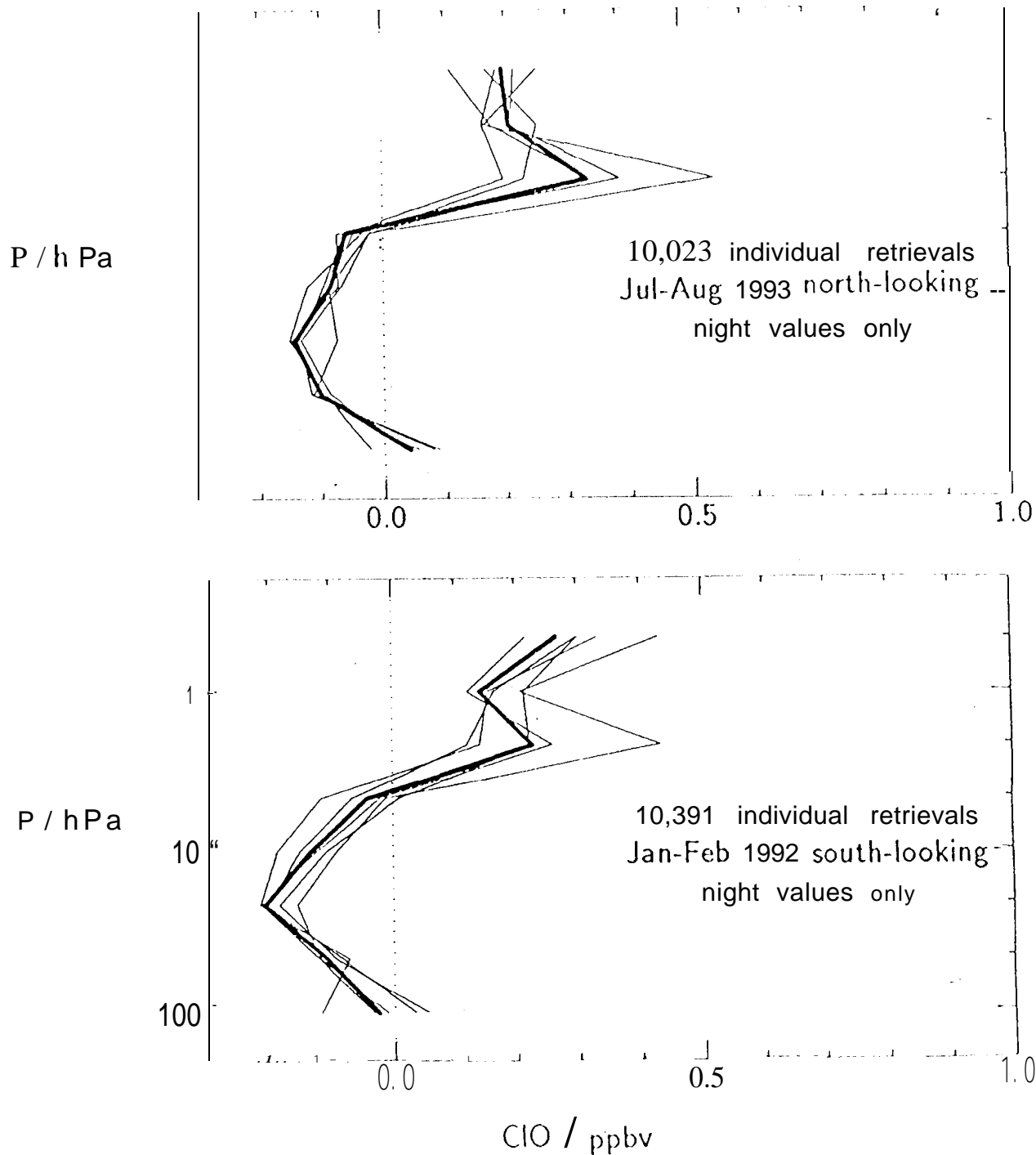


Figure 20. Averages of nighttime ClO retrievals. These are from data taken during 9 July through 7 August 1992 in the northern hemisphere (top panel), and 15 January through 14 February in the southern hemisphere (bottom panel). Only measurements made in early morning (local solar times between midnight and 6 am; solar zenith angles greater than 95°), and those having MMAF_STAT=G and QUALITY_CLO=4, were included. The thick line gives averages of all data (more than 10,000 individual retrievals from each of the hemispheres), and thin lines give 20° wide zonal averages in separate latitude ranges.

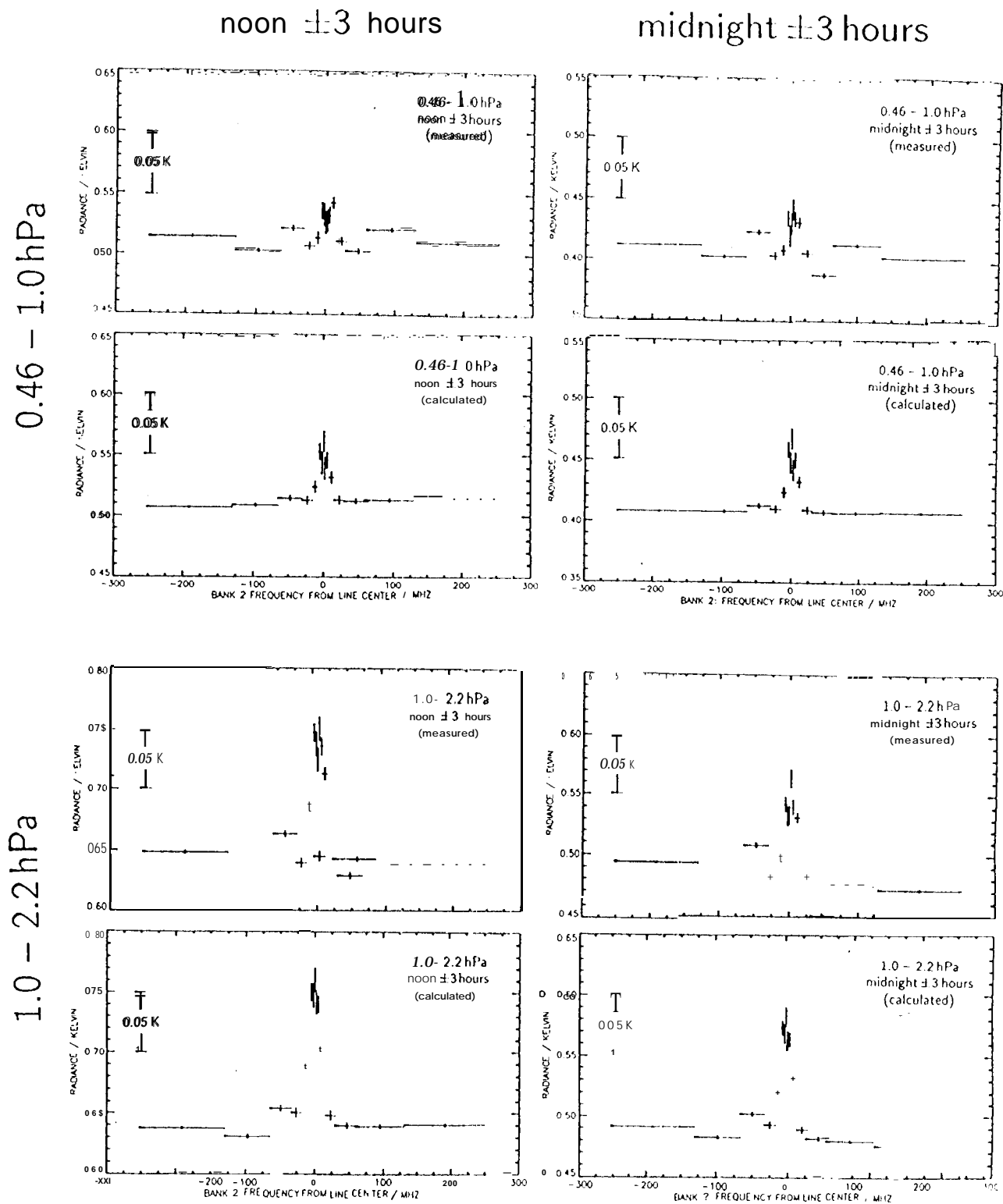


Figure 21, Measured and calculated ClO spectra at highest altitudes. The left panels are for averages of measurements made within 3 hours of local noon, and the right panels for those made within 3 hours of local midnight. The average is over all latitudes for measurements made on 19 and 26 January, and on 2 and 8 February 1992 (selected days covering the period shown in Figure 5-10). Only data having MMAF_STAT=G and QUALITY_CLO=4 have been included. The upper block of panels is for measurements made with the FOV between 0.46 and 1.0 hPa tangent height (~48-54 km), and the bottom block is for the FOV between 2.2 and 1.0 hPa (~42-48 km). The average of spectra calculated from the individually retrieved ClO profiles is shown below each measured spectra.

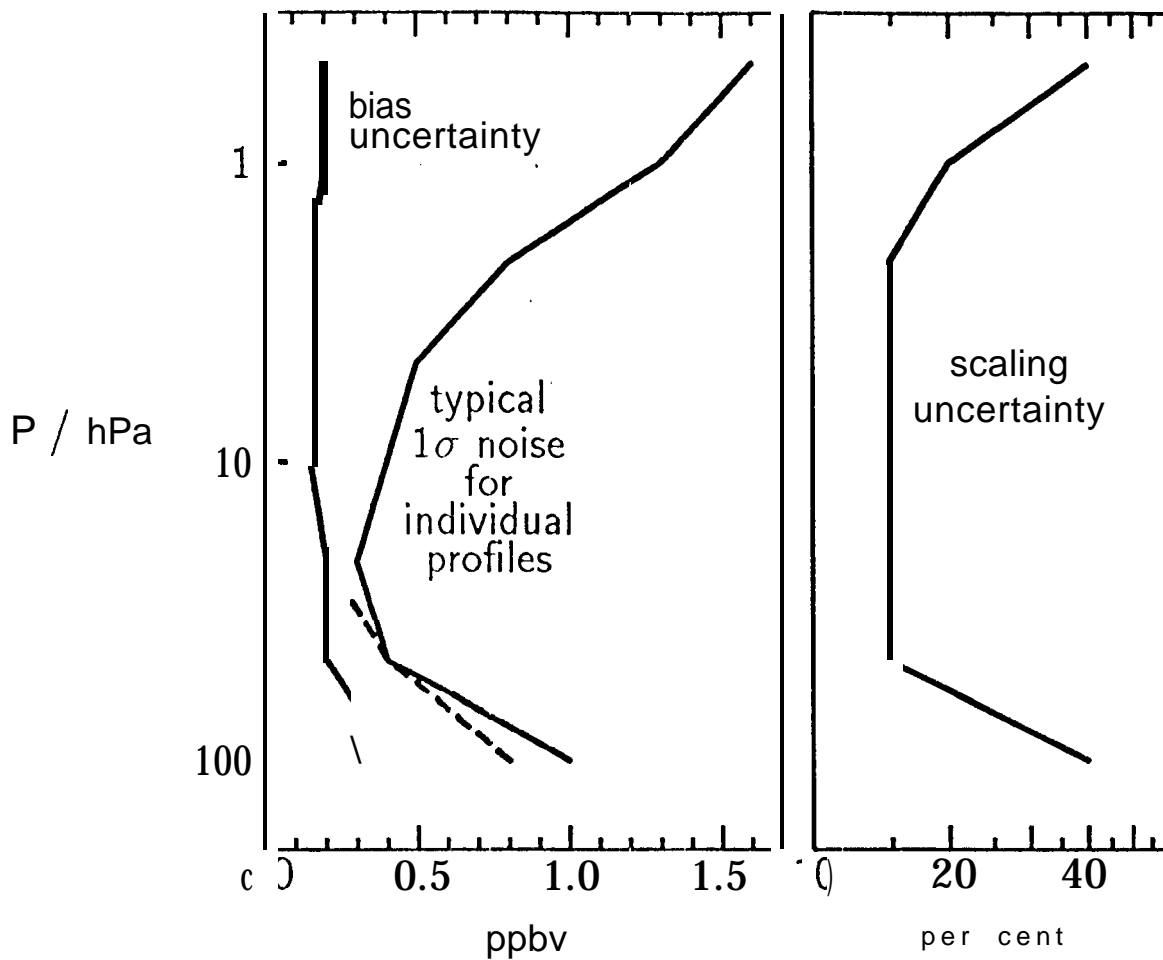
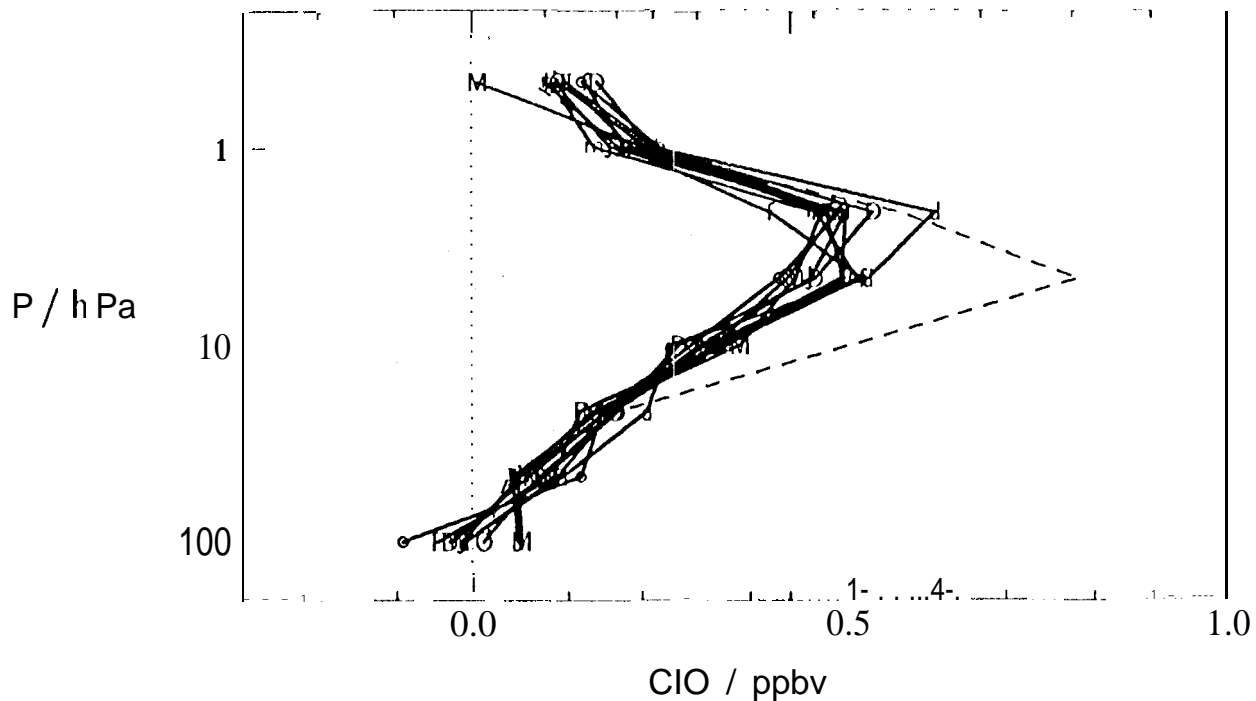


Figure 22. Summary of estimated uncertainties for MLS Version 3 ClO. The dashed curve for 'bias' applies to conditions of enhanced lower stratospheric ClO, and the solid curve to typical mid-latitude conditions.



O: 27 Sep 1991-3 Nov 1992 UARS days 16-53
 d: 5 Dec 1991 - 14 Jan 1992 UARS days 85-125
 f: 15 Feb 1992 - 23 Mar 1992 UARS days 157-194
 m: 2 May 1992-1 Jun 1992 UARS days 234-264
 j: 18 Jul 1992-13 Aug 1992 UARS days 311-337
 O: 22 Sep 1992 - 29 Oct 1992 UARS days 377-414
 D: 30 Nov 1992-9 Jan 1993 UARS days 446-486
 F: 10 Feb 1993 - 19 Mar 1993 UARS days 518-555
 M: 27 Apr 1993-28 May 1993 UARS days 594-625
 J: 9 Jul 1993-8 Aug 1993 UARS days 626-666

dashed: a priori profile

Figure 23. Monthly 20-40° N monthly zonal averages of ClO profiles from MLS. Only data taken at solar zenith angles less than 80° and with local solar times between 9am and 3pm were included in the average. Values from the night side of the orbit (solar zenith angles greater than 95°) have been subtracted from at 10 hPa and greater pressures to remove biases at lower altitudes. Only data having MMAF_STAT=G and QUALITY.CLO=4 were included in the averages.

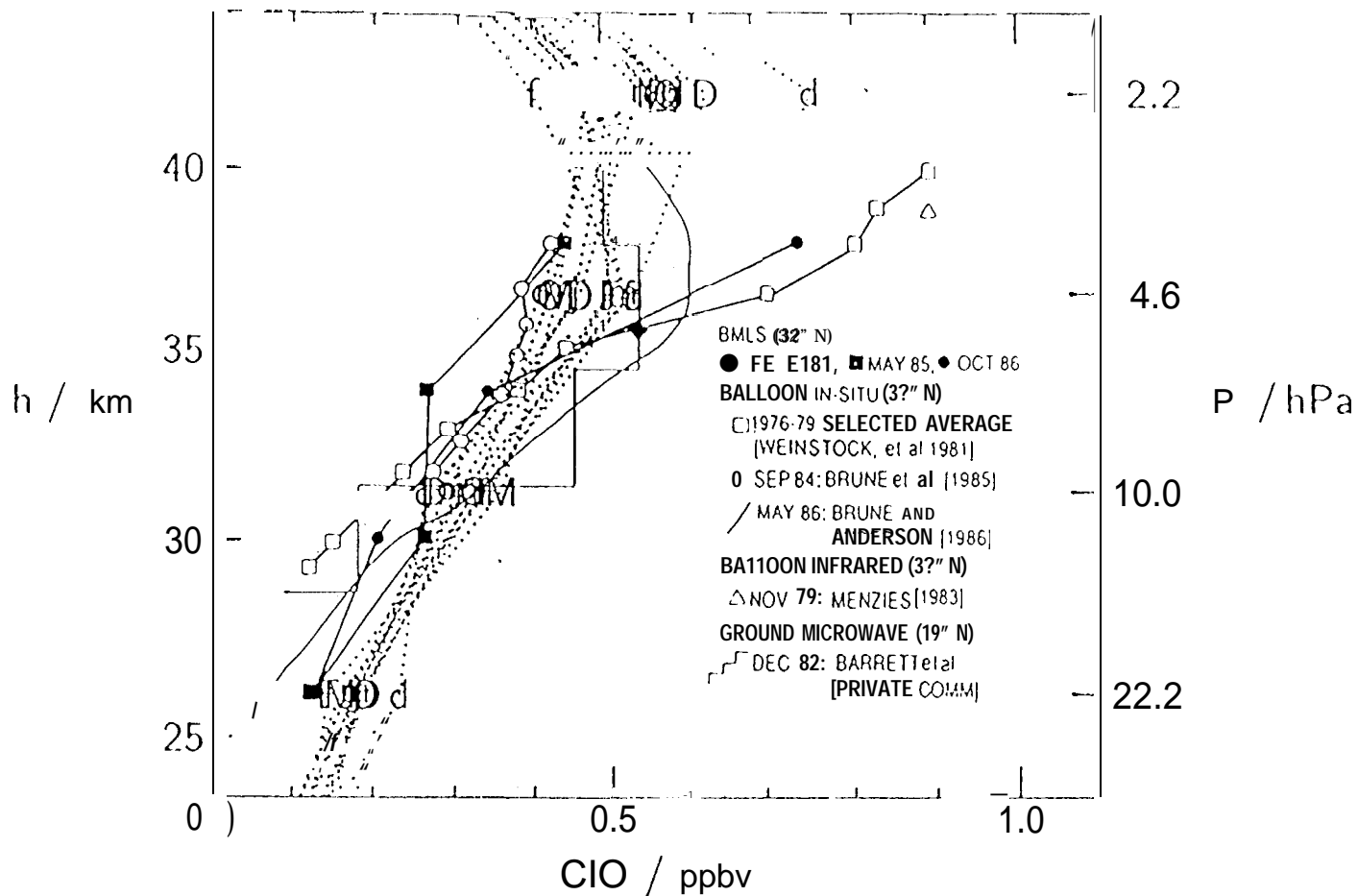
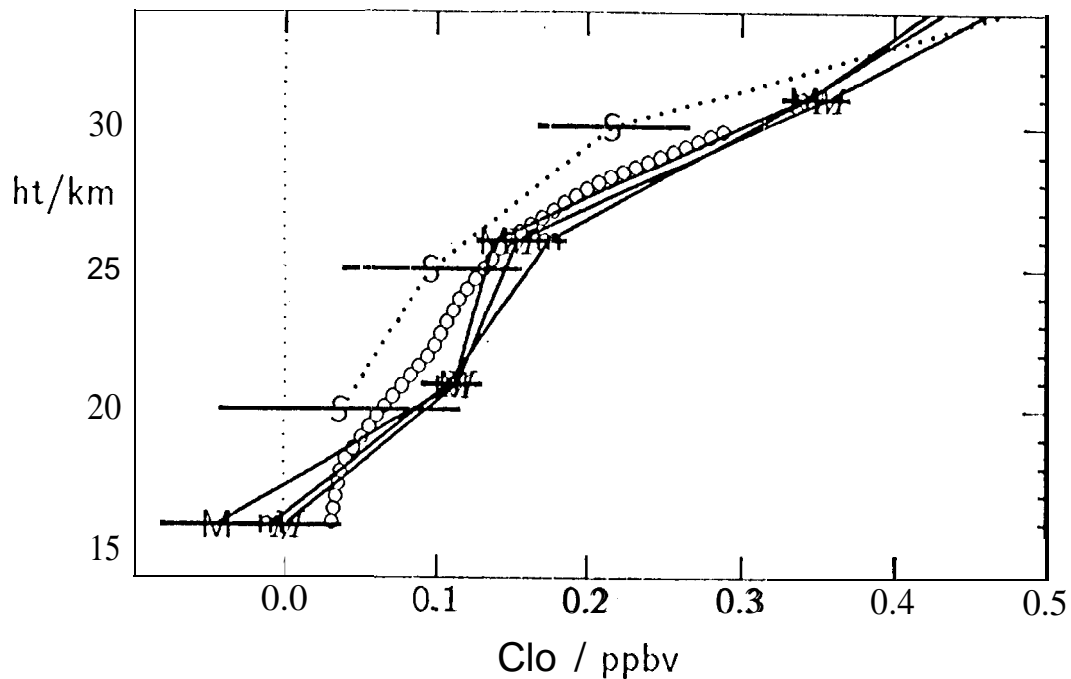
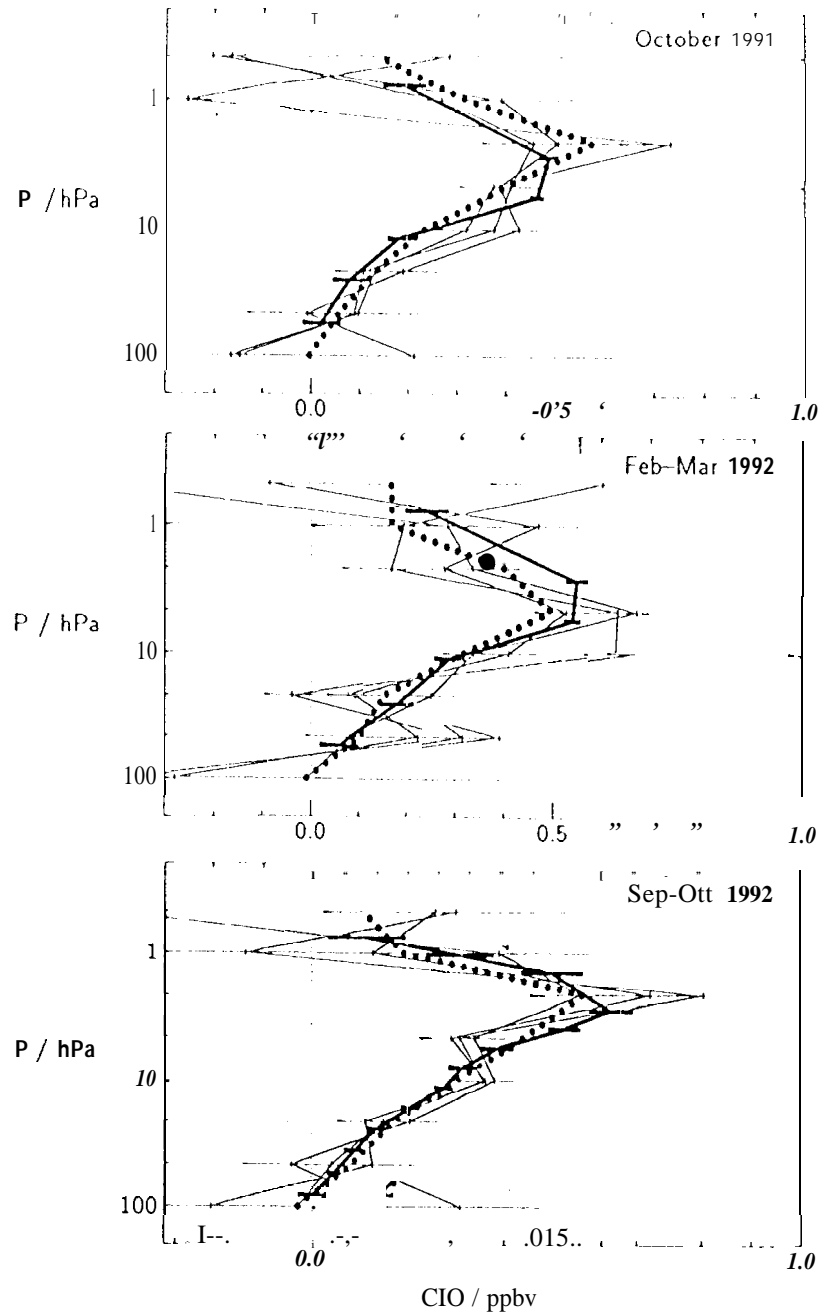


Figure 24. Comparison of MLS 20-40° N zonal mean CIO profiles with pre-UARS profiles measured at these latitudes as summarized in Figure 3 of Waters et al., [1988]. The MLS profiles are dotted, and are the same (and labeled the same) as those shown over a larger vertical range in Figure 23. [This figure will be redrawn before public at ion,]



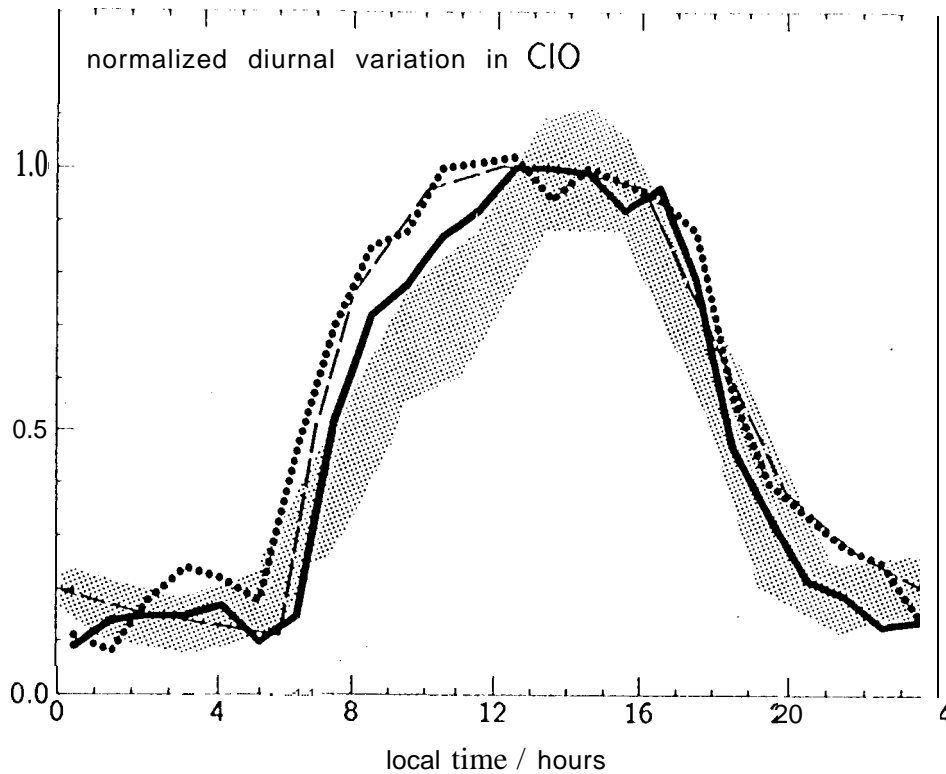
m MLS 30-40° N day-night zonal average, 15 Feb -23 Mar 1992
 M MLS 30-40° N day-night zonal average, 10 Feb -19 Mar 1993
 M MLS 30-40° N day-night zonal average, 5 Feb -14 Mar 1994
 S SLS 34° N, 9 April 1991 [Stachnik et al., 1992]
 o *in situ* 34° N, 31 March 1991 [Avallone et al., 1993a]

Figure 25. Comparison of 30-40° N lower stratospheric CIO zonal means from MLS north-looking Feb-Mar periods in 1992, 1993 and 1994 with SLS [Stachnik et al., 1992] and *in situ* [Avallone et al., 1993a] measurements for approximately the same season in 1991. The MLS values are day-night differences, with 'day' measurements having local solar zenith angles (sza) <80°, and 'night' measurements having sza >110°. Approximately 1200 individual MLS profiles were averaged for day and for night, including only data with MMAF_STAT=G and QUALITY_CIO=4. The horizontal extent, of the bars for the MLS is the observed standard deviation of the retrieved values divided by the square root of the number of measurements (and rss'd for the day-night difference).



thick line: SLS measurements at 350N
 thin lines: MLS 30-40° N daily zonal means
 dots: MLS 30-40° N monthly zonal mean

Figure 26. Comparison of Submillimeter Limb Sounder (SLS) CIO measurements at ~35° N with 30-40° N zonal mean CIO measured by MLS during the same time periods for SLS flights: (top) on 1 October 1991 from Ft. Sumner, New Mexico, (middle) on 20 February 1992 from Daggett, California, and (bottom) on 29 September 1992 from Ft. Sumner. All measurements were made during mid-day, and CIO values from the 'night' side of the orbit have been subtracted from the MLS data at 10 hPa and greater pressures to remove known biases of 0.1-0.2 ppbv at lower altitudes. The MLS daily zonal means are averages of approximately 40 individually-retrieved profiles, and the monthly zonal means are averages of approximately 1200 individual profiles. Only MLS data having QUALITY_CIO=4 and MMAF_STAT=G have been used. The horizontal extents of the bars give the estimated $\pm 1\sigma$ uncertainty of the SLS measurements and the MLS daily zonal means.



stippled	Ground-based 19° N measurements: Ott and Dec 1982 averages
solid	MLS 10–30° N monthly zonal mean for December 1991
dotted	MLS 10–30° N monthly zonal mean for October 1992
dashed	Model of Ko and Sze [1984]

Figure 27. Comparison of observed diurnal variation in upper stratospheric ClO measured by MLS and by ground-based techniques [Solomon, et al., 1984]. The quantity plotted is the column above 30 km for the ground-based results and the column above 10 hPa (~31 km) for MLS. The horizontal axis gives local solar time. Both sets of measurements have been normalized to unity peak value, and the 4 am MLS value has been slightly shifted to coincide with the ground-based value. Only MLS data having MMAF_STAT=G and QUALITY_CLO=4 have been included. The MLS measurements have been binned in one-hour intervals and the horizontal axis gives the local solar time of the measurements (the earlier sunrise and later sunset in October are evident in the MLS data); between 100 and 500 individually-retrieved profiles were averaged for each local time bin. The ground-based measurements were binned in two-hour intervals.

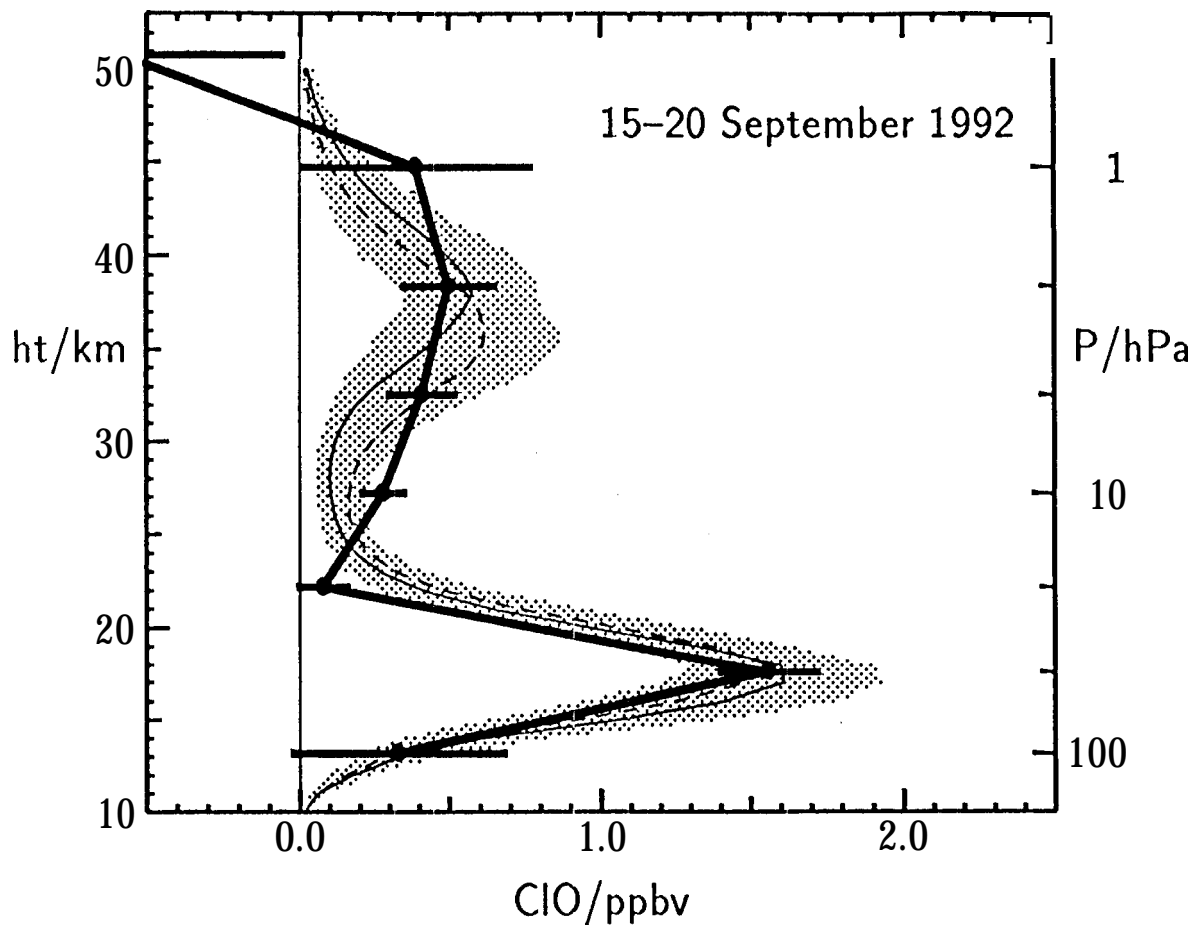


Figure 28, Comparison of ground-based and MLS measurements of the ClO profile over McMurdo Station (78° S, 166° E) Antarctica during 15-20 September 1992. The thick line is the average of all MLS profiles measured at latitudes 75- 80° S and longitudes 140-190° E (within ~500 km of McMurdo) during 15-20 September 1992. Only data having MMAF_STAT=G and QUALITY_CLO=4 were used. Horizontal bars are the estimated $\pm 1\sigma$ uncertainty in the precision of the MLS averages. Heights of the MLS pressure surfaces are from geopotential height obtained from the MLS data. Thin lines show the profiles obtained from the ground-based measurements [Shindell et al., 1994]. The thin solid curve is for measurements on 15 September 1992, and the dashed curve is for measurements on 19-20 September. The shaded area is the $\pm 1\sigma$ total uncertainty (including calibration, atmospheric parameter uncertainties, and retrieval algorithm limitations) estimated by the ground-based team. Day-night differences have been taken at 10 hPa and below for both MLS and ground-based results.

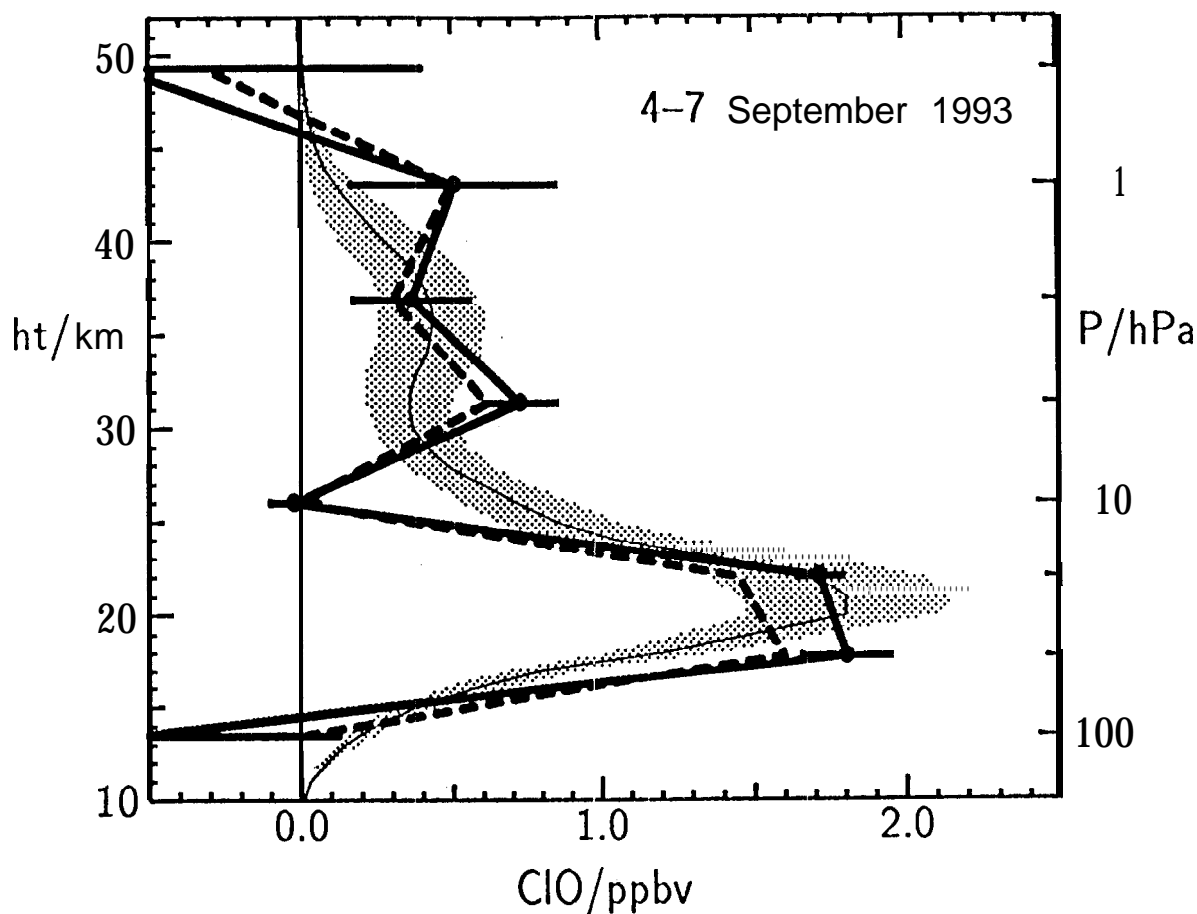


Figure 29. Comparison of ground-based and MLS measurements of the C10 profile over McMurdo Station (78°S, 166°12) Antarctica during 4-7 September 1993. The thick solid line is the average of profiles measured at latitudes 75-80°S and longitudes 140-190°E (within ~500 km of McMurdo) from the MLS Version 3 data. The thick dashed line is an average of the same MLS observations, but from an iterative retrieval performed after averaging the measured radiances. Only MLS data having `MMAF_STAT=G` and `QUALITY_C10=4` were used. The horizontal range of the bars on MLS profile retrieval points are the estimated uncertainty of the MLS average. The thin line is the profile obtained from the ground-based measurements [deZafra et al. 1994 b]. The shaded area is the $\pm 1\sigma$ total uncertainty (including calibration, atmospheric parameter uncertainties, and retrieval algorithm limitations) estimated by the ground-based team. Day-night differences have been taken at 10 hPa and below for both MLS and ground-based results.

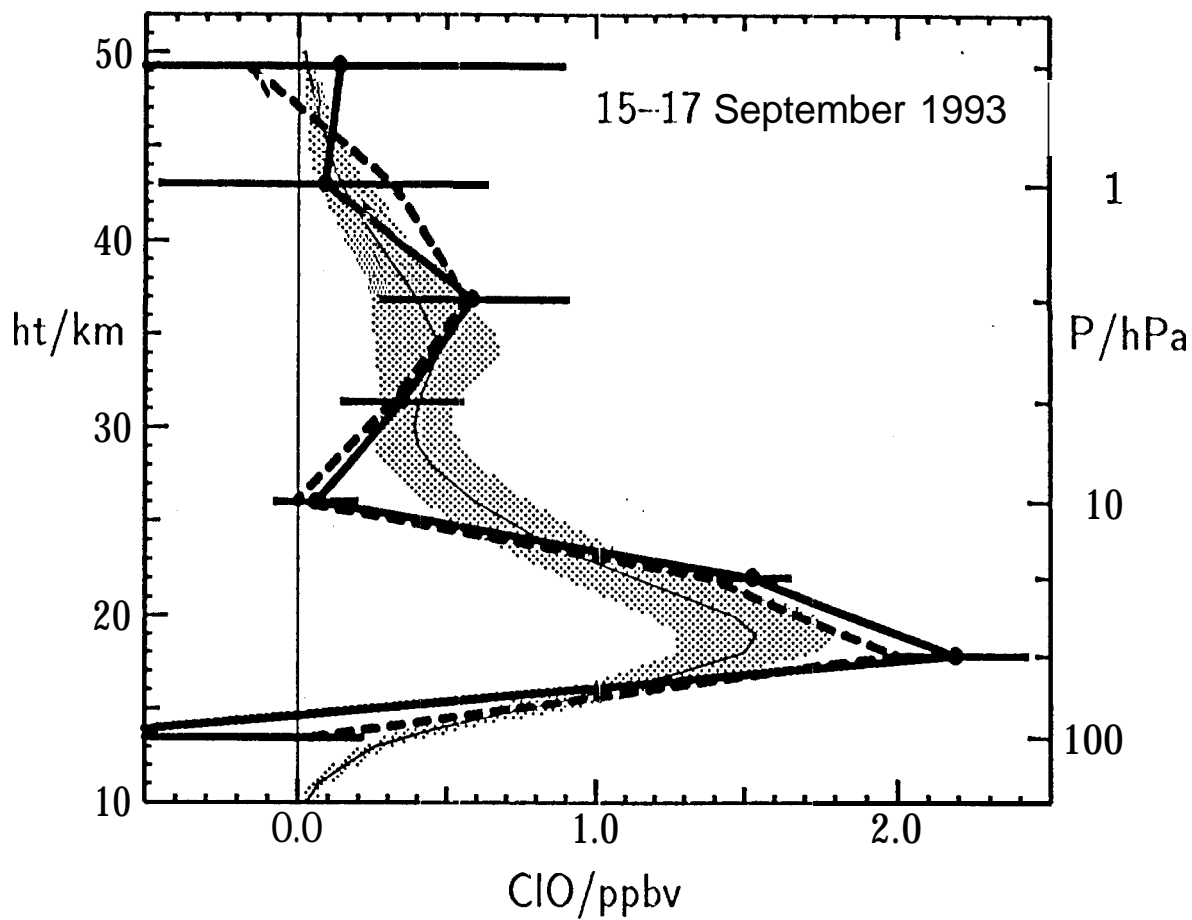


Figure 30, Same as Figure 29, except that the ground-based profile (thin line) is for 17 September 1993 and the MLS profiles (thick lines) are for 15-16 September (MLS turned to north-viewing on 17 September 1993).

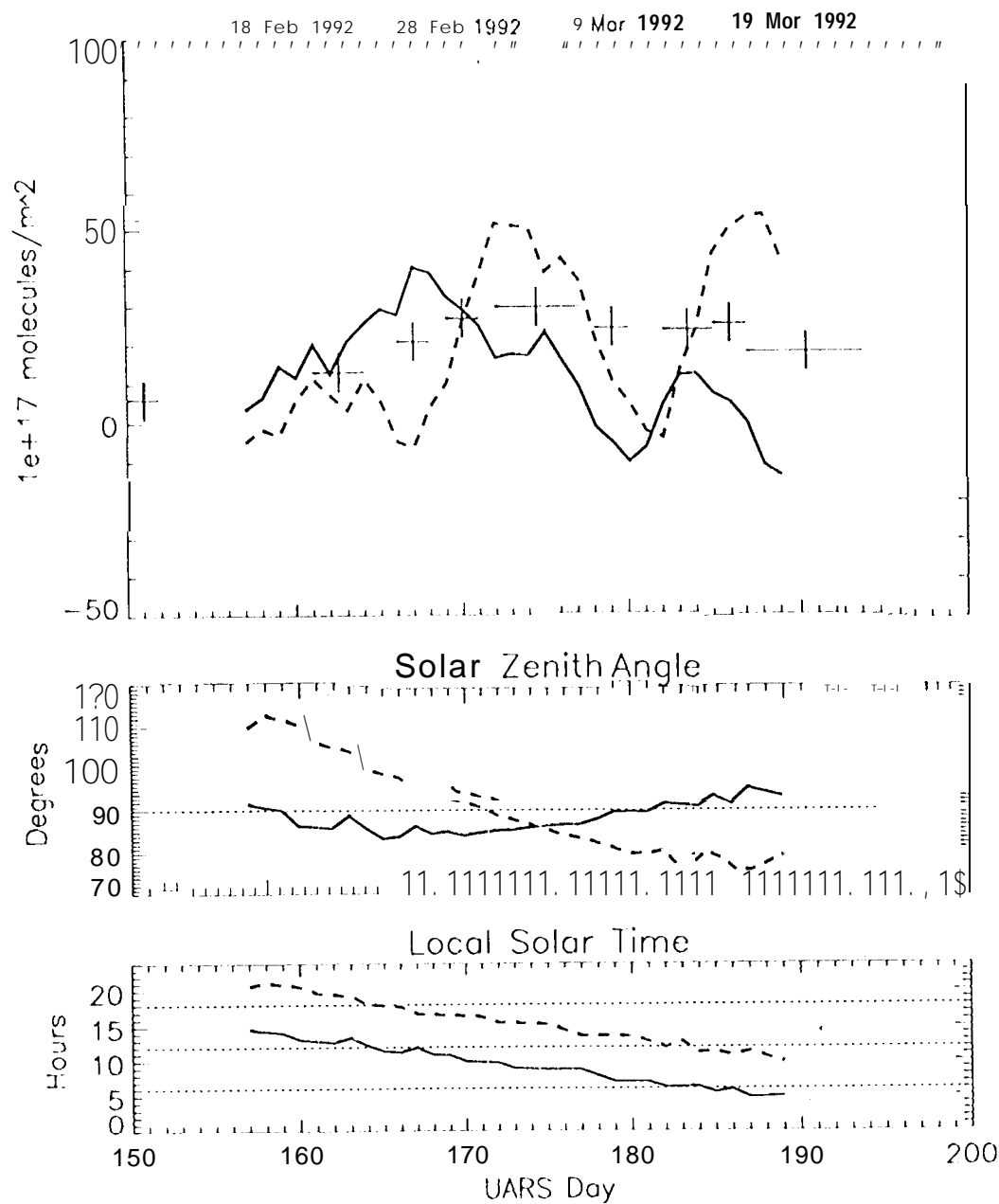


Figure 31. Comparisons of column ClO measurements over Thule, Greenland, in February and March 1992. The crosses are ground-based measurements [deZafra et al., 1994a], and the lines are from MLS. The ground-based measurements have been averaged over a period of 3-5 days, and the MLS measurements have been averaged by a running 5-day smoothing. The MLS measurements are each day's values measured nearest Thule; the solid line gives measurements on the ascending side of the orbit, and the dashed line gives measurements on the descending side of the orbit. Only data having MMAF_STAT=G and QUALITY_CLO=4 have been included. The solar zenith angle and local solar time of the MLS measurements are shown in the two bottom panels. Prior to UARS day 175 the ascending side of the orbit gave measurements nearest mid-day (when the ground-based measurements were taken, and following day 175 the descending side of the orbit gave measurements nearest mid-day. Thus the solid curve should be used for comparisons before day 175 and the dashed curve following day 175.

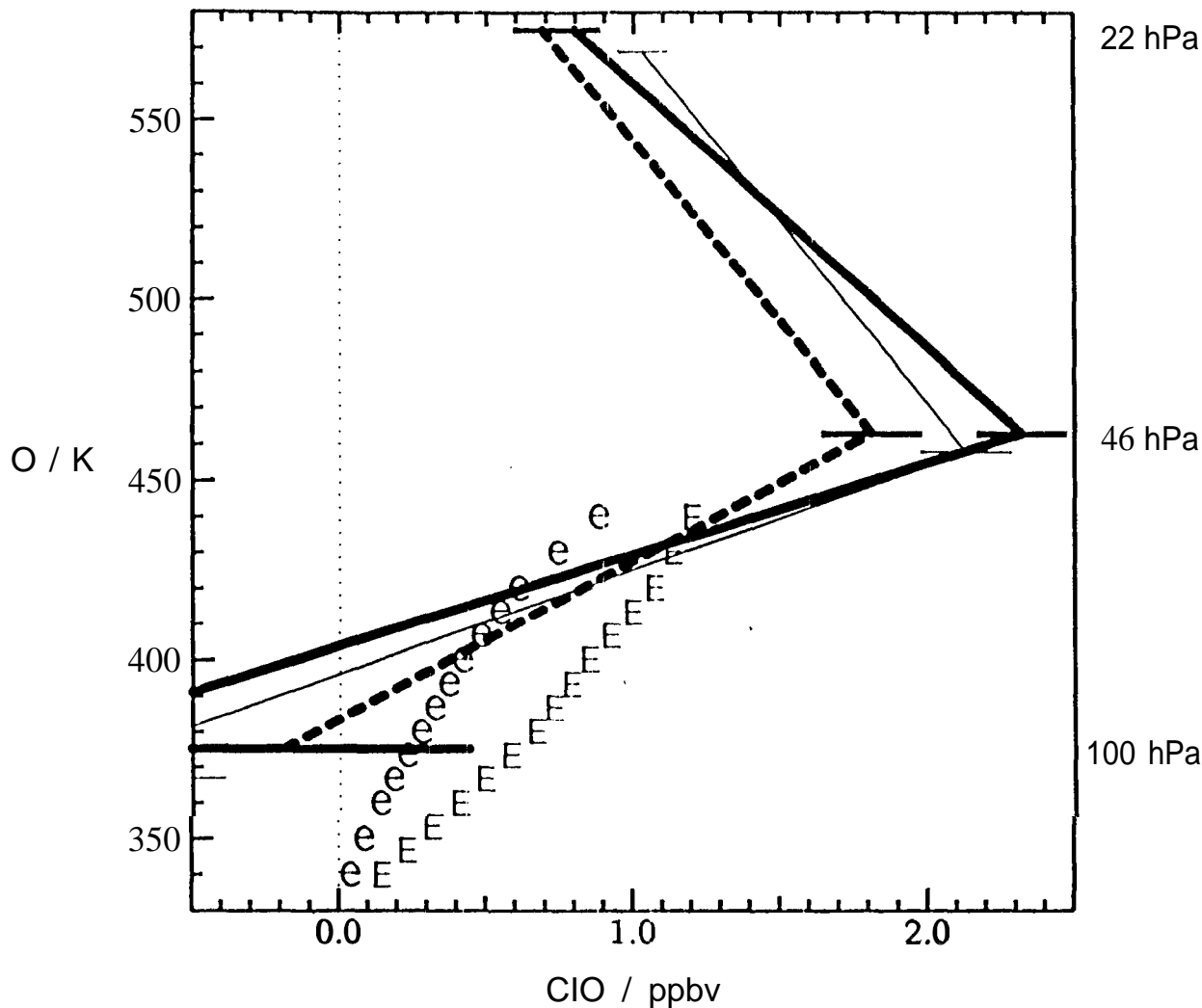


Figure 32. Comparisons of MIS September 1992 and 1993 Antarctic ClO profiles with that measured by the RR-2 aircraft in September 1987. The vertical coordinate indicated on the left is potential temperature, and pressures at MIS retrieval points are indicated on the right. The MIS measurements shown here are averages over 71–73° S latitude and 0–140° W longitude, for the periods 6–11 September 1992 (thin lines) and 7–12 September 1993 (thick lines). These periods were chosen to be in the middle of the corresponding 1987 dates of the RR-2 flights, and when MIS maps showed the edge of enhanced ClO to be at approximately the same location as seen by the RR-2 in 1987. Solid lines are averages of individual MIS Version 3 profiles; dashed lines are iterative retrievals on averaged radiances from the same data sample. The iterative retrievals use the revised O_2 linewidth for pointing and account for the effects of HNO_3 . Day–night differences have been taken for all the MIS data shown here, and horizontal bars give the estimated $\pm 1\sigma$ precision. The RR-2 profiles (e,E) were made at approximately 72° S, 70° W. The lower values (e) are the averages from 10 flights occurring between 23 August and 22 September 1987 reported in *Anderson et al., [1989]*; the higher values (E) are the RR-2 results after recalibration. The uncertainty in the absolute values of the recalibrated RR-2 data is $\pm 25\%$, at 90% confidence limits [*Anderson et al., 1991*].

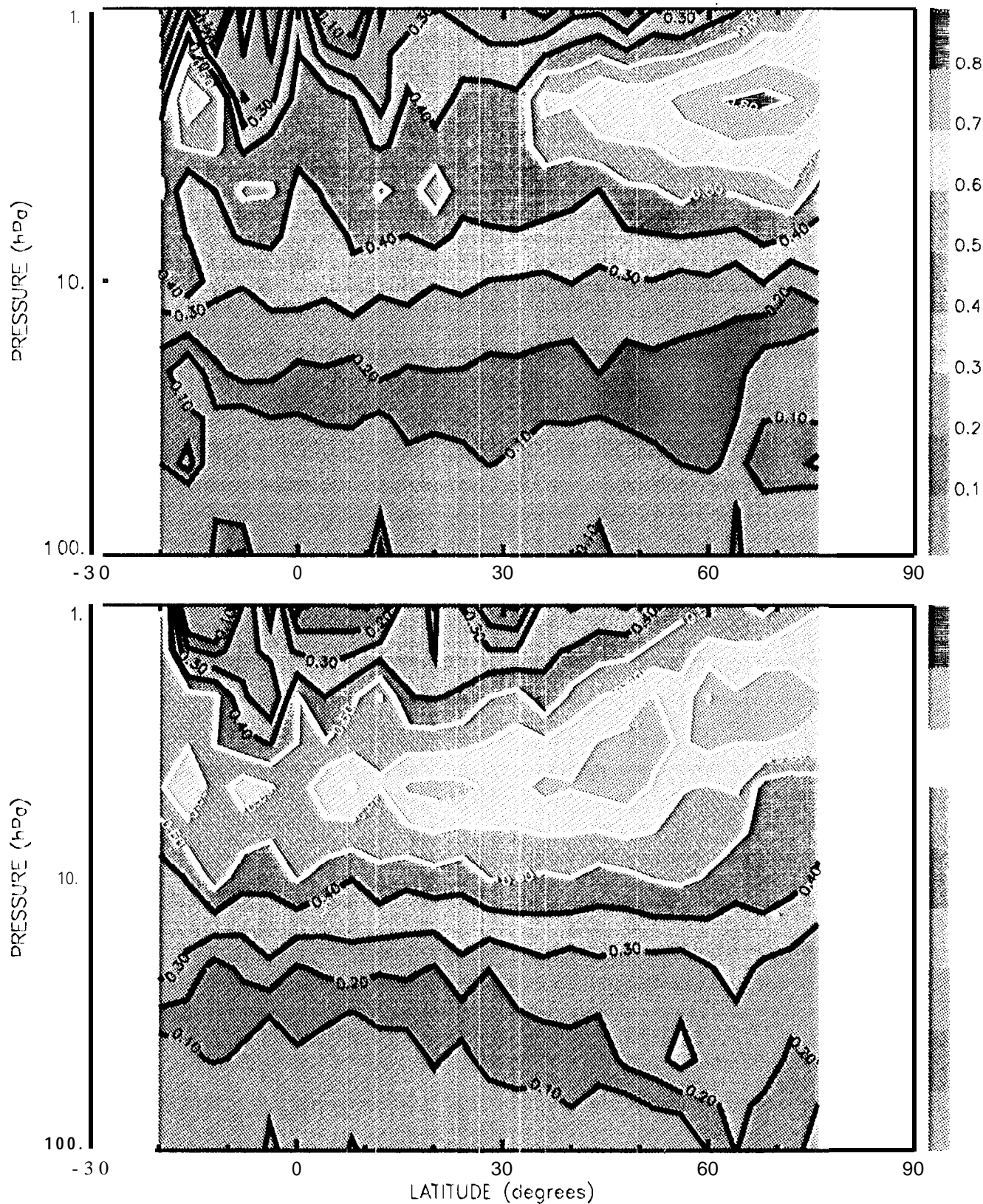
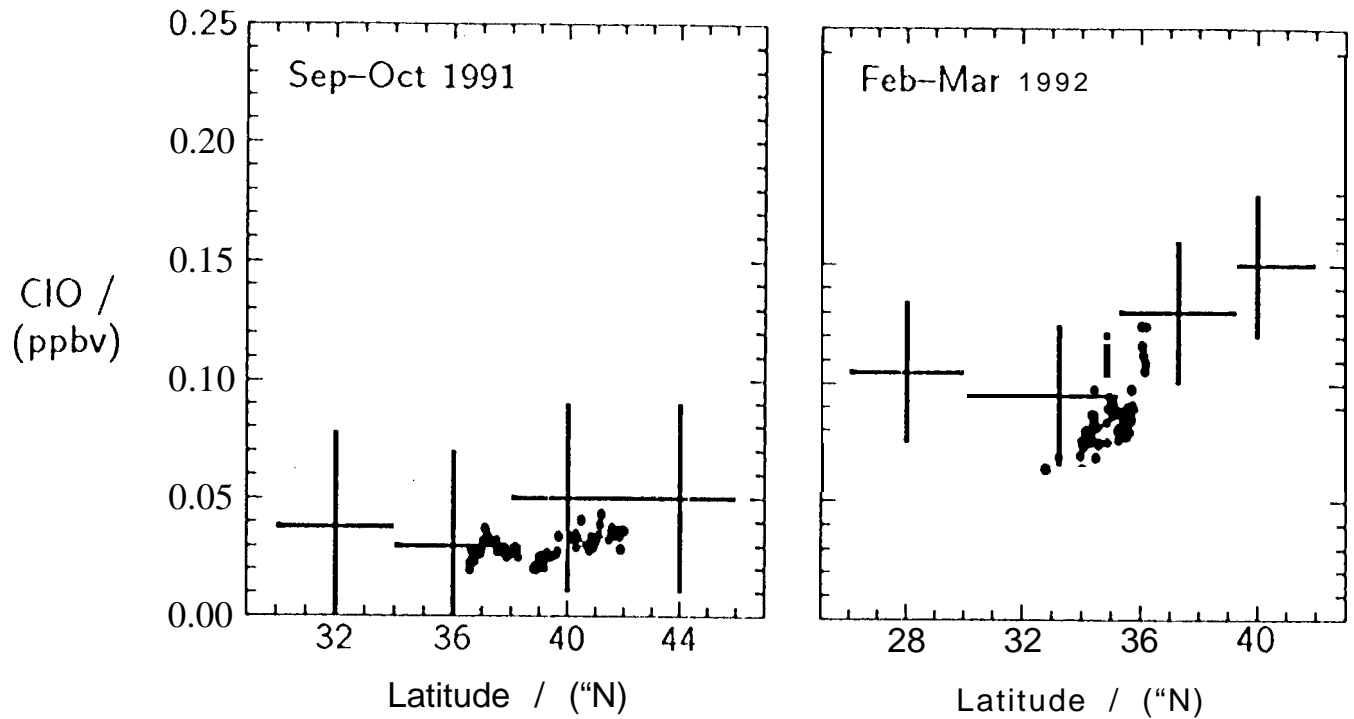


Figure 33. Zonal mean of MLS daytime ClO measurements for 1 to 31 October 1991 (top) and 15 February to 22 March 1992 (bottom). The latitude interval is 4° and each latitude bin is an independent sample (i.e., there has been no ‘smoothing’ of the data). The color scale is ClO abundance in ppbv. Only data having MMAF_STAT=G and QUALITY_CLO=4 have been included. Day-night differences have been taken at 4.6 hPa and below.



points: ER-2 measurements on 17 Sep 1991 and 22 Mar 1992
 crosses: MLS zonal averages for 2-31 Oct 91 and 15 Feb --22 Mar 92

Figure 34. Comparison of *in situ* ER-2 lower stratospheric ClO measurements with zonal means from MLS. ER-2 values, from Figure 3a of *Fahney et al.*, [1593] are individual measurements made between 50 and 65 hPa on the indicated dates. MLS values, taken from higher-resolution versions of the contour plots shown in the previous figure, are day-night differences of zonal averages at the same altitudes as the ER-2 measurements.

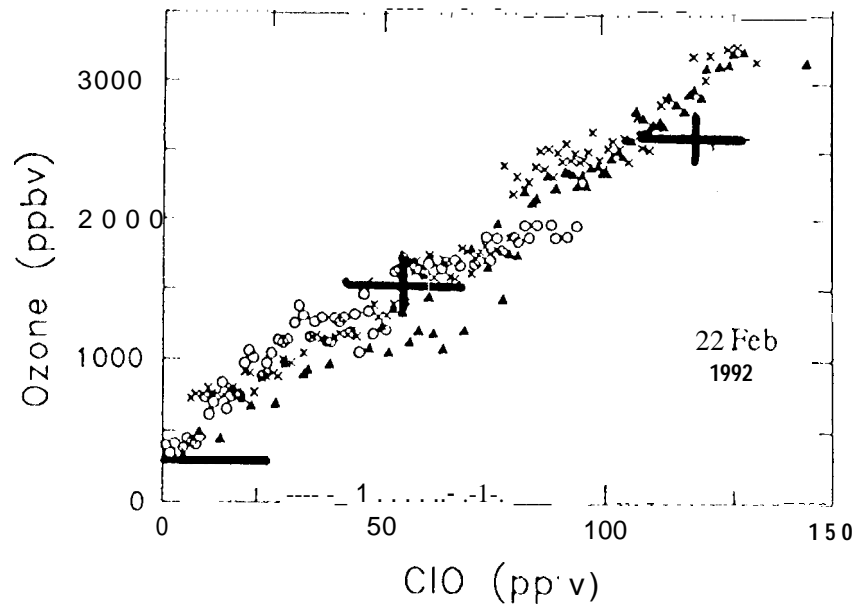
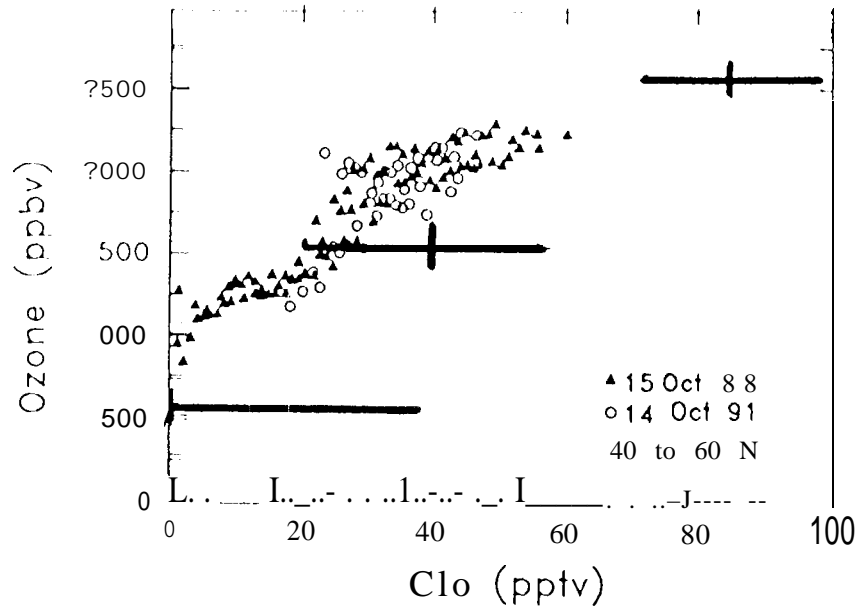


Figure 35. Lower stratospheric ClO plotted versus ozone from (symbols) ER-2 *in situ* measurements [Avallone *et al.*, 1993b] and from (crosses) MIS. The upper panel is for October (dates shown in 1988 and 1991 for ER-2; 1-30 October 1991 for MIS) and covers 40-60 N latitudes. The lower panel is for February 1992 (22 February for ER-2; 15 February through 22 March for MIS) and covers 20-50° N. The upper crosses are MIS values at 46 hPa, the middle crosses at 68 hPa, and the lower crosses at 100 hPa. Note the different ranges (of both ozone and ClO) in the two panels. MIS values are monthly zonal means with day-night differences taken. The horizontal extent of the crosses gives the observed standard deviation of MIS ClO measurements divided by the square root of the number which were averaged. Only MIS data having MMAF_STAT=G and QUALITY_CLO=4 have been included. [Note: this figure will be redrawn before publication.]

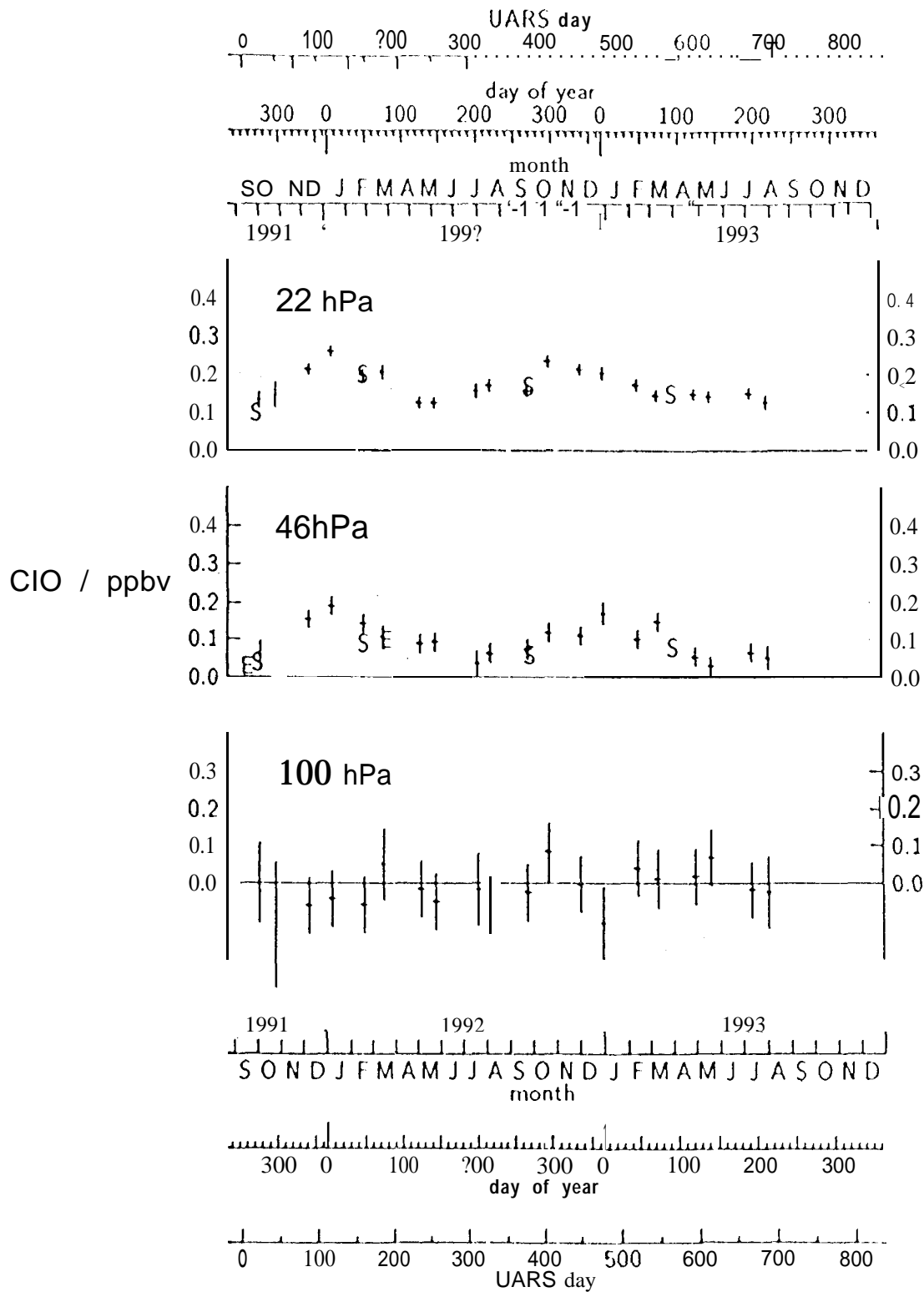


Figure 36. Time-series of 30-50° N monthly zonal means of MLS lower stratospheric ClO data (crosses) compared with ER-2 (E) and SLS (S) measurements. MLS data from the night side of the orbit have been subtracted to remove biases. The vertical extents of the crosses give the estimated precision of the MLS means, and the horizontal extents give the time period over which the data were taken. The ER-2 measurements [Fahey et al., 1993] were made at 50-65 hPa.

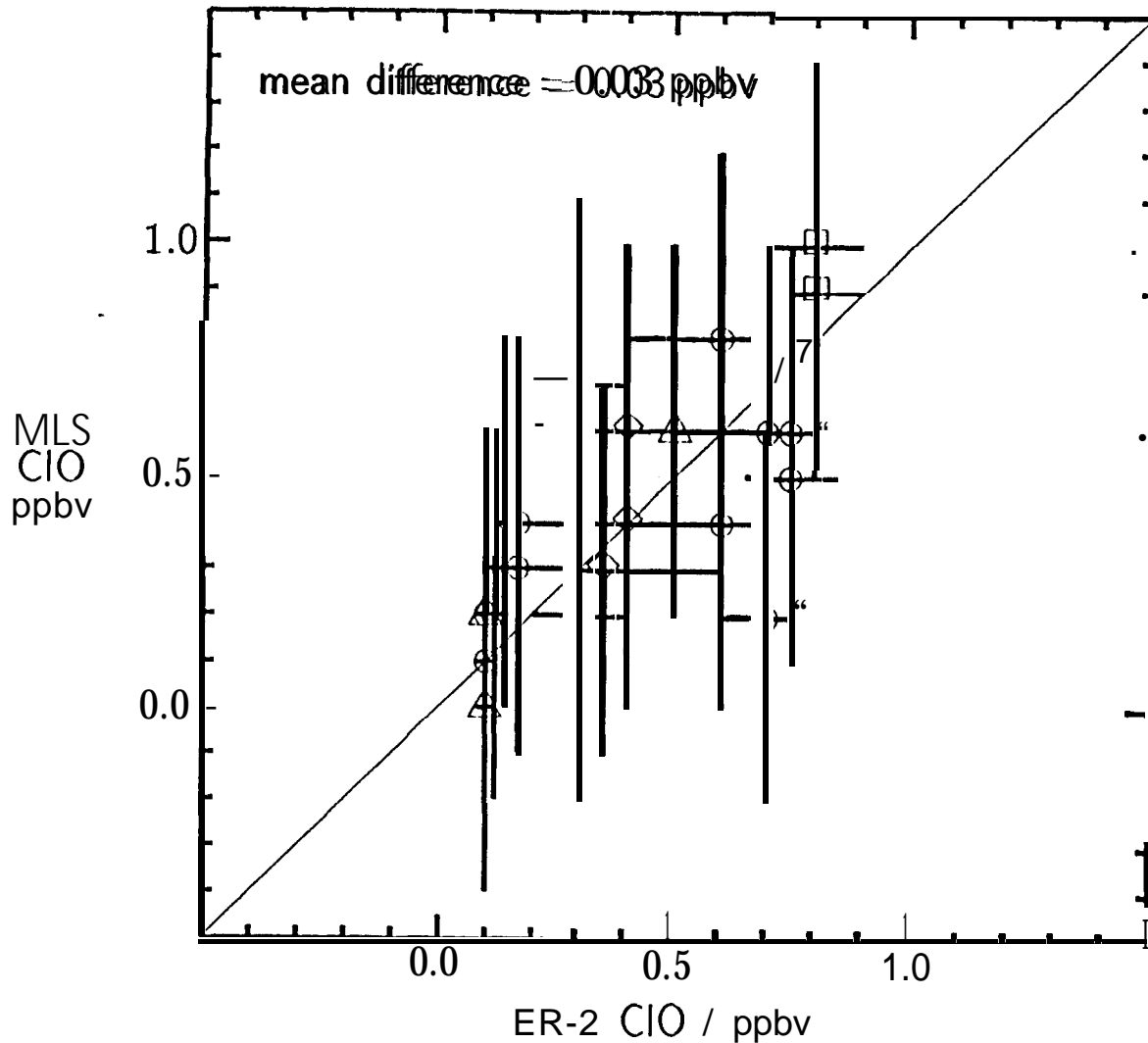


Figure 37. Scatterplot of individual MLS ClO measurements versus near-coincident ER-2 measurements. The ER-2 measurements were made during flights north from Bangor, Maine, as part of the AASE-II campaign [Toohey *et al.*, 1993]. The MLS values (Version 3 data) are taken from MLS vertical profiles at the potential temperature of the ER-2 measurement. Numerical values, locations and times of the measurements are given in Table 4. Symbols indicate measurements on 4 January (A), 6 January (D), 8 January (O), and 17 February (O) 1992. The vertical extent of each cross is the $\pm 1\sigma$ MLS measurement noise, and the horizontal extent indicates the range of values measured by the ER-2 over the approximate spatial area sampled by MLS. The diagonal straight line is where points would lie if there were perfect agreement. The mean difference of 0.03 ppbv is the average value of the difference (MLS-ER2) in all measurements shown here.

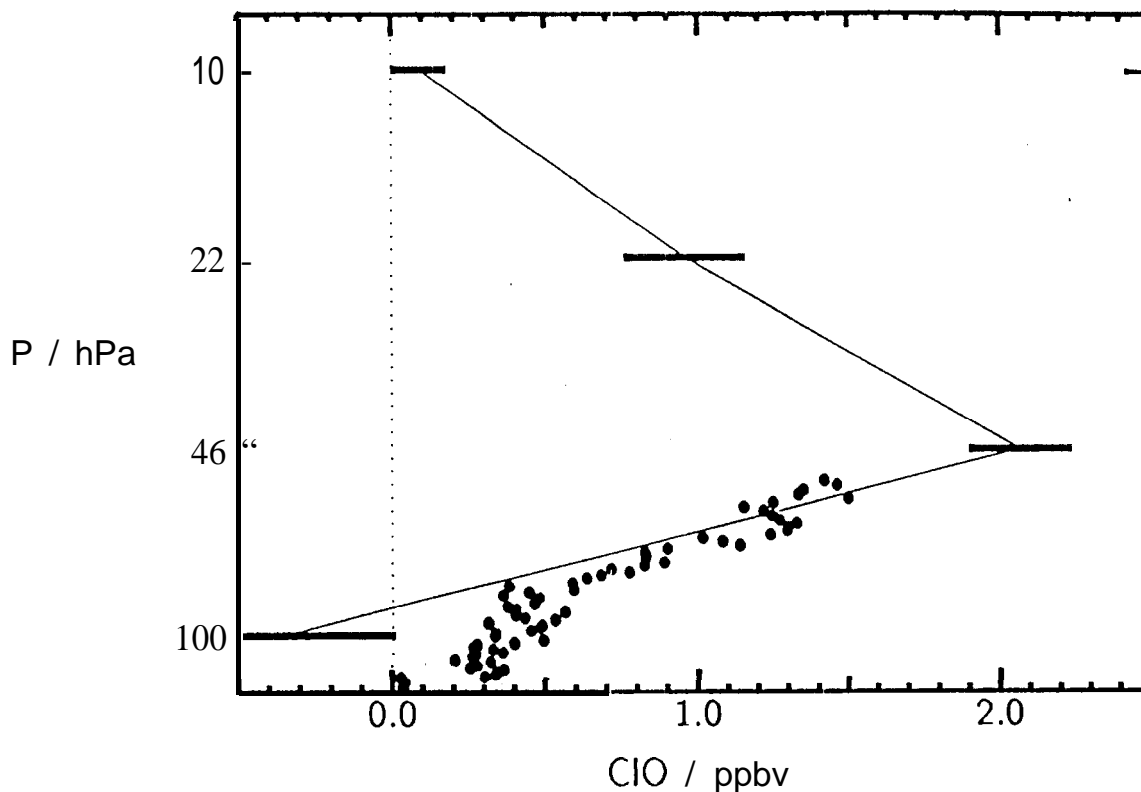


Figure 38. Comparison of largest CIO abundances from MLS Version 3 (line) and ER-2 (•) measured in the Arctic vortex during January 1992. The MLS profile is the average of all measurements made during 9-11 January between 55- 65° N and 0- 60° E (see Figure 4 of Waters et al. [1993a]). The ER-2 measurements [Tohey et al., 1993b] are a combination of two profiles measured within the vortex on 20 January: one at 68° N, 60° W measured at local times within one-half hour of noon, and the other at 54° N, 67° W measured between 1:30 and 2:15 pm local times. There is almost no difference between the two ER-2 profiles. The MLS measurements are averages of day-night differences, and only data having X14 AF_STAT=G and QUALITY_CIO=4 are included. The MLS day measurements were at local solar times within one hour of noon (solar zenith angles of 77- 86°); the night measurements were at local solar times between midnight and 2 am. The horizontal extent of each bar gives the estimated $\pm 1\sigma$ precision for the MLS day-night average. Systematic uncertainties for the MLS measurements are discussed in the text. Uncertainty in the absolute values of the ER-2 measurements is $\pm 15\%$ ($\pm 2\sigma$).